REGULATION OF ATR SIGNALING BY CINP AND RPA

By

Xin Xu

Dissertation

Submitted to the Faculty of the

Graduate School of Vanderbilt University

in partial fulfillment of the requirements

for the degree of

DOCTOR OF PHILOSPHY

in

Biochemistry

August, 2009

Nashville, Tennessee

Approved:

Professor David Cortez

Professor Ellen Fanning

Professor Scott Hiebert

Professor Lawrence Marnett

Professor Neil Osheroff

To my parents

and

To my daughter, Lydia

and

To my beloved wife, Zhe Li, infinitely supportive

ACKNOWLEDGEMENTS

I thank my thesis advisor, Dr. David Cortez for the training and support without which this research would not have been possible. Dave showed me how to think critically, keep an open mind, and plan projects wisely. His enthusiasm for science motivated me to start a rotation in his lab when I was in the first year IGP program. Dave has been very patient to exchange thoughts with me about projects and seminars. He is always willing to help his students, and his advice has benefited me in many aspects including for my future career and also my personal life. I feel very fortunate to have had the opportunity to train under Dave's supervision.

I also thank the members of my thesis committee: Dr. Ellen Fanning, Dr. Scott Hiebert, Dr. Larry Marnett, and Dr. Neil Osheroff for their scientific expertise and advice. They helped me prioritize projects and kept me focused. Their criticism and encouragement helped me on my thesis projects and also for my future career. I especially want to thank Dr. Fanning. Her expertise in the field of studying DNA replication directly benefited my first project.

My collaborators, Dr. Walter Chazin and Dr. Sivaraja Vaithiyalingam contributed to this research. Their expertise in structure biology and NMR experiment is a part of foundation for this research. I also thank Dr. Sivaraja Vaithiyalingam for his help in protein purification. Other collaborations are acknowledged where applied inside of the thesis.

I also am grateful to all the members of the Cortez laboratory, who make up of this great team. Gloria Glick is the lab manager who makes sure the lab supplies are

sufficient and organized. Without her dedication, my work would have taken much longer to accomplish. Also she cares about the productivity of students, which are essential towards graduation. In addition, her work directly contributed to my research was recognized inside of this thesis. She also cared for my family, especially after my daughter was born two years ago. I also thank other lab members, past and present, for helping me in many aspects including scientific experiments and English communication. I would especially like to thank Heather Ball, Courtney Lovejoy, Jeremy Myers, and Daniel Mordes who have been in the lab with me the longest. Heather has always been a good source of scientific ideas and an initiator of fun parties. She was an example of the student life in the Cortez laboratory which stimulated my decision to join the lab. Courtney and I joined the Cortez laboratory at the same time, and she graduated two months before me. She is always willing to share ideas, reagents, and experimental protocols. It is also my pleasure to collaborate with her for the recent project about studying the function of CINP. Dr. Jeremy Myers not only contributed to my graduate research, but also shared his experiences and his understanding of science. He is a good friend that I can ask for honest advice for my work and future career. Daniel Mordes provided valuable ideas and suggestions to many projects in the lab. One of his ideas initiated one of my projects which became a part of this research. Finally, I would like to thank Eddie Nam and Tim Wiltshire for reading my thesis and their advices on English writing.

I thank the members of Dr. Pietenpol laboratory and Dr. Sun laboratory for their suggestions and discussion about my projects. They are generous to share equipments and ideas. I would also like to thank members of the Biochemistry Department who have

supported me as a graduate student. Marlene Jayne kindly reminded me all the deadlines for graduation. I appreciate her and other administrative supports from Robert Dortch, Peggy Fisher, Brenda Bilbrey, and Melvin Fitzgerald, which are essential for keeping our department and graduate school requirements in order. I also thank the graduate school for supporting travel to conferences.

I thank all of my friends for their friendship, which makes me feel home in the U.S. Special thanks to the Cretins, the Thurmans, the Lowes, the Lins, and the Shis. They have been caring for my family and my career. I will miss them. Also I would like to thank Jenna Ray, Kay Eaves, Jennifer Stadler, Shelia Thurman, and C. T. for reading my thesis and their help on English writing.

Finally, I want to thank my family. My parents are very supportive to my education and career. Their encouragements and supports are always with me. My wife, Zhe supports me in every way. I specially thank her for understanding that I have to work long hours many days. I also thank my daughter, Lydia. Her big hugs and smiles bring me joy and happiness after my bench work.

TABLE OF CONTENTS

LIST OF TABLES

LIST OF FIGURES

LIST OF ABBREVIATIONS

2D	two dimensional
6-4PPs	(6-4) photoproducts
9-1-1	Rad9-Hus1-Rad1
AAD	ATR activation domain
APC	anaphase-promoting complex
ATM	Ataxia Telangiectasia Mutated
ATR	ATM and Rad3 Related
ATRIP	ATR Interacting Protein
BER	base excision repair
bp	base pair
BRCT	BRCA1 C-terminal domain
CAK	Cdk-activating kinase
Cdk	cyclin-dependent kinase
CHIP	chromatin IP
CINP	Cdk2—interacting protein
CPD	cyclobutane pyrimidine dimer
CRD	checkpoint recruitment domain
DDR	DNA damage response
DMEM	Dulbecco's Modified Eagle medium
DNA	deoxyribonucleic acid
DNA-PKcs	DNA dependent protein kinase catalytic subunit

dNTP	deoxyribonucleotide triphosphate
DSB	double strand break
dsDNA	double-stranded DNA
EBV	Epstein-Barr virus
FEN1	flap endonuclease 1
HR	homologous recombination
ICL	inter-strand cross-link
INK4	inhibitors of Cdk4
IP	immunoprecipitation
IR	ionizing radiation
LOH	loss of heterozygosity
MCM	mini-chromosome maintenance
MMC	mitomycin C
MMS	methyl methane sulfonate
MRN	Mre11-Rad50-NBS1
NER	nucleotide excision repair
NHEJ	non-homologous end joining
NLS	nuclear localization signal
NMR	nuclear magnetic resonance
OB-fold	oligonucleotide/oligosaccharide-binding fold
ORC	origin recognition complex
PRC	pre-replication complex
PAGE	polyacrylamide gel electrophoresis

PCD	programmed cell death
PCNA	proliferating cell nuclear antigen
PCR	polymerase chain reaction
pso	psoralen
RDS	radio-resistant DNA synthesis
RFC	replication factor C
RNA	ribonucleic acid
RPA	replication protein A
SSA	single strand annealing
ss-DNA	single stranded DNA
siRNA	small interfering RNA
TCL	total cell lysate
TFO	triple helix forming oligonucleotides
TLS	translesion synthesis
TopBP1	topoisomerase-II-binding protein 1
UV	ultra violet
XP	xeroderma pigmentosum

CHAPTER I

INTRODUCTION

All organisms are composed of cells. Every cell comes from a pre-existing cell (1). Each cell contains a set of instructions and the production facilities for making the materials that will form a new cell. The instructions are encoded in the sequence of DNA, which is the genetic information, and the totality of genetic information for a cell is called the genome. During cell proliferation, the genome has to be duplicated precisely, and two copies of the genome have to be evenly propagated into two daughter cells. Maintaining genome integrity is critical for cellular viability and disease prevention in multicellular organisms including humans.

DNA is composed of two strands that twist together to form a helix and is packed into a set of chromosomes (2, 3). The DNA replication process is a semi-conservative process (4). Parental DNA strands are unwound and used as templates to synthesize complementary strands. As a result, each new copy of the DNA helix will have one strand of parental DNA and one nascent strand when DNA replication is finished. Cells are constantly challenged by DNA damaging agents from endogenous and exogenous sources. Free oxygen radicals, by-products of normal cellular metabolism, and ultraviolet radiation from environmental sources cause DNA lesions. The ability of cells to deal with DNA damage is essential for maintaining genome integrity. Damaged DNA will result in erroneous DNA replication if the damage is not corrected. The altered genetic information will be passed into daughter cells permanently after chromosome

propagation and cell division. When mutations arise, activation of oncogenes and inactivation of tumor suppressor genes can occur. This can promote more mutations. Accumulated mutations are a characteristic of tumors in humans.

In this chapter, I will discuss how the DNA replication process is regulated in cells, how DNA damage causes problems during DNA replication, and how cells respond to these problems to maintain genome integrity.

The Cell Cycle and DNA Replication

Cell proliferation is a complex process that includes duplication of the cellular components and division into two cells. This process is called the cell cycle and can be separated into four different phases by functional purposes (Figure 1.1A). DNA replication occurs during S phase (DNA synthesis), and cell division occurs in M phase (mitosis). Two gap phases (G1 and G2) separate the S and the M phases. Cells prepare for DNA replication in G1 phase and prepare for cell division in G2 phase.

Regulation of eukaryotic cell cycle

Cell cycle progression is controlled by a series of cyclin-dependent kinases (Cdks) (5). Cdk activation requires their binding partners, cyclins. Cyclins are expressed in a cyclical fashion (6, 7). They have no catalytic activities. The expression of Cdks is not changed in different phases throughout the cell cycle. The oscillating expression of cyclins results in oscillating activities of Cdks by forming corresponding Cdk-cyclin complexes in different phases (Figure 1.1A).

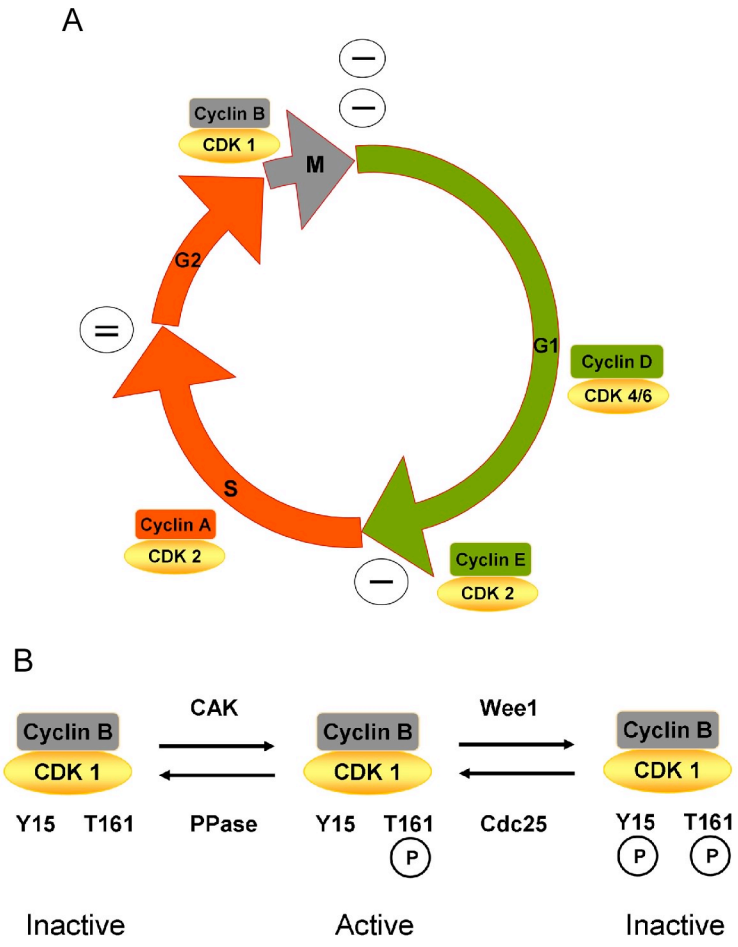

Figure 1.1. Cdk activities control the cell cycle progression. (A) Cell cycle progression. The cell cycle consists of four phases, G1, S, G2, and M phases. Oscillating expressed cyclins activate correspondent Cdks for different phases. DNA replication occurs in S phase, and cell division occurs in M phase. Colors of cyclins correspond to different phases of the cell cycle. (B) Kinase activity of Cdk-cyclin is regulated through phosphorylation, one activatory phosphorylation (T161 on Cdk1) and one inhibitory phosphorylation (Y15 on Cdk1).

Cyclin D expression is stimulated in response to mitogenic factors in the extracellular environment in G1 phase (8). Cyclin D binds to Cdk4 or Cdk6. Cdk4/6-cyclin D complexes phosphorylate the tumor suppressor protein Rb, which results in the release of transcription factors including E2F (9, 10). This promotes the expression of cyclin E (11, 12). Cyclin E associates with Cdk2 and activates Cdk2. Activation of the Cdk2-cyclin E complex drives cells entering S phase through phosphorylation of various targets including Rb (11, 13). Upon entry into S phase, cyclin E undergoes degradation mediated by the proteasome (14, 15). Cyclin A expression results from the activation of Cdk2-cyclin E. The activity of Cdk2-cyclin A drives cells through S phase and regulates DNA replication (3, 16). Cyclin A remains present throughout the G2 phase and associates with Cdk1 during the transition from G2 to M phase. Upon entry into M phase, cyclin A is degraded, and cyclin B associates with Cdk1 to drive cells through M phase (17).

In addition to cyclins, the activities of Cdks can also be regulated by cellular inhibitors and phosphorylation. The inhibitors of Cdk4 proteins (INK4), p16, p15, p18, and p19, specifically bind to and inhibit Cdk4 and Cdk6 (18). The Cip/Kip family of proteins including p21 and p27 act as broad inhibitors for Cdk4, Cdk6, Cdk2, and Cdk1 (19). Cdk2 and Cdk1 undergo two types of phosphorylation for activating and inhibiting their kinase activities (Figure 1.1B). Cdk2 phosphorylation on threonine 160 is required for activities of Cdk2-cyclin E and Cdk2-cyclin A and is accomplished through Cdk-activating kinase (CAK) (20-22). Cdk2 is also phosphorylated on inhibitory sites, threonine 14 and tyrosine 15 (19, 20). The inhibitory phosphorylations are relieved by the action of the phosphatase Cdc25 (23). Cdk1 also undergoes similar positive and negative

regulations by phosphorylation. Both the phosphorylation of threonine 161 and dephosphorylation of threonine 14 and tyrosine 15 are required for Cdk1 activity (24).

DNA replication

While DNA replication occurs in S phase, the assembly of replication fork components starts in M phase. DNA replication starts from the region of DNA called replication origins, marked by origin recognition complexes (ORC) (25). In metazoans, DNA replication origins are less understood than in yeast, although a handful of origins has been mapped including the β-globin gene clusters (26). In G1 phase, ORC assembly promotes the pre-replication complex (PRC) formation on replication origins by recruiting Cdc6 and Cdt1 (25).

The mini-chromosome maintenance (MCM) complex consists of six-subunits, Mcm2-7, and functions as a DNA helicase to unwind the parental DNA while the replication fork moves (25). The MCM complex is required for DNA replication initiation and elongation (27). The MCM complex is recruited to DNA through the coordination of Cdc6 and Cdt1 in G1 phase (28-30). The stabilization of MCM complexes on DNA is achieved by Cdc45 and GINS [Go, Ichi, Nii, and San; five (Sld5), one (Psf1), two (Psf2), and three (Psf3) in Japanese] complex (31-34).

DNA replication elongation is carried out by many proteins, forming replication forks (Figure 1.2). DNA synthesis is accomplished by DNA polymerases starting from a primer with a direction from 5' end to 3' end (3, 35). Replication protein A (RPA) has a strong affinity for single stranded DNA (ss-DNA) (36). Parental DNA unwinding generates ss-DNA, and RPA is loaded onto the ss-DNA followed by the recruitment of

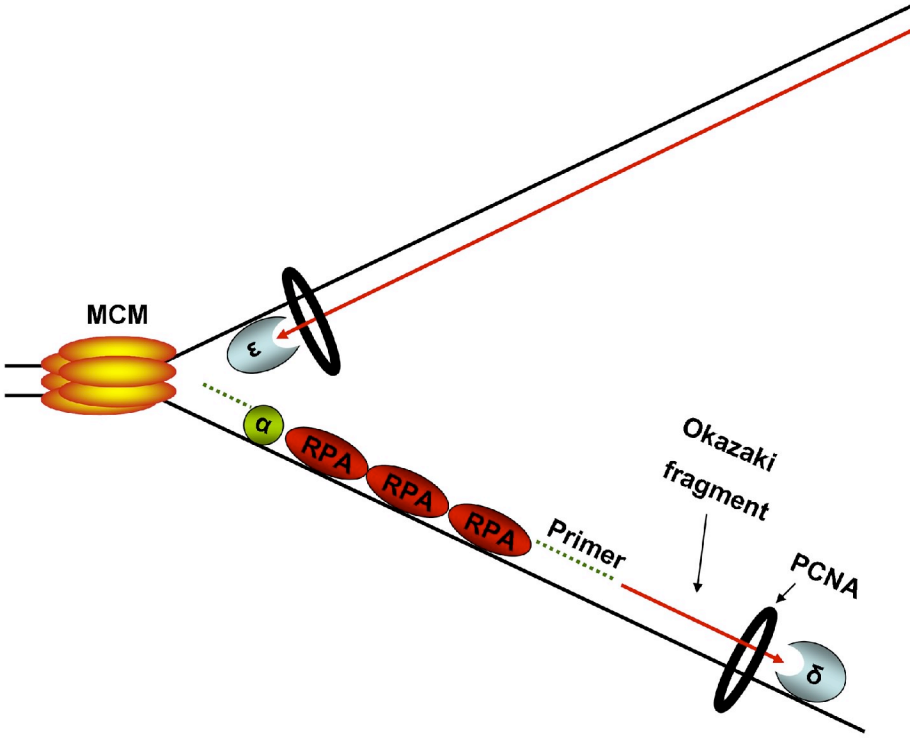

Figure 1.2. A simplified replication fork. MCM complex functions in unwinding parental double strand DNA. Polymerase α (α) generates RNA-DNA primers for DNA synthesis. Polymerase ε functions in leading strand thesis, and Polymerase δ functions in lagging strand synthesis. The leading strand synthesis is continuous, and the lagging strand synthesis is discontinuous with okazaki fragments synthesis. PCNA stabilizes polymerases on DNA. RPA binds to single strand DNA.

primase/polymerase α (pol α) (37). The primase forms an RNA primer followed by a short DNA primer to pair with the template DNA. DNA synthesis starts from the RNA-DNA primer. The RNA-DNA primer synthesis promotes the loading of proliferating cell nuclear antigen (PCNA). PCNA functions in stabilizing DNA polymerase δ (Pol δ) and DNA polymerase ε (Pol ε) on DNA (25, 38, 39). Both Pol ε and Pol δ are high fidelity DNA polymerases for leading strand and lagging strand synthesis respectively. For leading strand synthesis, priming is only required once. Lagging strand synthesis is accomplished through the synthesis of okazaki fragments (35).

Model systems used to study DNA replication

Several model systems have been used to study the regulation of DNA replication. The budding yeast model system has several advantages for studying DNA replication. The replication origins are well defined and conserved from cell to cell (25). Genetic background manipulation is easier in yeast than in mammalian cells. The *Xenopus* egg extract system has also been used to study DNA replication as a model system (40). In this system, the concentrated S phase components support a robust DNA replication *in vitro*. A particular protein deficient background can be achieved by immuno-depletion with a specific antibody. Any region on DNA can serve as a replication origin.

In mammalian cells, both SV40 and oriP episomes have been used to study DNA replication. The SV40 episome is derived from the simian virus. DNA replication on the SV40 episome starts from the SV40 origin in both directions. The SV40 episome replication bypasses the requirement for pre-replication complex formation (41). Large T antigen functions as a DNA helicase and binds to the SV40 origin (42, 43). This is

sufficient for replication initiation and elongation of SV40 episomes (41). Because of this unique characteristic, the SV40 episome can replicate constantly in S phase. Also, the SV40 episome can replicate *in vitro* with cell extracts from S phase, supplemented with the large T antigen protein (44, 45). The oriP episome is derived from the Epstein-Barr virus (EBV). Replication starts from the oriP origin in one specific direction (46). EBNA-1 is the only viral protein required to support oriP episome replication in mammalian cells (47). EBNA-1 contributes to recruiting the ORC complex to the oriP origin, and then the DNA replication machinery is utilized to support episome replication (48, 49). This regulation limits the oriP episome replication to only once per cell cycle (50).

Cellular Responses to DNA Damage

The activities of DNA helicases and DNA polymerases are coordinated to function in replication fork progression. The DNA replication process is challenged by various DNA damaging agents from internal and external sources. Cells have evolved complex mechanisms including DNA repair, cell cycle checkpoint activation, senescence, and apoptosis to safeguard the precise duplication of DNA and to maintain genome integrity.

DNA repair

Damaged DNA can be repaired by different mechanisms according to the type of damage (51). Base excision repair (BER) continually acts to correct non-bulky damage to bases resulting from hydrolysis, oxygen free radicals, and simple alkylating agents or spontaneous loss of the DNA base itself (52). Activation of BER is independent of DNA

replication or transcription. The damaged base is removed by DNA glycosylase. The apurinic/apyrimidinic (AP) endonuclease then removes the abasic site by niching the DNA, and the gap is filled by DNA polymerase β and DNA ligase. This gap can be a single nucleotide (nt) or up to 13 nt in length (52).

Nucleotide excision repair (NER) removes DNA lesions that often cause both a helical distortion of the DNA duplex and a modification of the DNA chemistry (53). The most significant of these lesions are pyrimidine dimers, cyclobutane pyrimidine dimers (CPDs) and (6-4) photoproducts (6-4PPs), two major kinds of DNA damage produced by the shortwave UV component of sunlight (54, 55). In addition, numerous bulky chemical adducts and DNA intra-strand cross-links are eliminated by this process (56). Although NER is not essential for viability, patients younger than 20 years with the inherited syndrome xeroderma pigmentosum (XP) have a roughly 1000-fold increased incidence of skin cancers (57). The XP gene products (XPA to XPG) are now known to perform various functions during damage recognition and DNA incision of NER (51). DNA endonucleases cleave the DNA strand with the lesion and generate a repair patch about 25-30 nt long (51). RPA binds to and stabilizes the exposed ss-DNA. DNA polymerase δ and ε are required for DNA synthesis to fill this gap, and the gap is sealed by DNA ligase. Transcription can enhance NER efficiency when the damaged site falls in a transcriptionally active region.

DNA double strand breaks (DSBs) can result from exogenous agents such as ionizing radiation (IR) and certain chemotherapeutic drugs including mitomycin C (MMC) and etoposide, from endogenously generated reactive oxygen species, and from mechanical stress on the chromosomes (58). Failure to rejoin breaks properly can lead to

loss of portions of chromosomes or chromosomal rearrangements. End-joining can be achieved through single strand annealing (SSA), non-homologous end joining (NHEJ), and homologous recombination (HR). SSA and NHEJ often result in the loss or gain of a few nucleotides (59). For the SSA repair pathway, the ends of DSB are resected to single strand DNA with 3' overhangs by exonucleases followed by Rad52 binding. Rad52 facilitates the annealing of complementary single strand DNA at these termini (60). DSB ends also can be directly ligated through NHEJ. The Ku heterodimer, consisting of Ku70 and Ku80, forms a complex with the DNA dependent protein kinase catalytic subunit (DNA-PKcs) and facilitates NHEJ repair (61, 62). During HR, a sister chromatid or a homologous chromosome is utilized as a repair template (63). Break ends are resected to single strand DNA with 3' overhangs. Rad52 binds to the single strand DNA filaments followed by the recruitment of Rad51. Rad51 directs a strand invasion into a homologous chromosome followed by DNA synthesis (63). Although HR is an error-free repair pathway for the DSB, it can result in loss of heterozygosity (LOH) (64).

DNA inter-strand cross-links (ICL) are highly cytotoxic (65). ICL occurs when cells are treated with cancer therapy drugs including cisplatin. It is not well understood how ICL is repaired. It has been proposed that both NER and HR are involved in ICL repair (66).

Cell cycle arrest

Cell cycle progression has to be coordinated with DNA repair in order to safeguard genome stability (67). Cell cycle checkpoints function to halt cell cycle progression in a particular phase and provide more time for DNA repair before entering

the next phase (68). Cell cycle progression is regulated by oscillating Cdk activities. Arresting cell cycle progression is achieved through inhibition of Cdk activities. According to the different phases of the cell cycle, there are four cell cycle checkpoints, G1-S checkpoint, intra-S phase checkpoint, G2-M checkpoint, and spindle checkpoint (Figure 1.3).

Replication of damaged DNA will cause genetic alteration. The G1-S checkpoint functions to arrest cells in the G1 phase and to allow cells to repair the damaged DNA. This arrest is achieved by inhibition of Cdk2 through induction of p21 and reduction of cyclin E (13). DNA damage induced signaling results in stabilization of p53 in the nucleus (69, 70). P53 is a transcription factor that stimulates the expression of p21, an inhibitor of Cdk2 (69, 71). When cell size is less than the threshold or when nutrient levels are reduced, Cdk4/6 activity is inhibited due to reduction of cyclin D expression. This results in suppression of Rb hyperphosphorylation. Hyperphosphorylation of Rb is required for releasing E2F, a transcription factor regulating gene expression for entering S phase including cyclin E (11, 12).

While the function of the intra-S phase checkpoint is not well understood in humans, cells with a defective intra-S phase checkpoint exhibit radio-resistant DNA synthesis (RDS). In yeast, this checkpoint initiates at least three cellular actions (72). First, it slows DNA replication by inhibiting the initiation of additional replication origins. Second, it inhibits the onset of mitosis while replication is active. Third, it acts to resolve the problem at the stalled replication fork. Stabilization of stalled replication forks is the essential function of the intra-S phase checkpoint (73, 74). Intra-S phase checkpoint signaling is activated upon stalling of replication forks and results in rapid degradation of

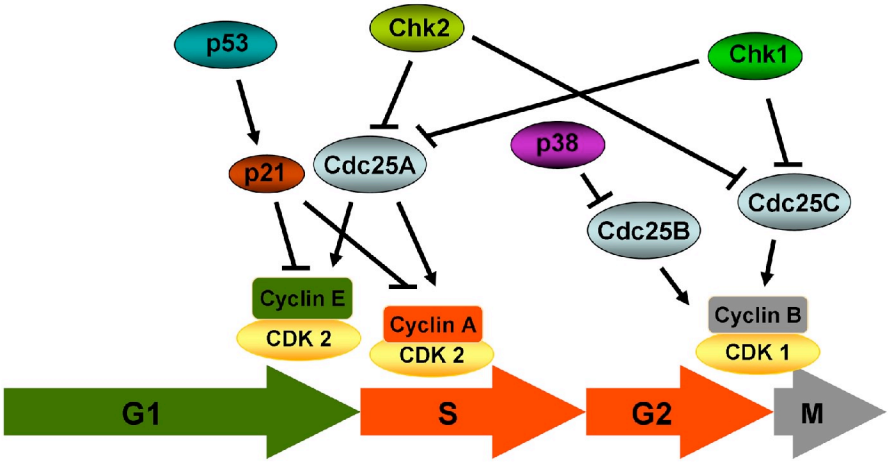

Figure 1.3. Cell cycle checkpoints arrest the cell cycle progression. Cell cycle arrest is achieved by inhibition of Cdk-cyclin activities. DNA damage results in p53 stabilization, which stimulates p21 transcription. P21 inhibits the kinase activity of Cdks. Chk1 and Chk2 are activated upon checkpoint signaling. Then they phosphorylate Cdc25A and Cdc25C. Phosphorylation of Cdc25A leads to its rapid degradation. This functions as S phase checkpoint. P38 phosphorylates Cdc25B upon induction of DNA damage. Cdc25B and Cdc25C phosphorylation creates a binding site for 14-3-3, and this binding inhibits the phosphatase activity of Cdc25B and Cdc25C. Inhibition of Cdc25B functions in initiation of G2-M checkpoint, and inhibition of Cdc25C functions in maintenance of G2-M checkpoint.

Cdc25A (75, 76). Cdc25A removes the inhibitory phosphorylation of Cdks and is required for Cdk2 activity (77). Degradation of Cdc25A inhibits Cdk2 activity, which is required for the DNA replication process.

Prematurely entering mitosis with broken DNA or incompletely replicated DNA causes chromosome aberration in cells (3). The G2-M checkpoint functions to arrest cells in G2 phase through inhibition of Cdk1 activity (72). The G2-M checkpoint is initiated by p38 through phosphorylation of Cdc25B (78) and is maintained through phosphorylation of Cdc25C by Chk1 and Chk2 (77, 79, 80). Both phosphorylation of Cdc25B and Cdc25C facilitate their interaction with the protein 14-3-3, which inhibits the phosphatase activities of Cdc25B and Cdc25C (81, 82). Inactive Cdc25B and Cdc25C fail to remove the inhibitory phosphorylation of Cdk1, which results in inhibition of Cdk1 (23).

Until all chromosomes are properly attached to the spindles, the spindle checkpoint blocks a cell from undergoing mitosis into anaphase by inhibiting the anaphase-promoting complex (APC) (83). To achieve proper segregation, the two kinetochores on the sister chromatids must be attached to the opposite spindle poles, and tension of spindles has to be generated. Only this pattern of attachment will ensure that each daughter cell receives one copy of the chromosome (83).

Senescence and apoptosis

Apoptosis is the process of programmed cell death (PCD) that may occur in multicellular organisms, and senescence is a state of irreversible cell growth arrest (3). Both senescence and apoptosis can prevent cell proliferation and be induced by telomere

shortening and accumulation of DNA damage through the p53 and Rb pathways (84). Premalignant cells acquire the heritable capacity to grow beyond normal cell growth and escape from the control of apoptosis and senescence. Once premalignant cells acquire the ability to invade their surrounding tissues, cancer is developed.

DNA damage response is an anti-cancer barrier

Genetic instability is a hallmark of most cancers (85). Cells sense DNA damage and facilitate DNA repair along with cell cycle arrest. Genetically unstable cells are eliminated by apoptosis. Activation of oncogenes and inactivation of tumor suppressor genes will allow cells to bypass senescence or apoptosis (86, 87). Therefore, the DNA damage response (DDR) acts as an anti-cancer barrier by fixing the problem or eliminating genetically unstable cells. Patients with many inheritable diseases resulting from DDR deficiency exhibit cancer predisposition syndromes (Table 1.1).

The cell cycle checkpoint is also an inducible barrier against tumor progression. This is evidenced by the fact that markers of DSB and DSB-induced checkpoint signaling are present in many precancerous lesions before p53 mutations are acquired (88, 89). Furthermore, oncogene-induced senescence requires DSB induced checkpoint signaling (90, 91). This checkpoint signaling results from DNA replication stress, characterized by multiply fired replication origins and prematurely terminated replication forks (90, 91). Thus, premalignant cells are under the pressure of selection by DDR mediated senescence during tumor progression. Overcoming the effects of the DDR allows genetically unstable cells to continuously proliferate.

Table 1.1. Examples of DDR genes associated with human diseases.

Disease	Functional defect	Genetic deficiency
Fanconi anemia	Cross-link repair, checkpoint signaling	Fanconi Anemia complementation group genes
Ataxia-telangiectasia	DSB repair, checkpoint signaling	ATM
Xeroderma pigmentosum	Nucleotide excision repair	XPA-G
Nijmegen breakage syndrome	DSB repair, checkpoint signaling	NBS1
Li-Fraumeni	Checkpoint signaling, apoptosis, senescence	p53 heterozygosity, Chk2
HNPCC (hereditary nonpolyposis colon cancer)	Mismatch repair, checkpoint signaling	MSH2/6, MLH1
Early onset breast and ovarian cancer	DNA repair, checkpoint signaling	BRCA1, 2
Blooms syndrome	DNA replication, DNA repair	BLM
Werner syndrome	DNA replication, DNA repair	WRN
RIDDLE syndrome	DSB repair, checkpoint signaling	RNF168
ATLD syndrome	DNA repair, checkpoint signaling	Mre11
Seckel syndrome	DNA replication, checkpoint signaling	ATR

ATM and ATR signaling mediates the DNA Damage Response

The DDR is a signal transduction pathway that coordinates DNA replication with DNA repair, cell cycle checkpoint, and apoptosis during cell cycle progression (Figure 1.4). The major regulators of the DDR are the phosphoinositide 3-kinase related protein kinases (PIKKs) including ATM (ataxia-telangiectasia mutated) and ATR (ATM and Rad3 related) (92).

Like DNA-PK, both ATM and ATR are protein kinases with a strong preference to phosphorylate serine or threonine residues followed by glutamine (S/TQ) (61, 92-94). ATM phosphorylates Chk2 (79, 95), and ATR phosphorylates Chk1 respectively (96, 97). ATM and ATR also phosphorylate many of the same substrates including p53 (98-103). Chk1 and Chk2 are protein kinases and can also phosphorylate some substrates of ATM and ATR including p53 (104-106). The substrates of ATM and ATR function in repairing damaged DNA, arresting the cell cycle, regulating transcription, and inducing senescence and apoptosis (68).

ATM Signaling Pathway

The ATM-dependent pathway primarily responds to double strand breaks (DSBs) (92). This pathway can be activated throughout the cell cycle. Ionizing radiation (IR) causes DSBs in cells (58). When cells are irradiated with IR, the Mre11-Rad50-NBS1 (MRN) complex and ATM form intranuclear foci rapidly (107-110). Phosphorylation of histone variant H2AX (γH2AX) is a known marker of DNA damage (111-113). Co-localization of γH2AX with the MRN complex and ATM suggests that the MRN complex and ATM are recruited to the damage sites (114).

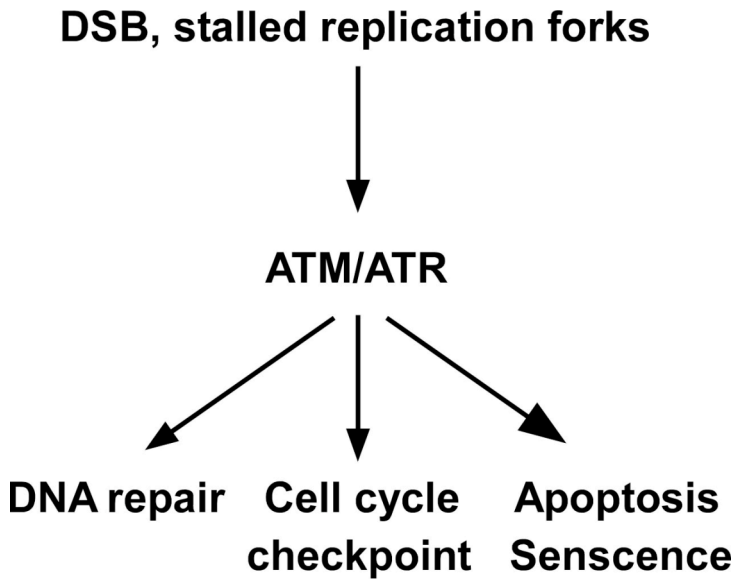

Figure 1.4. ATM and ATR signaling mediates DNA damage response. ATR and ATM are major regulators to mediate DDR. Upon DNA damage, ATM and ATR signaling regulates cellular events, DNA repair, cell cycle arrest, apoptosis, and senescence to either correct the errors or eliminate cells.

The MRN complex is required for ATM activation. The Mre11-Rad50 complex forms a dimer at DSB sites through Mre11 (115, 116). This suggests that the Mre11-Rad50 complex functions in tethering DNA break ends. MRN foci formation after DSB is independent of ATM (108). ATM foci formation and activation of ATM requires the MRN complex (117, 118). The C-terminal region of NBS1 is required for ATM recruitment to DSB sites (119). This suggests that the MRN complex functions upstream of ATM activation. Consistently, patients with mutated Mre11 (A-TLD) or Nbs1 (NBS) exhibit defective ATM activation in response to DSB (120).

The MRN complex also functions downstream of ATM to facilitate ATM signaling. Nbs1 is phosphorylated by ATM on several sites including S343, and the S343A mutant of Nbs1 causes hypersensitivity of these cells to IR (121). Mre11 possesses both endonuclease and exonuclease activities (122). However, the nuclease activity of Mre11 is not required for ATM signaling (123).

Upon DSB induction, ATM undergoes autophosphorylation on several sites including S1981 in the FAT domain (124, 125). The phosphorylated ATM promotes a conformation change from inactive dimers to active monomers (124). ATM phosphorylates many substrates including Chk2, p53 and MDM2 (67, 98, 126-129). Chk2 is a protein kinase and can phosphorylate p53, Cdc25A, and Cdc25C (75, 77, 79, 126, 130). Phosphorylation of p53 on S20 by Chk2 contributes to stabilization of p53 by inhibiting the interaction of p53 with MDM2, the negative regulator of p53 (126, 130). Phosphorylation of MDM2 by ATM stabilizes p53 in the nucleus (127). Phosphorylation of p53 on S15 by ATM enhances transactivation activity of p53 (98, 128, 129). ATM also phosphorylates other proteins to facilitate DSB repair including H2AX (67). H2AX is

phosphorylated at the DSB site, and the signal is then spread to adjacent regions at least 10 kb in humans and about 50 kb in yeast (131, 132).

ATR Signaling Pathway

ATR is activated during every S-phase to regulate the firing of replication origins, to stabilize and repair damaged replication forks, and to prevent premature onset of mitosis (133, 134). ATR exhibits a similar organization of functional domains as ATM (Figure 1.5). Sequence homology between ATM and ATR is exclusive to the C-terminal half of the proteins, a region that includes their kinase domains (92). The ATR signaling pathway includes recognizing DNA damage, stimulating the kinase activity of ATR, and amplifying the checkpoint signaling (Figure 1.6). Briefly, two checkpoint complexes, ATR-ATRIP and 9-1-1 complexes recognize a specific DNA-protein structure with single strand DNA (ss-DNA), RPA, and a 5' DNA junction. This allows ATR activity to be stimulated by TopBP1. Several mechanisms exist to amplify the signal of ATR activation towards Chk1 phosphorylation. This pathway is conserved in yeast and humans (Table 1.2).

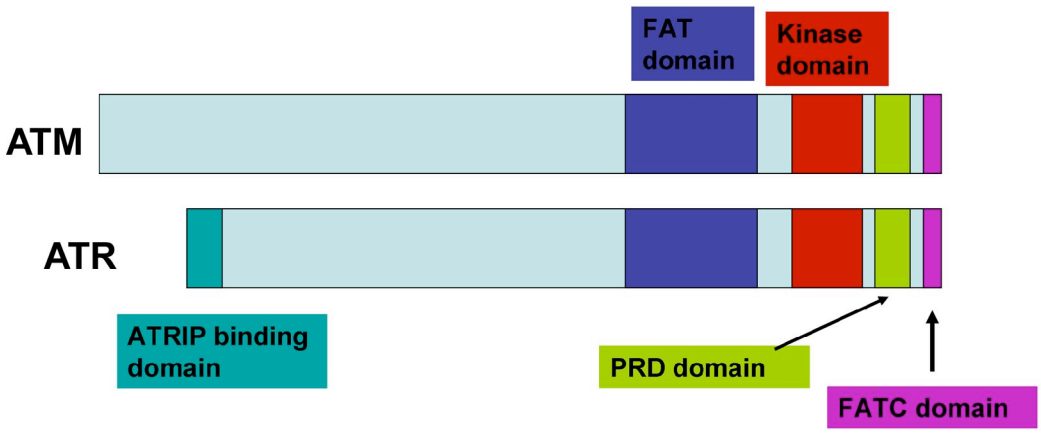

Figure 1.5. Functional domains of ATM and ATR. The PIKK recruitment domain (PRD) domain of ATM interacts with Mre11-Rad50 complex. The PRD domain of ATR interacts with TopBP1. The sizes of domains are not to scale.

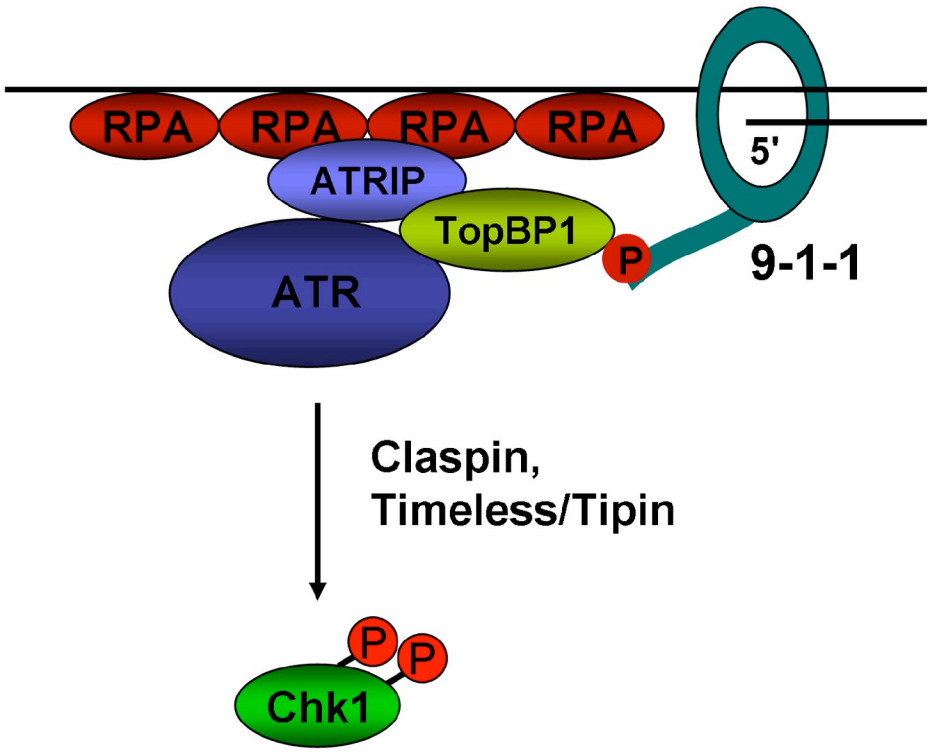

Figure 1.6. A simplified model of ATR signaling pathway. Two checkpoint complexes, ATR-ATRIP and 9-1-1 complexes are loaded to an ATR activation structure with single strand DNA, RPA, and a 5′ DNA junction. The kinase activity of ATR is enhanced by TopBP1, which is concentrated by 9-1-1 complex at the sites of DNA damage. Several mechanisms exist to amplify the signal of ATR activation including Claspin (see text).

Table 1.2. Protein orthologs in ATR signaling pathway.

Protein Function	***H. sapiens***	***S. cerevisiae***	***S. pombe***
PIKK kinase	ATR	Mec1	Rad3
	ATRIP	Ddc2	Rad26
Effector kinase	Chk1	Rad53	Chk1
Clamp loader	Rad17	Rad24	Rad17
	Rfc2-5	Rfc2-5	Rfc2-5
9-1-1 clamp	Rad9	Ddc1	Rad9
	Rad1	Rad17	Rad1
	Hus1	Mec3	Hus1
Kinase activator	TopBP1	Dpb11	Cut5
Chk1 adaptor	Claspin	Mrc1	Mrc1
Replication fork stabilizer	Timeless	Tof1	Swi1
	Tipin	Csm3	Swi3

Recognizing DNA damage

ATR is activated in response to many types of DNA damage including DSB and replication stress. Two checkpoint complexes are required for ATR signaling, ATR-ATR interacting protein (ATRIP) and Rad9-Hus1-Rad1 (9-1-1) complexes (133). Loading of both complexes to DNA requires a DNA-protein structure with single strand DNA (ss-DNA), Replication protein A (RPA), and a 5' DNA junction. In *S. cerevisiae*, artificially manipulated co-localization of $Mec1^{ATR}$-$Ddc2^{ATRIP}$ and 9-1-1 checkpoint complexes on DNA can activate $Mec1^{ATR}$ signaling in the absence of DNA damage (135).

A ss-DNA motif has been suggested as the primary signal for ATR localization (136, 137). This DNA motif can be generated during DNA replication and DNA repair (25, 133). It is suggested that ATR activation in unperturbed cells at a basal level is required to regulate normal DNA replication (134, 138). An enhanced level of ATR activation is induced in comparison to the basal level activation of ATR in response to replication stress. Replication stress can result from insufficient deoxyribonucleotide triphosphate (dNTPs) or inhibition of primase. Long stretches of ss-DNA is the signal for the enhanced activation of ATR (139, 140). This type of ATR activation will be discussed in this chapter.

Replication stress and DNA lesions cause stalled replication forks, which can form long stretches of ss-DNA. The coordination of DNA helicase and DNA polymerases is required for replication fork progression (25). The MCM complex unwinds parental DNA while pol ε and pol δ synthesize the complementary strands. Stalled replication forks can be caused by stalling DNA helicases or stalling the DNA polymerases. For example, a DNA inter-strand cross-link will stall DNA helicase

movement, and an intra-strand cross-link will only stall DNA polymerase movement. Only the latter type of stalled forks will form long stretches of ss-DNA, resulting from continued unwinding of the parental DNA by MCM helicases (37, 139).

It is unclear whether ATR is activated at different levels when a polymerase is stalled on the leading strand or the lagging strand. A lesion on the lagging strand might yield a small gap between two Okazaki fragments since re-priming naturally happens all the time. Indeed, the length of ss-DNA generated varies by stalling DNA polymerases on the leading strand and the lagging strand. It is reported that the lesion induced by ultraviolet radiation (UV) generates long stretches of ss-DNA of up to 3 kb when the lesion is on the leading strand and up to 400 bases pairs when the lesion is on the lagging strand (141). This suggests that a DNA lesion on the leading strand may cause higher levels of ATR activation than a DNA lesion on the lagging strand.

RPA coats most of the ss-DNA in cells (36). RPA is a heterotrimer complex consisting of three subunits: RPA70, RPA32, and RPA14, and is essential for DNA replication and DNA repair of eukaryotic cells (142). RPA binds tightly to ss-DNA with a defined 5'→3' polarity (143-145) and an affinity of up to about 10^{-9}–10^{-10} M (146).

The ability of RPA binding to ss-DNA is carried out by oligonucleotide/oligosaccharide-binding fold (OB-fold) domains (36). RPA70 contains four OB-fold domains, DBD-N, DBD-A, DBD-B, and DBD-C, and one OB-fold domain exists on RPA32 and RPA14 respectively. Four OB fold domains possess strong affinity (μM) to ss-DNA including three OB-fold domains on RPA70 (DBD-A, DBD-B, and DBD-C) and one OB-fold domain on RPA32 (DBD-D) (36, 147). In the 30 nucleotide binding mode, the DBD-A, DBD-B, DBD-C, and DBD-D bind to ss-DNA (Figure 1.7A).

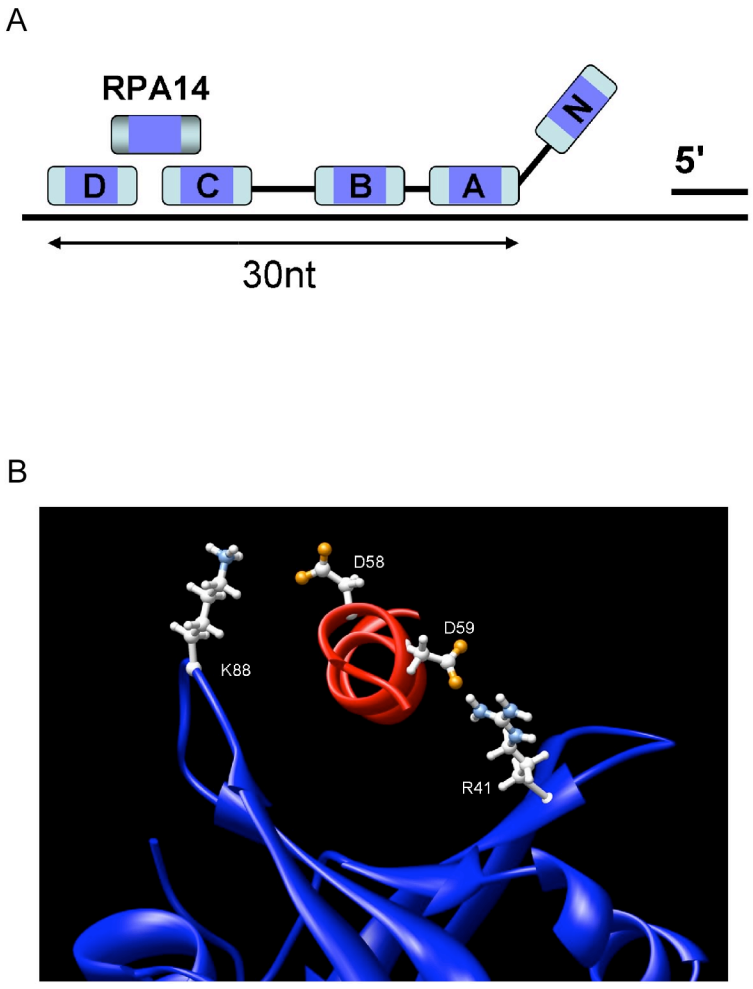

Figure 1.7. Models of RPA binding to DNA and proteins. (A) An RPA molecule binds to a single strand DNA with 30 nucleotides. DBD-A, DBD-B, and DBD-C on RPA70, and DBD-D on RPA32, four OB-fold domains bind DNA directly. RPA14 hinge RPA70 and RPA32 together by linking the DBD-C and DBD-D domains. (B) Predicted electrostatic interactions between basic RPA70N basic residues K88 and R41 with ATRIP acidic residues D58 and D59 [adapted from (151)].

The OB-fold domain on RPA14 does not bind DNA. Instead, it functions as a hinge between the DBD-C and the DBD-D domain (148). The RPA70N OB-fold domain has a relatively weak affinity (mM) to ss-DNA (36, 149, 150). Instead, it binds to many proteins including ATRIP and p53 (149, 151).

RPA undergoes phosphorylation in an unperturbed cell cycle and also upon induction of DNA damage. RPA32 is phosphorylated in S and G2 phase in human and yeast cells with unknown functions (152). Both RPA70 and RPA32 are hyperphosphorylated in response to DNA damage and replication stress (153, 154). RPA70 hyperphosphorylation is conducted by ATR and Chk1 (154), and RPA32 hyperphosphorylation is conducted by DNA-PK, ATR, and Chk1 *in vitro* (154, 155). Functional significance of hyperphosphorylation of RPA70 and RPA32 remains unknown. Hyperphosphorylation of RPA alters its affinity with ss-DNA *in vitro* (154, 156). This suggests that it may function in changing the mode of RPA binding with ss-DNA (36).

RPA70N forms a basic cleft structure [Figure 1.7B and reference (149, 151). In *S. cerevisiae*, the $Rfa1^{RPA70}$–t11 mutation causes a charge reversal mutation, K45E within this basic cleft (157). Localization of $Ddc2^{ATRIP}$-$MEC1^{ATR}$ and 9-1-1 complex to DSB sites is impaired in cells with the Rfa1-t11 mutant (137, 158, 159). The interaction of RPA70N with ATRIP localizes ATR-ATRIP complex to DNA damage sites (151, 160).

In addition to RPA coated ss-DNA, a 5' DNA junction rather than a 3' DNA junction is also required for ATR activation [Figure 1.8A and reference (140)]. The 9-1-1 complex is preferentially loaded to DNA with a 5' DNA junction but not the 3' DNA junction (159, 161). RPA is critical for the loading (159, 161). The specific polarity of

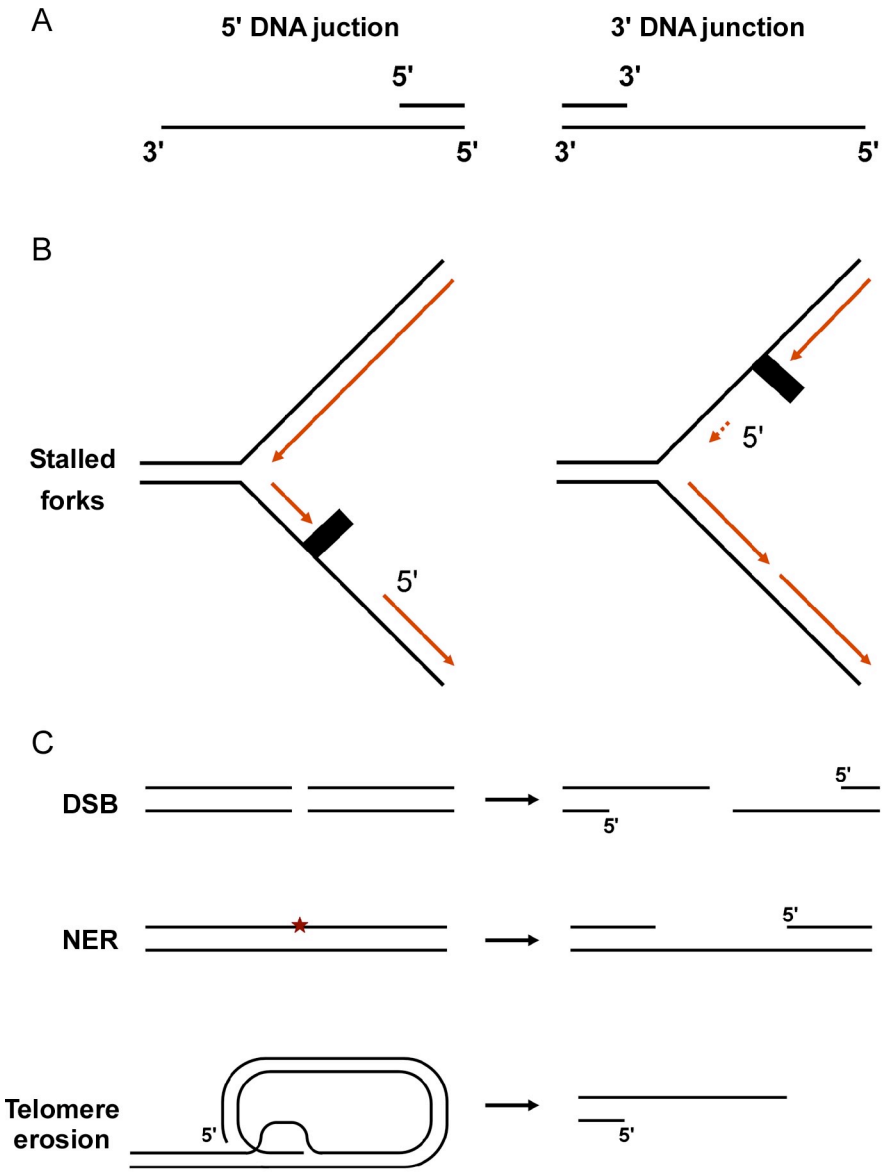

Figure 1.8. A common ATR activation structure. (A) Illustration of a 5′ DNA junction and a 3′ DNA junction. (B) ATR activation structure is formed when replication fork is stalled by a lesion on leading strand (left panel) and lagging strand (right panel). (C) ATR activation structure can be formed from DSB ends resection (top panel), NER processing (middle panel), and telomere erosion (bottom panel). Adapted from (133).

RPA binding to ss-DNA may contribute to this 9-1-1 complex preferential loading. The DNA motif with a 5' DNA junction is generated during the priming process facilitated by primase for lagging strand synthesis during normal DNA replication (25). Therefore, a stalled replication fork induced by stalling the lagging strand synthesis is more likely to activate ATR than by stalling the leading strand synthesis. However, it is also possible that a re-priming process occurs downstream of a lesion on the leading strand.

The ATR activating structure, including ss-DNA, RPA, and a 5' DNA junction, can also be generated during processing of DSB, NER, and telomere erosion [Figure 1.8B and reference (133)]. Both DSB and telomere erosion can activate ATR signaling (162). However, ss-DNA with only up to 30 nt is generated during NER. It is not clear whether this together with a 5' DNA junction is sufficient for ATR activation.

ATR-ATRIP complex

ATRIP was identified as an ATR interacting protein (163). ATR and ATRIP form co-localized damage inducible foci (163). ATRIP constitutively interacts with ATR, and the stability of ATR and ATRIP are linked (163). This relationship between ATRIP and ATR is conserved in yeast. In *S. pombe* and *S. cerevisiae*, $Rad26^{ATRIP}$ interacts with $Rad3^{ATR}$, and $Ddc2^{ATRIP}$ interacts with $Mec1^{ATR}$ (164-167). ATRIP can be considered an obligate subunit of the ATR kinase. Loss of ATRIP copies the phenotypes of loss of ATR and vice versa (163). ATRIP regulates ATR activation through several mechanisms including localization and kinase activity of ATR (Figure 1.9).

ATRIP interacts with ATR through the N terminal region of ATR and the C terminal region of ATRIP [Figure 1.9 and reference (160)]. The coiled-coil domain of

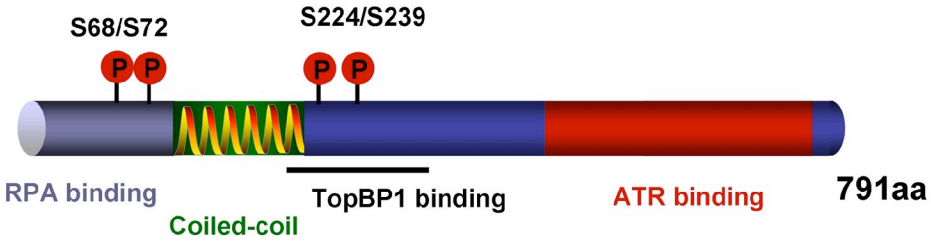

Figure 1.9. Functional domains of ATRIP. ATRIP N terminal region binds RPA. The coiled-coil domain of ATRIP is required for ATRIP oligomerization. ATR binding domain is in the C terminal region. Four phosphorylation sites are marked (S68, S72, S224, and S239). Phosphorylation of S68 and S72 is induced by DNA damage with unknown function. Phosphorylation of S224 and S239 are required for the maintenance of G2-M checkpoint.

ATRIP regulates ATRIP oligomerization, which contributes to stabilizing the ATR-ATRIP complex and is required for ATR signaling (168).

The localization of the ATR-ATRIP complex to DNA damage sites is achieved through the interaction between ATRIP and RPA (137). Biochemical studies indicate that ATRIP directly interacts with RPA through the evolutionarily conserved N-terminal region of ATRIP and the RPA70N OB-fold domain of RPA (160). Disruption of the interaction between ATRIP and RPA by deletion of the ATRIP N-terminal region greatly reduces the ability of both ATR and ATRIP to localize to DNA damage sites (160). This interaction is the major mechanism by which ATRIP interacts with RPA-ssDNA; although, some residual interaction exists when the N-terminal region of ATRIP is deleted (169). Although disruption of this interaction in yeast causes a defect in ATR signaling after MMS treatment (151), disruption of this interaction does not affect ATR signaling in human cells (160). It is possible that additional means of ATR-ATRIP localization are largely sufficient for ATR activation. Indeed, ATRIP localizes to DNA damage sites in the absence of RPA. In *S. cerevisiae*, a DNA-binding domain on $Ddc2^{ATRIP}$ promotes the localization of $Mec1^{ATR}$-$Ddc2^{ATRIP}$ to DNA damage sites (170). *In vitro*, the ATR-ATRIP complex exhibits the ability to bind ss-DNA in the absence of RPA (171).

In addition to ATRIP interaction with RPA, localization of ATRIP to sites of DNA damage is also regulated by ATR in a complex with ATRIP. ATRIP interaction with ATR is through the C terminal region of ATRIP (160). Deletion of this region does not alter ATRIP interaction with RPA, but impairs ATRIP localization to sites of DNA damage (160). Although no functional significance of ATRIP phosphorylation by ATR

has been reported, ATR kinase activity contributes to the ATRIP localization (163, 172, 173). In *S. pombe*, the replication protein $Cdc18^{Cdc6}$ directly interacts with $Rad26^{ATRIP}$ and is required for the recruitment of $Rad3^{ATR}$-$Rad26^{ATRIP}$ to chromatin (174).

ATR is a protein kinase with similar organization of functional domains to ATM. Unlike ATM, no autophosphorylation sites have been reported on ATR. Four phosphorylation sites have been identified on ATRIP including S68, S72, S224, and S239 (173, 175, 176). S68 and S72 are substrates of ATR and are phosphorylated upon DNA damage. Although it is suggested that phosphorylation of S68 and S72 is upstream of ATR activation (173), the functional significance is unclear. Because they fall in the region of the RPA interaction domain on ATRIP, they may contribute to the interaction between ATRIP and the basic cleft of RPA70N. This will be further discussed in chapter V. Both ATRIP S224 and S239 phosphorylation are required for ATR signaling. This will be discussed in more detail in chapter III.

9-1-1 complex

The 9-1-1 complex consists of three subunits, Rad9, Hus1 and Rad1 (177). This complex is evolutionarily conserved in yeast and humans (178, 179). The structure of the 9-1-1 complex in yeast was predicted to resemble the structure of the DNA replication clamp, proliferating cell nuclear antigen (PCNA), by molecular modeling techniques [Figure 1.10A and reference (180-182)]. PCNA forms a homotrimer with a ring-shaped structure through the PCNA domains (183). Rad9, Hus1, and Rad1 have a PCNA domain in the N terminal region (180-182). The 9-1-1 complex forms a heterotrimer through the PCNA domains of Rad9, Hus1, and Rad1 (Figure 1.10B).

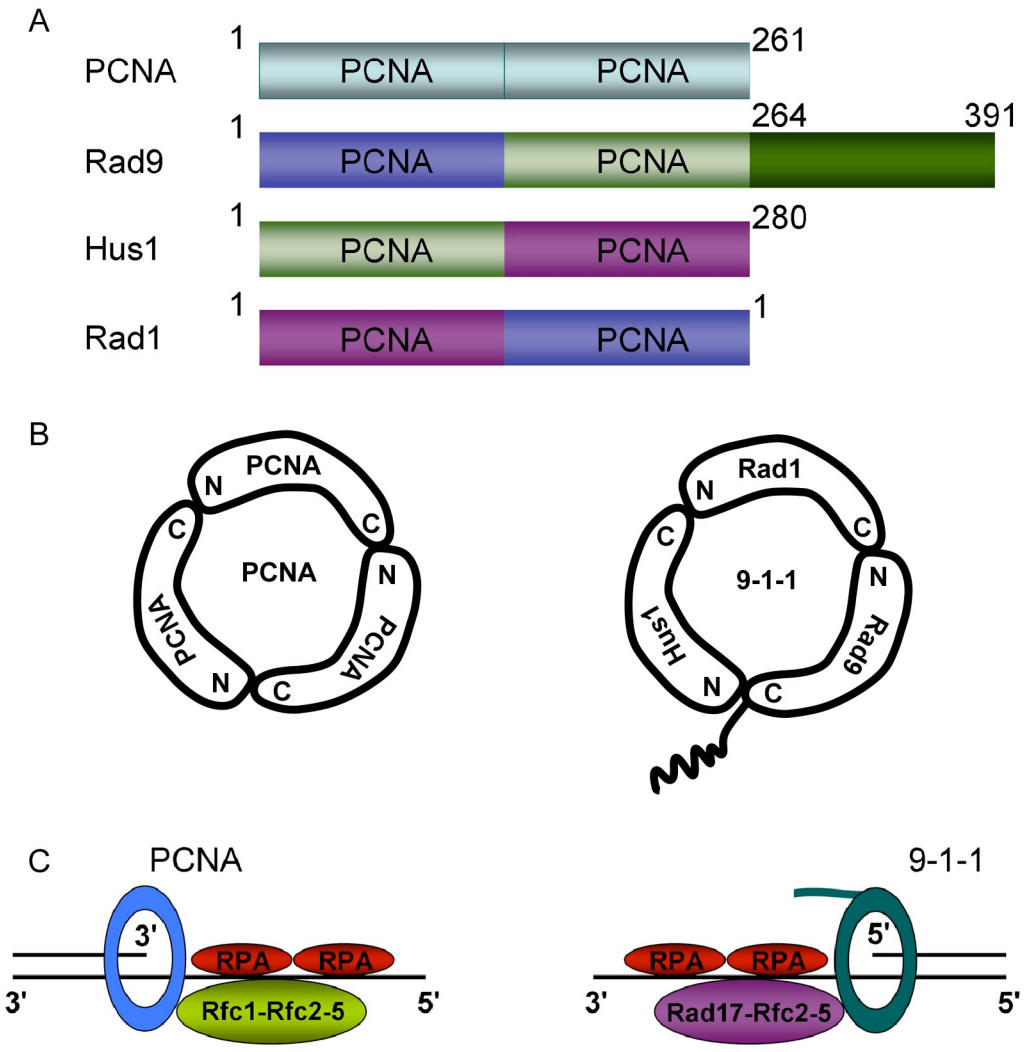

Figure 1.10. DNA replication clamp and checkpoint clamp. (A) PCNA has two PCNA domains. Rad9, Hus1, and Rad1 all have two PCNA domains. The matched colors indicate the regions interacted directly in the complex. (B) PCNA forms a homotrimer, and Rad9, Hus1, and Rad1 form a heterotrimer complex. (C) PCNA and 9-1-1 complex are loaded by clamp loaders Rfc1-Rfc2-5 and Rad17-Rfc2-5 complexes respectively. PCNA complex is loaded onto a 3′ DNA junction, and 9-1-1 complex is loaded onto a 5′ DNA junction. Both loading requires RPA.

The 9-1-1 complex is constitutively formed in cells. Depletion of Hus1 or Rad1 decrease the stability of the other two components of the 9-1-1 complex in cells (184). Genetic knockout of Hus1 or Rad9 in mice causes embryonic lethality (185, 186). Cells exhibit reduced clonogenicity when Rad1 is depleted (184). Moreover, loss of Rad9, Hus1, or Rad1 produces similar defects including ATR signaling and sensitivities to genotoxic agents (184, 185, 187). This suggests that components of the 9-1-1 complex function together as a whole protein like the ATR-ATRIP complex.

Both PCNA and the 9-1-1 complex are loaded onto DNA by clamp loaders (Figure 1.10C). The PCNA complex is loaded onto DNA by the replication factor C (RFC) complex, which consists of a large subunit, Rfc1 (p140), and four small subunits, Rfc2-5 (p40, p38, p37, p36) (188, 189). 9-1-1 complex loading onto DNA is carried out by the Rad17-Rfc2-5 complex (161, 190-194). Compared to the PCNA clamp loader, the Rfc1 subunit is replaced by Rad17 in this complex. The Rad17-Rfc2-5 complex interacts with the 9-1-1 complex and directly loads the 9-1-1 complex on DNA in an ATP dependent manner (190).

PCNA is preferentially loaded onto the 3'-DNA junction in an ATP hydrolysis dependent manner [Figure 1.10C and reference (161)]. In contrast, the 9-1-1 complex is preferentially loaded onto the 5'-DNA junction (159, 161). Both PCNA and 9-1-1 complex loading require RPA (161). In *S. cerevisiae*, $Rfa1^{RPA70}$ can bind directly to Rfc4 (195), and the rfa1-t11 mutant exhibits less efficiency than wild type Rfa1 to load the yeast 9-1-1 complex on DNA *in vitro* (159). RPA can directly load the Rad17-Rfc2-5 complex onto DNA (196). It is unclear whether RPA interacts with PCNA or the 9-1-1 complex directly.

It is also reported that topoisomerase-II-binding protein 1 (TopBP1) is required for 9-1-1 complex loading to DNA (197). In this study, depletion of TopBP1 inhibits primase, Rad17, and 9-1-1 complex loading in the *Xenopus* egg extract system. TopBP1 is required for the chromatin loading of DNA polymerases and Cdc45 in replication initiation but is not required for DNA replication elongation (198-200). Therefore, the requirement of TopBP1 to load the 9-1-1 complex is distinct from TopBP1 function in replication initiation. The mechanism of TopBP1 recruitment to sites of DNA damage before 9-1-1 complex loading remains unknown.

Similar to PCNA, the 9-1-1 complex can stimulate the activity of flap endonuclease 1 (FEN1), cleaving the RNA on the RNA-DNA primer generated by primase (201). This suggests that the 9-1-1 complex may function to generate a preferential loading site prior to its loading. However, it is unclear whether the 5'-RNA/DNA junction is able to activate ATR as the 5'-DNA junction.

Rad9, Hus1, and Rad1 are phosphorylated upon induction of DNA damage. Phosphorylation of Rad1 and Hus1 occurs in an ATR and TopBP1 dependent manner, but the functional significance remains unknown (202). The C-terminal tail of Rad9 undergoes phosphorylation on at least nine serine or threonine sites [Figure 1.11 and reference (203, 204)]. Rad9 is loaded upon induction of DNA damage, and the Rad9 mutant with all nine phosphorylation sites to alanine can be efficiently loaded onto DNA as wild type (205). Rad9 S272 site indicates a favorable substrate of ATM/ATR and is phosphorylated upon induction of DNA damage (205). The phosphorylation sites of Rad9, S277, S328, S336, and T355, are candidate substrates of Cdk (204). Rad9 phosphorylation on S387 occurs constitutively (204). This is the only Rad9

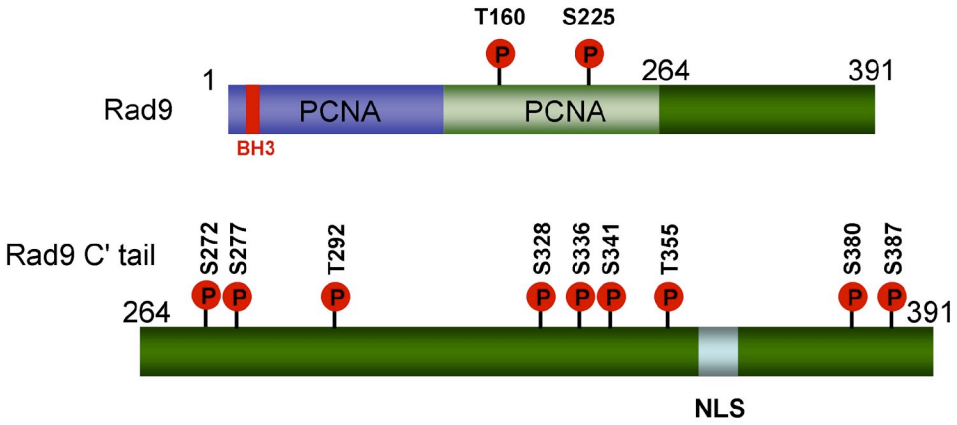

Figure 1.11. Functional domains of Rad9. Rad9 has two PCNA domains and a unique C terminal tail compared to Rad1 and Hus1. A BH3 like domain on the very N terminal region interacts with BCL-2 and BCL-x_L (top panel). This BH3 like domain of Rad9 is required for apoptosis induced by over-expression of Rad9. Phosphorylation of Rad9 on S160 is required for MMR function of Rad9, and phosphorylation of T225 is required for Rad9-mediated translesion synthesis. The C terminus tail of Rad9 contains nine phosphorylation sites and an NLS signal (bottom panel). Phosphorylation of S272 is induced by DNA damage, and S272 is a favorable substrate of ATM and ATR. Phosphorylation of S387 is required for Rad9 interaction with TopBP1. Deletion of the C terminus tail of Rad9 does not affect the 9-1-1 complex formation.

phosphorylation site on the tail of Rad9 with known functional significance. Phosphorylation of Rad9 on S387 functions in concentrating TopBP1 at the DNA damage site through direct interaction with TopBP1 and is required for ATR signaling (203, 206). The Rad9 mutant, with all other phosphorylation sites in the C terminal tail mutated except S387, functions normally as wild type Rad9 in ATR signaling (203).

Rad9 contains a nuclear localization signal (NLS) on the C-terminal tail (Figure 1.11). The NLS domain of Rad9 is required for 9-1-1 complex nuclear localization, but deletion of the NLS domain of Rad9 does not affect Rad9 forming a complex with Hus1 and Rad1 (207). The PCNA domains of Rad9 are involved in 9-1-1 complex formation. Over-expression of the PCNA domains of Rad9 induces apoptosis (207). Over-expression of Rad9 induces apoptosis by antagonizing the anti-apoptotic activities of Bcl-2 family proteins, BCL-2 and BCL-x_L (208). Both BCL-2 and BCL-x_L contain a BH-3 domain (BCL-2 homology domain 3) (208). Rad9 also contains a BH3-like domain in the N terminal region (Figure 1.11). This BH-3 like domain of Rad9 regulates its localization to the nuclear envelope through interaction with BCL-2 and BCL-x_L after MMS treatment (208). It is unclear whether the apoptosis induced by over-expression of Rad9 requires the other two components of the 9-1-1 complex, Hus1 and Rad1.

Loss of Rad9 causes hypersensitivity to IR, and this sensitivity can be inhibited by the Rad9 mutant, which is defective in checkpoint signaling (205). This suggests that the 9-1-1 complex may play a role in DSB repair. Moreover, Rad9 and Rad1 exhibit 3' to 5' exonuclease activity, which indicates that Rad9 can process DSB ends to 3' overhangs (209, 210). In *S. cerevisiae*, the 9-1-1 complex is required for $Ddc2^{ATRIP}$-$Mec1^{ATR}$

localization to HO endonuclease-mediated but not IR induced DSB site in G1 (211). This further supports that 9-1-1 complex contributes to the processing of DSB ends.

The 9-1-1 complex plays a role in BER and DNA translesion synthesis (TLS). Thymine DNA glycosylase (TDG) is a key DNA glycosylase that recognizes a wide array of DNA lesions, and FEN1 removes the displaced flaps generated by long-patch BER (52). The 9-1-1 complex interacts with TDG, and the interaction is enhanced with *N*-methyl-*N*′-nitro-*N*-nitrosoguanidine (MNNG) treatment (212). The activity of TDG can be stimulated by Hus1, Rad1, and Rad9 separately, and also by the 9-1-1 complex *in vitro* (212). The 9-1-1 complex also can stimulate the activity of FEN1 *in vitro* (201). The 9-1-1 complex can interact with DNA polymerase β and enhance its lesion bypass activity (213). In *S. cerevisiae*, the 9-1-1 complex is required for UV-induced mutagenesis, which requires the bypass TLS polymerase, polymerase ζ (214). In *S. pombe*, Rad9 interacts with the bypass polymerase, polymerase κ (215). Phosphorylation of Rad9 on T225 is required for this interaction, which functions in loading polymerase κ onto DNA (215).

Rad9 also plays a role in mismatch repair (MMR) independent of Hus1 and Rad1 (216). MLH1, a protein involved in mismatch repair, has been shown to interact with Rad9 (216). The minimum requirement of Rad9 for the interaction is the region containing residues 130 to 270 (216). Loss of Rad9 or the Rad9 mutant with S160 to alanine compromise MMR activity (216). However, this function of Rad9 is not required for the function of Rad9 in checkpoint signaling (216).

TopBP1

TopBP1 functions in checkpoint signaling in addition to its function in replication initiation. TopBP1 contains eight BRCT (BRCA1 C-terminal domain) domains. The region between the 6th and the 7th BRCT repeats of TopBP1 was named ATR activation domain (AAD) (217). This domain enhances ATR kinase activity *in vitro* and is required for ATR signaling *in vivo* (217, 218). TopBP1 interacts with the ATR-ATRIP complex (217). Disruption of the interaction of TopBP1 with the ATR-ATRIP complex by mutation of ATRIP or ATR does not disrupt the ATR-ATRIP complex, but severely suppresses the stimulation of ATR kinase activity (218). The 1st and 2nd BRCT domains of TopBP1 interact with Rad9, and this interaction concentrates TopBP1 to damage sites for ATR activation (203, 206).

Chk1

Chk1 is an effector protein of ATR signaling (97, 219). Chk1 is phosphorylated by ATR on S345 and S317 (97, 220, 221). Chk1 phosphorylation occurs at the DNA damage site, and phosphorylated Chk1 dissociates from chromatin and diffuses in the nucleus to facilitate checkpoint signaling (222). Phosphorylation of Chk1 activates kinase activity of Chk1 towards Cdc25C on S216 (80). Phosphorylation of Cdc25C on S216 creates a binding site for the protein 14-3-3, which inhibits phosphatase activities of Cdc25C (80, 82). Inhibition of Cdc25C regulates the G2-M checkpoint as discussed previously. Chk1 also phosphorylates Cdc25A and promotes its degradation (76). This rapid destruction of Cdc25A inhibits Cdk2 activity and functions as an intra-S phase checkpoint (76). Similar to Chk2, Chk1 can phosphorylate p53, which results in

stabilization of p53 (106). This stabilization induces transcription of p21, which inhibits Cdk2 activity and cell cycle progression (69, 71). Thus, ATR activation arrests cell cycle progression through multiple mechanisms.

Chk1 phosphorylation by ATR is regulated by several signal amplification mechanisms. Phosphorylation of Chk1 by ATR requires Claspin, which functions as an adapter protein to bring Chk1 to ATR (223). It is unclear whether Claspin is required for phosphorylation of other ATR substrates besides Chk1 (224). Claspin is phosphorylated by Chk1 in response to replication stress, and this phosphorylation promotes Claspin interaction with Chk1 (225, 226). This is one mechanism of signal amplification. Claspin is found at the replication fork (223). Claspin interacts with phosphorylated Rad17, and this interaction is required for sustained Chk1 phosphorylation (227). Rad17 phosphorylation is ATR dependent (228). This may provide another mechanism for signal amplification. The Timeless-Tipin complex mediates Chk1 activation and the intra-S-phase checkpoint (229). Depletion of Timeless or Tipin decreases Chk1 phosphorylation after DNA damage and replication stress. The Timeless-Tipin complex interacts with Claspin and RPA (229). This may be a third mechanism for signal amplification.

Cross-Talk between ATM and ATR Pathways

While ATM is not essential for cell viability, people with mutations in both alleles of ATM exhibit the neurodegenerative and cancer predisposition disorder ataxia-telangiectasia (230). ATR is essential for cell viability (163, 231, 232). ATR mutations

are rare and probably are only compatible with viability when cells have heterozygous or hypomorphic ATR.

ATR forms intranuclear foci when cells are treated with IR (103, 160). Chk1 is phosphorylated when DSBs are induced in cells (233, 234). This ATR activation upon DSB induction is dependent on ATM (233-236). It is suggested that the resection of DSB ends is the signal to trigger ATR activation (133, 237, 238). DSB ends can be resected into 3'-overhangs by 5'-to-3' exonucleases including Exo1 and BLM in yeast and humans (239, 240). Although Mre11 nuclease activity is not required for ATM activation in response to DSB, it is required for ATR activation (233, 234, 240). ATM dependent DSB end resection results in the ATR activation structure, a DNA-protein motif with long stretches of ss-DNA, RPA, and 5' DNA junction. Moreover, TopBP1 S1131 is phosphorylated by ATM, and this phosphorylation is required for ATR activation in *Xenopus* egg extract system in response to DSB (241). Thus, ATR activation requires ATM activation in response to DSB.

Replication stress results in stalled replication forks, which can activate ATR. The stalled forks can also result in DSBs (Figure 1.12). This is evidenced by γ-H2AX foci formation (242). However, induction of DSB is not the only signal to trigger ATM activation. One study suggests that ATM phosphorylation on S1981 is dependent on the kinase activity of ATR but not ATM (242). Moreover, this ATM activation is independent of the MRN complex (242). The ATM specific substrate Chk2 and the ATR specific substrate Chk1 function to regulate the G2-M checkpoint after replication stress (242). Thus, ATM and ATR cooperatively function to maintain genomic stability.

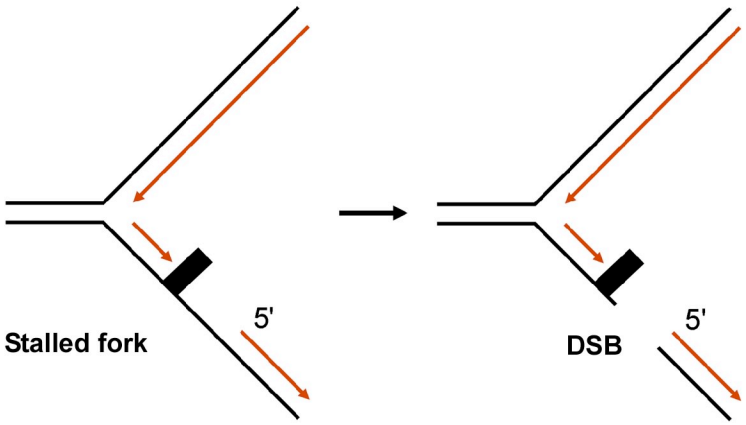

Figure 1.12. A stalled replication fork can be converted to a DSB. Replication fork stalling can form long stretches of single strand DNA, which can be attacked by DNA nuclease. This results in DSB.

ATR Signaling and Cancer

Mutations in many DDR genes lead to inherited diseases including neurodegenerative disorders, premature aging syndromes, and cancer predisposition syndromes (87). Hypomorphic mutations in ATR have been linked to rare cases of Seckel syndrome (67). These patients exhibit microcephaly and developmental defects (67). Seckel syndrome is the only disease that has been linked to mutations in proteins functioning in ATR signaling including Chk1, Claspin, and the 9-1-1 complex. This may be due to the fact that these proteins are essential for cellular viability (163, 185, 231). Therefore, these proteins are possible therapeutic targets for drug design to inhibit cell growth.

Cell cycle progression is regulated by Cdks and monitored by cell cycle checkpoints (5, 68, 87). Two of the major cell cycle checkpoints are the G1-S checkpoint and the G2-M checkpoint (92). The ATR-Chk1 pathway is a major player for regulating the G2-M checkpoint (133). In p53-defective cells, the ATR-Chk1 pathway is even more important for cell survival from treatments of replication stress or DNA damage than in p53 proficient cells (243). Inhibition of ATR signaling selectively sensitizes G1-S checkpoint deficient cells to replication inhibitors or DNA damage (243). This suggests that some cancer cells are under selection for high dependency on the ATR-Chk1 pathway to survive during tumorigenesis. Consistently, Rad9, Hus1, and Rad17 are required for ATR signaling (244), and increased expression of them has been seen in cancer cells (210, 245, 246). Depletion of Hus1 sensitizes non-small lung cancer cells to cisplatin (247). Therefore, proteins functioning in the ATR-Chk1 pathway can be good targets for designing therapeutic drugs, which are expected to selectively kill cancer cells.

Understanding how ATR Signaling is Regulated

Maintenance of high fidelity DNA replication and genome stability is essential for cellular viability and disease prevention. The process of cell proliferation is constantly challenged by many types of DNA damaging agents. ATR is activated in response to replication stress and DNA damage during every S phase (133). It mediates cell cycle checkpoint activation to coordinate with cell cycle progress and also stabilizes stalled replication forks.

The ATR-Chk1 pathway functions in stabilizing the stalled replication forks in yeast (248, 249). How does the ATR signaling pathway stabilize the replication forks? To answer this question, the first step is to identify the proteins on stalled replication forks. A system in which replication forks can be stalled at defined sites is needed. In chapter II, I establish a system in which a replication fork is stalled at a defined site. I attempt to detect proteins recruited to the stalled fork with this system.

How is ATR activation regulated? Many mechanisms by which ATRIP regulates ATR activation are already known. In chapter III, ATR activation regulated by a post-translational modification on ATRIP and a novel ATRIP interacting protein is discussed. In chapter IV, I characterize the RPA70N domain that interacts with multiple checkpoint proteins including ATRIP, Mre11, and Rad9. I characterize the interaction between Rad9 and RPA70N required for ATR signaling.

CHAPTER II

STALLING A REPLICATION FORK AT A DEFINED SITE

Summary

Genetic instability is one characteristic of cancer cells. Genomic DNA has to be duplicated faithfully before cell division during cell proliferation. The DNA replication process constantly experiences endogenous and exogenous challenges. One consequence of replication stress is replication fork stalling. We hypothesized that proteins are recruited to the stalled replication forks to sense DNA damage and activate cell cycle checkpoints, stabilize the replication forks, and repair the damaged DNA to promote replication resumption. Currently, protein localization to sites of DNA damage is detected by immunofluorescence microcopy. Here I established a model system to detect protein localization by CHIP. In this system, a single replication fork is stalled at a defined site on an episome. Modifying this system and making it useful to study protein recruitments to the stalled replication forks are to be continued.

Introduction

High fidelity DNA replication is essential for maintaining genome stability and preventing diseases (250, 251). During cell proliferation, genomic DNA is constantly exposed to varieties of DNA mutagens from endogenous and exogenous sources. The damaged DNA has to be repaired before cell division. Otherwise, permanent mutations on DNA will be generated and accumulated. Cell cycle checkpoints function in sensing these damages and arresting the cell cycle to allow more time for cells to repair the damaged DNA or inducing apoptosis or senescence to eliminate genetic unstable cells.

The faithful duplication of the genome is a complex process involving multiple enzymatic activities that must be coordinated. DNA pre-replication complexes and replication initiation complexes only assemble once per cell cycle, and disassemble after DNA replication initiation to prevent DNA re-replication (25). In eukaryotic cells, replication forks can be stalled by many causes. DNA lesion can block DNA helicases and polymerases from moving along the DNA templates. Replication fork movement is impeded when replication occurs in the heterochromatin region. DNA polymerase and RNA polymerase collisions also impede replication fork movement. Since the pre-replication complexes can not be re-assembled, stabilization of the stalled DNA replication forks is essential for the replication resumption (252).

In yeast, $Mec1^{ATR}$-$Rad53^{Chk1}$ signaling pathway is required for cells recovery from replication stress or methyl methanesulphonate (MMS) treatment accompanied with accumulated unusual DNA structure at replication forks and high rates of irreversible fork collapse (248, 249). Currently very little is known about what happens at the stalled replication forks and how cell cycle checkpoints act to promote the recovery of fork

stalling in mammalian cells. Many proteins have been shown to form foci on sites of DNA damage and stalled replication forks including ATR and ATRIP detected by immunofluorescence microscopy (160, 163). The details of protein localization on the stalled forks are unclear due to the limitation of resolution with immunofluorescence microscopy technique.

The chromatin immunoprecipitation (CHIP) method provides a higher resolution than immunofluorescence to study protein localizations on DNA. The finest resolution of an optical microscope is about 0.2 μm (3). CHIP is a PCR-based approach to analyze DNA interaction with protein. An extended 100 bp DNA is 0.034 μm in length (3). In addition, CHIP is a more sensitive approach than immunofluorescence because PCR is used to amplify the DNA fragments bound by proteins. To utilize CHIP to detect protein interaction with DNA, the information of DNA sequence is needed for PCR. Therefore, a model system with stalled replication forks at defined sites is needed.

The model system of a single double strand break (DSB) at a defined site has been used successfully in yeast and mammalian cells to study cellular responses to DSBs. In yeast, the HO mating-type switch endonuclease cleaves a specific DNA sequence site on the genome (253). With this system, the kinetics of the protein recruitment to the DSB site were investigated (117, 254, 255). Recently, a single DSB was generated in mammalian cells to study protein recruitments to the DSB site by CHIP (131). We intended to establish a model system with a single replication fork stalling at a defined site similar to the above systems and expected that the CHIP would provide a high resolution and focused method to investigate the biologic events on stalled replication forks.

A DNA replication fork could be stalled at a defined site by inhibiting the separation of two strands of DNA templates. This inhibition of DNA strand separation can be achieved by cross-linking agents. It would be necessary to generate an inducible cross-link on the DNA if the chromosomal DNA was the cross-link target. Otherwise cells would either die or repair the cross-link to survive. Two model systems have been used to study the regulation of DNA replication in mammalian cells, SV40 and oriP episomes. The SV40 episome is derived from the simian virus, and the oriP episome is derived from the Epstein-Barr virus (EBV). Both SV40 and oriP episomes are convenient model systems to study DNA replication. The SV40 episome contains a bidirectional replication origin and bypasses the requirements of pre-replication complexes (41). The large T antigen (a viral protein) functions in DNA unwinding as the DNA replication helicases (41, 256). The oriP episome contains a unidirectional origin and utilizes all mammalian DNA replication machinery proteins in addition to EBNA-1, a viral protein to regulate episome replication (48, 49). It replicates once per cell cycle as does the mammalian genomic DNA (50). Thus these two episomes provide suitable vectors to generate a stalled replication fork.

Several oligonucleotides form a triple helix with a sequence-specific double stranded DNA (257, 258). Therefore, psoralen can be conjugated on the oligonucleotide to induce a site-specific cross-link (257). In this study, I established an episome-based model system with a single stalled replication fork at a defined site. Modifying this system to make it useful to study protein recruitment to the stalled replication forks is to be continued.

Materials and Methods

Cell culture, cell lines, and transfections

HeLa and COS-1 cell lines were grown in DMEM (Invitrogen) supplemented with 7.5% fetal bovine serum at 37°C in 5% CO_2. The HeLa cell line expressing the EBV viral protein EBNA-1 was established by retrovirus infection followed by G418 selection. Plasmid DNA transfections into HeLa cells were done with LipofectAMINE (Invitrogen). DNA transfections into COS-1 cells were done with Fugene 6 (Roche Applied Science) according to the manufacturer's instructions.

DNA constructs and oligonucleotides

Oligonucleotides for the TFO target and the APRT target were synthesized (Invitrogen) and annealed. The TFO target and the APRT target were cloned into oriP and SV40 plasmid vectors (Table 2.1). pXX2, pXX3, pXX27, and pXX28 are oriP episomes generated with pCEP4 vector (Invitrogen) as the backbone. pXX2: a stop codon was generated on the N terminal region of EBNA-1; the TFO target was inserted; the furan ring of psoralen-TFO can be cross-linked on the leading strand. pXX3: same as pXX3 except the TFO target was inserted with the opposite direction; the furan ring of psoralen-TFO can be cross-linked on the lagging strand. pXX27: same as pXX2 except the EBNA-1 gene is intact. pXX28: same as pXX3 except the EBNA-1 gene is intact. pXX15: the oriP origin was deleted from pXX2. pXX23, pXX60, and pXX61 are SV40 episomes generated with pcDNA3.1 vector (Invitrogen) as the backbone. The SV40 derived plasmid including pXX23 (the TFO target was inserted; the furan ring of psoralen-TFO can be cross-linked on the leading strand), pXX60 (two APRT targets were

inserted; the TFO target was inserted; the furan ring of psoralen-TFO can be cross-linked on the leading strand), and pXX61 (two APRT targets were inserted; the TFO target was inserted; the furan ring of psoralen-TFO can be cross-linked on the lagging strand) were cloned with pcDNA3.1 vector (Invitrogen) as the backbone.

The oligonucleotides of pso-TFO [5'-X_1TTTTX_2TTTTGGGGGGX_3 (X_1=psoralen C-6; X_2=5-Me-dC; X_3=C7 amine)] and pso-APRT [5'-X_1TGTGGTGGGGGGTTTGGGGX_2 (X_1=5' psoralen C-6; X_2=C3 spacer)] were purchased from Oligo Etc., Inc. The primers of pCEP4 PPT 1F (5'-ACCCCTCCTCTTCCTCTTCA) and pCEP4 PPT 1R (5'-TGCCACCTGACGTCTAAGAA) were purchased from Invitrogen.

Table 2.1. A summary of constructs used in chapter II.

Construct	Origin of episome	TFO cross-link specificity*	Other modifications
pXX2	oriP	Leading strand	Transcription stop codon is inserted in EBNA-1
pXX3	oriP	Lagging strand	Same as pXX2
pXX27	oriP	Leading strand	EBNA-1 is intact compared to pXX2
pXX28	oriP	Lagging strand	EBNA-1 is intact compared to pXX2
pXX15	none	Leading strand	Same as pXX2
pXX23	SV40	Leading strand	
pXX60	SV40	Leading strand	Two APRT target inserted
pXX61	SV40	Lagging strand	Two APRT target inserted

(*TFO cross-link specificity is defined by the strand cross-linked with the furan ring of psoralen.)

Triple helix formation and cross-link induction

Plasmid DNA 0.04 μM was incubated with 8 μM of pso-TFO in the TFM buffer I (10 mM Tris, pH 7.0, 50 mM NaCl, 10 mM $MgCl_2$, 1 mM EDTA) at 37°C for 16 hours in the dark. DNA was precipitated with NH_4Ac and ethanol and resuspended in TFM buffer I to achieve a concentration of 100 ng/μl) immediately followed by exposure to 1.8 J/m^2 UVA (365 nm) irradiation (Stratagene; split the DNA into 10 μl per drop on a piece of parafilm) or 400 nm light generated from a 150 W Xenon lamp at 37°C for 10 minutes [Rapid-Scanning Monochromator On-line Instrument System Inc., Olis Rsm 1000, 150 W Xenon lamp with output 140 W, 6.32 slits (40 nm band pass), 400±20 nm wavelength light will pass the slits]. I thank Dr. Frederick Guengerich for letting me use the machine and Dr. Emre Isin for helping me set up the machine. The psoralen-APRT oligonucleotide directed triple helix formation was performed the same as the pso-TFO directed triple helix formation except the TFM buffer II (10 mM Tris, pH 7.6, 10 mM $MgCl_2$, 10% glycerol) was used.

Determine cross-linking efficiency

*Dra*I protection assay was performed to determine the inter-strand cross-linking efficiency. DNA was digested with *Dra*I and then separated on 3.5% polyacrylamide gel in 1xTBE. The gel was stained with ethidium bromide and imaged with Gel Doc (Bio-Rad). The DNA bands were quantitated with the Quantity One software equipped with Gel Doc.

Primer extension was performed to determine the specificity and efficiency of the intra-strand cross-links. DNA was digested with restriction enzymes to yield a suitable

template for primer extension. The reaction was incubated at 65°C for 20 minutes to inactivate the enzymes. Primers were labeled on 5' ends with p^{32}-ATP by T4 Polynucleotide Kinase (NEB) and purified with the Sephadex G-25 columns (GE Healthcare Life Sciences). Primer extension was done with Taq DNA polymerase (Invitrogen) for 15 cycles according to the PCR protocol except only one primer was added. The primer extension products were dried by speed vacuum, resuspended in formamide loading buffer, and boiled for 5 minutes. Denatured samples were separated on 6% DNA sequencing gel containing 8 M Urea. The gel was dried with a filter paper as the supporter by Gel Drier (Bio-Rad) and imaged by phosphorimager. The target bands were quantitated with the equipped software.

Episomal DNA extraction

Episomal DNA was extracted with the Modified Hirt procedure as described (259). Briefly, $5.5x10^5$ cells were harvested, washed with PBS, and resuspended in 250 µl of buffer I (50 mM Tris, pH 7.5, 10 mM EDTA, 100 µg/ml RNase A). Cells were lysed by addition of 250 µl of 1.2% SDS. After being incubated at room temperature for 5 minutes, the lysate was neutralized with 350 µl of buffer II (3 M CsCl, 1 M KAc, and 0.67 M Acetic acid). After being incubated on ice for 5 minutes, the lysate was clarified by centrifugation. The supernatant was recovered and further purified with a miniprep column (Qiagen). After being washed with buffer III (80 mM KAC, 10 mM Tris, pH 7.5, 40 µM EDTA, 60% ethanol), the DNA was eluted with water.

Detection of DNA replication intermediates by 2-D agarose gel

The 2-D agarose gel was performed as described (260). I thank Dr. Katherine Friedman for her technical help. COS-1 cells $3.4x10^5$ were plated on a 60 mm dish. After being incubated for 24 hours, cells were transfected with 2 µg of DNA. Eight hours after transfection, episomal DNA was extracted as described above and resuspended in 10 µl water followed by restriction enzyme digestion with *Xmn*I. Digested DNA was separated on the first dimension gel made with 0.4% low melting temperature agarose under the condition of 1 V/cm for 17 hours in 1xTBE. The lane with the molecular weight marker on the gel was cut out and stained. The locations 1cm below the 1.5 kb molecular weight marker and 1cm above the 3 kb molecular weight marker were marked. The gel strips of the sample area were excised according to the marked locations on the stained gel and embedded into the second dimension gel made with 1.2% agarose containing 0.3 µg/ml ethidium bromide. The second dimension gel was run under the condition of 5 V/cm at 4°C for 4 hours (avoiding intensive light to keep DNA from damaged). The separated DNA was transferred onto a nylon membrane followed by Southern hybridization.

Southern hybridization

The DNA on nylon membranes were fixed by exposure to UVC (254 nm) generated from the UV cross-linker (Stratagene). The membrane was incubated with the QuickHyb hybridization solution (Stratagene) at 68°C for one hour. The ^{32}P labeled DNA probes were generated by random primers labeling kit (Invitrogen) followed by purification with the Sephadex G-50 columns (GE Healthcare Life Sciences). The labeled probes were denatured and added to the hybridization bottle followed by one hour

incubation at 65°C. The membranes were washed with wash buffer [0.1xSSC (15mM NaCl and 1.5mM trisodium citrate) and 0.1% SDS] at 65°C for 30 minutes and imaged by phosphorimager. The image was quantitated with the equipped software.

Xenopus egg extract preparation

The *Xenopus* Egg extract was prepared as described (139).

Results

Episomal DNA replicates in cells

Episomal DNA containing SV40 origin or oriP origin can replicate in cells (41, 261). They provide convenient model systems to study DNA replication. We intended to generate a site specific cross-link on an episome *in vitro*. After being transfected into cells, the episomal DNA replicates in the S phase. The cross-links on episomes are expected to stall replication forks.

To test whether the episomal DNA replicates in cells, an oriP episome, pXX2 was transfected into HeLa cells expressing EBV viral protein EBNA-1. The plasmid pXX15 served as a negative control for DNA lacking the oriP origin. After transfection, episomal DNA was recovered from cells and detected by southern blot. The template DNA contains dam methylation and is *Dpn*I sensitive. The replicated DNA is resistant to *Dpn*I because of lacking dam methylation. 17.8% of the total extracted DNA is the product of pXX2 replication in cells in 48hours after transfection, and 26.2% of the total extracted DNA is the pXX2 replication products in 72 hours after transfection (Figure 2.1A). In contrast, the control episome, pXX15 only yielded 5.1% and 5.3% replication product in

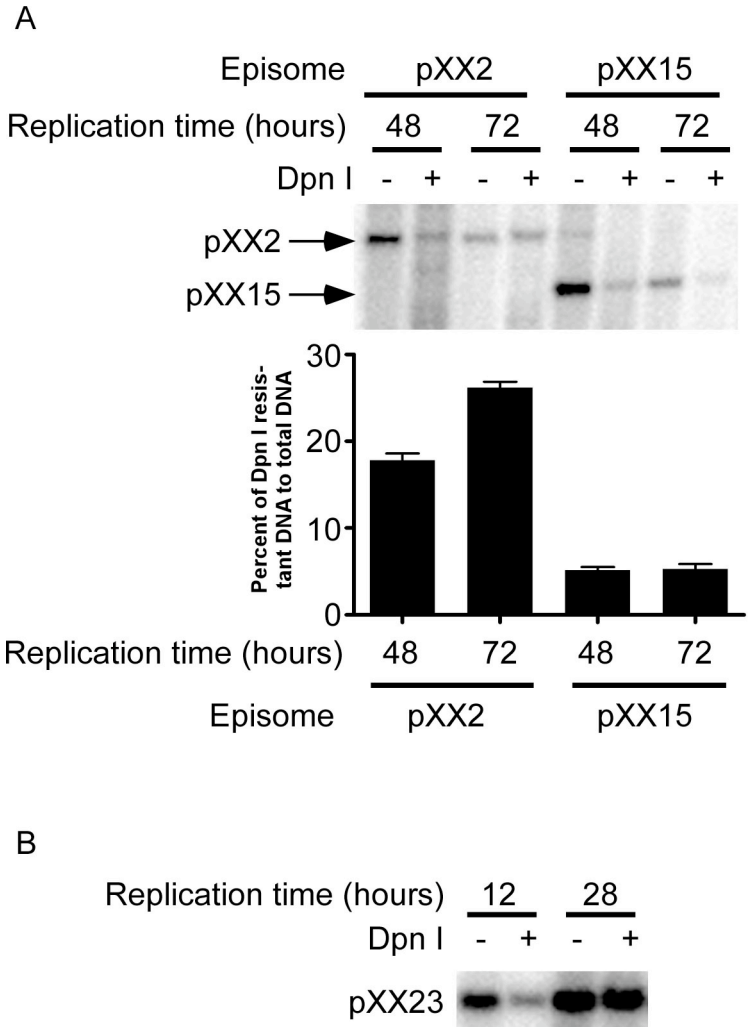

Figure 2.1. OriP and SV40 episomes transiently replicate in mammalian cells. (A) OriP episome replicates in HeLa cells. Plasmid DNA with oriP origin (pXX2) or plasmid DNA lacking oriP origin (pXX15) was transfected into HeLa cells expressing EBNA-1. 48 or 72 hours after transfection, episomal DNA was extracted. 2 µl DNA was digested with *Kpn*I to yield linear DNA, and 8 µl DNA was digested with *Kpn*I and *Dpn*I for quantification of replicated DNA. Southern hybridization was performed with pXX15 as probe (upper panel). The ratio of *Dpn*I resistant DNA to the total DNA represents replication efficiency of oriP episome (lower panel). Error Bars represent standard error calculated from 3 experiments. (B) SV40 episome replicates in COS-1 cells. Plasmid DNA with SV40 origin (pXX23) was transfected into COS-1 cells. 12 or 28 hours after transfection, episomal DNA was extracted. 4 µl DNA was digested with *Hin*dIII to yield linearized DNA. 10 µl DNA was digested with *Hin*dIII and *Dpn*I for quantification of replicated DNA. Southern hybridization was performed with pXX23 as probe.

48 hours and 72 hours respectively (Figure 2.1A). The replication efficiencies of the plasmid DNA containing SV40 origin in COS-1 cells were determined as 24% and 40% in 12 hours and 28 hours respectively (Figure 2.1B).

DNA cross-link can be formed by psoralen at a specific site

Triple helix forming oligonucleotides (TFO) forms a triple helix structure with sequence-specific double stranded DNA (257). The 16 bp polypurine tract (TFO target, figure 2.2A) is a good target for triple helix formation with TFO, a previously reported 15 bp oligonucleotide [Figure 2.2A and reference (262, 263)]. Psoralen is a bi-functional photo-reactive DNA intercalator. It preferentially reacts with thymine (264). The psoralen was conjugated on the 5'-end of TFO (pso-TFO). Psoralen forms covalent links with its furan ring upon exposure to 400nm light generated from xenon lamp and with both furan and pyran rings upon UVA irradiation (365 nm), which forms intra-strand cross-link and inter-strand cross-link respectively [Figure 2.2B and reference (265)].

Inter-strand cross-links were formed initially, which were expected to inhibit the DNA helicase passing the cross-link site. To determine the cross-linking efficiency, a *Dra*-I protection assay was performed (Figure 2.2C, top panel). The *Dra*-I site is inactivated where the cross-link is formed. Therefore, the disappearance of fragment 1 is an indicator of cross-links. The fragment 2 generated by *Dra*I digestion is not affected by the cross-links and serves as an internal control for normalization. The pXX2 plasmid DNA was incubated with pso-TFO to form triplex followed by exposure to UVA. The cross-linked DNA was digested, and separated DNA fragments were quantitated and normalized to the plasmid without any treatment (Figure 2.2C, bottom panel, lane 1).

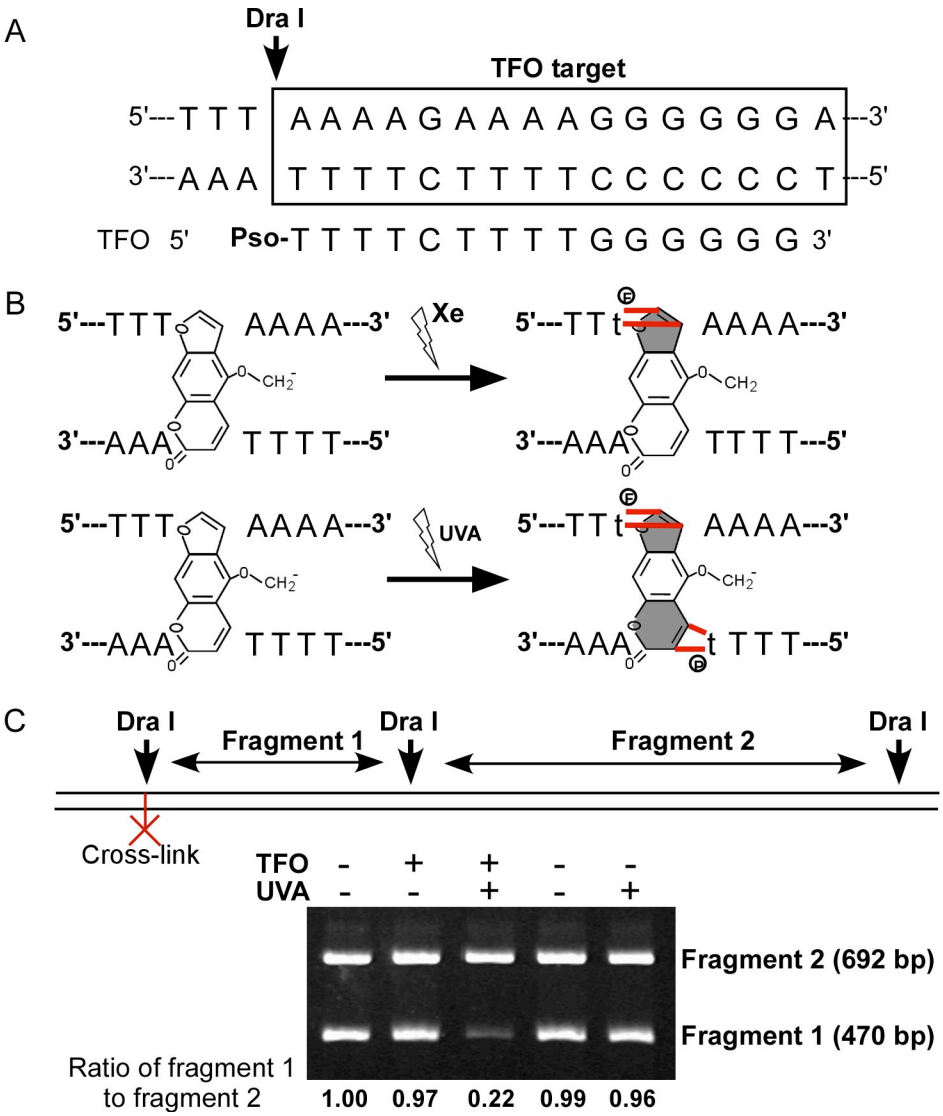

Figure 2.2. Cross-link formation at a defined site. (A) An illustration of a psoralen conjugated triplex formation oligo (TFO) binding to a double strand DNA with specific sequence (TFO target, highlighted in the box), and this forms a DNA triplex motif. (B) Two reactions demonstrate how the psoralen is covalently cross-linked with DNA on single strand by lights generated from Xenon lamp or on double strand by UVA light. Intra-strand link occurs between the furan ring of psoralen and the DNA bases (top panel, red lines). Inter-strand cross-link occurs through both the furan and pyran rings of psoralen (bottom panel, red lines). (C) Analyzing cross-linking efficiency. The top panel is a demonstration of the method for analyzing the cross-linking efficiency. The bottom panel is an analysis of measuring the efficiency. TFO target containing plasmid (pXX2) forms a triplex with psoralen-TFO followed by UVA treatment. DNA was purified by ethanol precipitation. 500 ng DNA was digested with *Dra*I and separated on 3.5% polyacrylamide gel followed by staining with ethidium bromide. The image was taken on Geldoc (Bio-Rad), and DNA bands were quantitated by Quantity One software (Bio-Rad). The ratio of fragment 1 to fragment 2 represents the uncross-linked DNA.

22% of the DNA can be digested to produce the fragment 1, which suggests the cross-linking efficiency about 78% (Figure 2.2C, lane 3). Both triple helix DNA without UVA irradiation and DNA treated with UVA irradiation preserve the *Dra*I site to generate the fragment 1 (Figure 2.2C, bottom panel, lanes 2 and 5).

Inter-strand cross-links inhibit DNA replication

OriP origin fires only in one specific direction (261). The pso-TFO with UVA irradiation induces a cross-link on the plasmid DNA. Also it leaves a third strand at the cross-link site. I generated two DNA constructs with different orientations of TFO targets. For the cross-linked pXX2 (pXX2x), the replication fork encounters the psoralen mediated cross-link before it encounters the TFO. For the cross-linked pXX3 (pXX3x), the fork encounters the 3'-end of the TFO before it encounters the cross-link (Figure 2.3A and 2.3B). Both pXX2 and pXX3 forms cross-link with efficiency of 65% and 84% respectively (Figure 2.3C).

To test whether the cross-link inhibits DNA replication, pXX2x and pXX3x were transfected into HeLa cells expressing EBNA-1 and allowed to replicate. At 48 hours after transfection, the percentages of replicated DNA are not different between the uncross-linked DNA pXX2 and the cross-linked DNA including pXX2x ($p=0.98$) and pXX3x ($p=0.069$, Figure 2.3D). At 72 hours after transfection, 20.4% of recovered episome from pXX3x transfected cells was replicated (Figure 2.3C). Although this is significantly different from pXX2 transfected cells (26.2%, $p=0.002$), the inhibition efficiency of replication (from 26.2% to 20.4%) does not match with the cross-linking

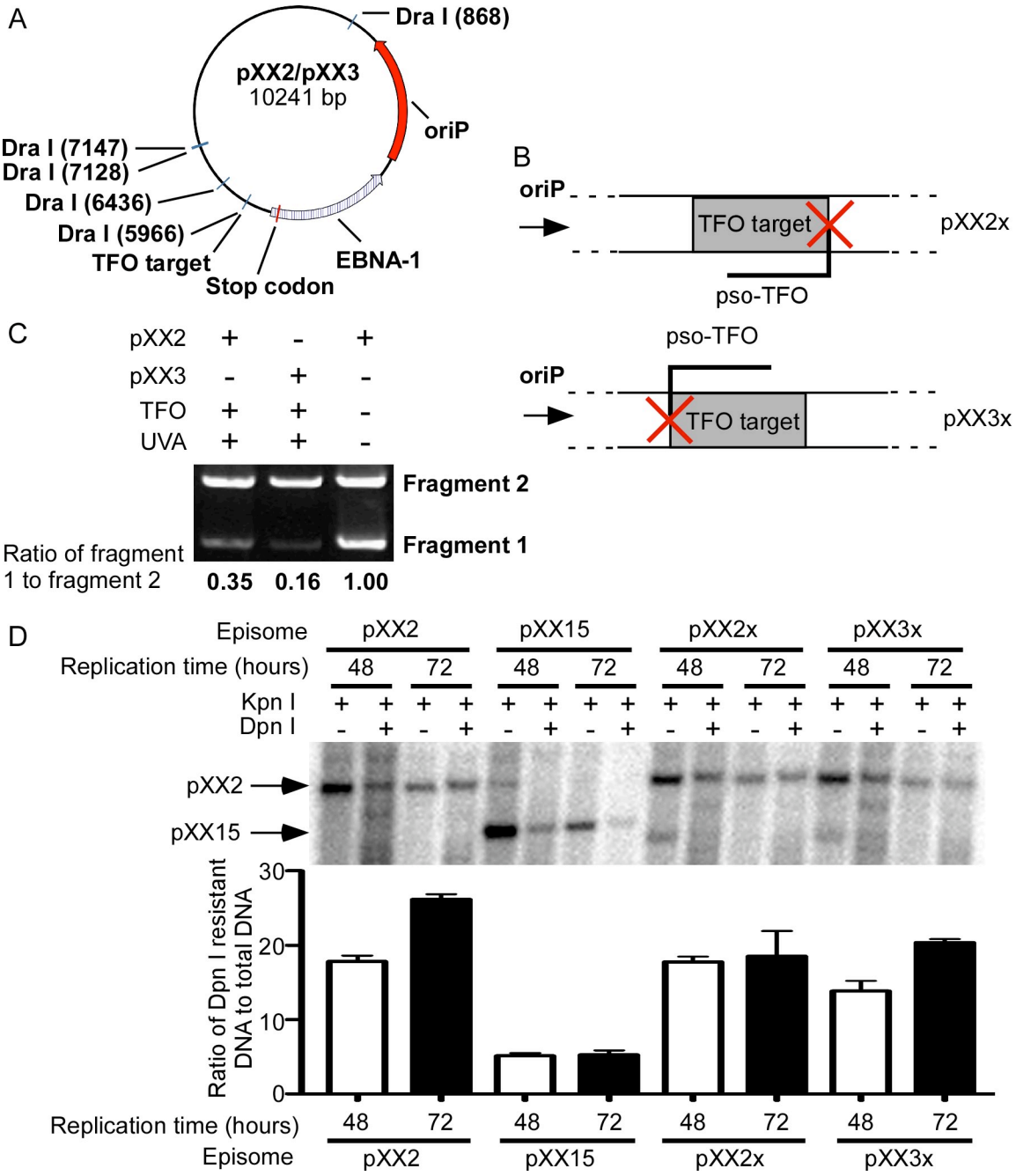

Figure 2.3. Inter-strand cross-link inhibits oriP episome replication in mammalian cells. (A) A diagram of oriP episomes used. (B) Demonstration of two oriP derived episomes containing different directions of the TFO target (pXX2 and pXX3). (C) PXX2 and pXX3 form triplex followed by induction of cross-link. The cross-linking efficiency was analyzed by Dra I protection assay as previously. (D) Episomes (pXX2 and pXX15) or episomes with cross-links (pXX2x and pXX3x) were transfected into HeLa cells expressing EBNA-1. 48 or 72 hours after transfection, episomes were extracted. 2ul of DNA was linearized with Kpn I, and 8ul of DNA was digested with Kpn I and Dpn I. Digested DNA was separated on agarose gel and quantitated by Southern blot with pXX15 as probe (top panel). The ratio of Dpn I resistant DNA to total DNA was presented (bottom panel).

efficiency of pXX3x (84%). Also the pXX2x did not inhibit replication compared to pXX2 at 72 hours after transfection (p=0.089, Figure 2.3D).

The SV40 episome has higher replication efficiency than the oriP episome because it can replicate multiple rounds in one cell cycle. We then tested whether the inter-strand cross-link inhibits replication with the SV40 episome model system. The cross-link was formed on pXX23, an SV40 episome (Figure 2.4A). The cross-linking efficiency was determined by *Dra*I protection assay to be 84% (Figure 2.4B).

The assay of competitive replication of SV40 episomes can determine replication efficiency (257). In this assay, another SV40 plasmid with a different size than pXX23 (pcDNA3.1) was used as an internal control for normalization. The pLNCX2 plasmid does not contain SV40 origin and served as a negative control. The pXX23 DNA was cross-linked with two different efficiencies, 84% (pXX23xa) and 42% (pXX23xb). The ratio of replicated DNA to the internal control was calculated and normalized to the uncross-linked pXX23. The replication efficiencies of pXX23xa and pXX23xb are about 30% and 70% of the uncross-linked pXX23 respectively (Figure 2.4C). The sample of pXX23/UVA is pXX23 treated with UVA without incubation with TFO oligo, and it serves as a control for UVA treatment. The pXX23/UVA episome replicates efficiently as pXX23. These data suggest that the inter-strand cross-link inhibits DNA replication of SV40 episome.

The replication fork is paused at the inter-strand cross-link site

Although the inter-strand cross-link inhibits replication of SV40 episome, it is unclear whether the origin is fired on the cross-linked DNA. Two-dimensional agarose

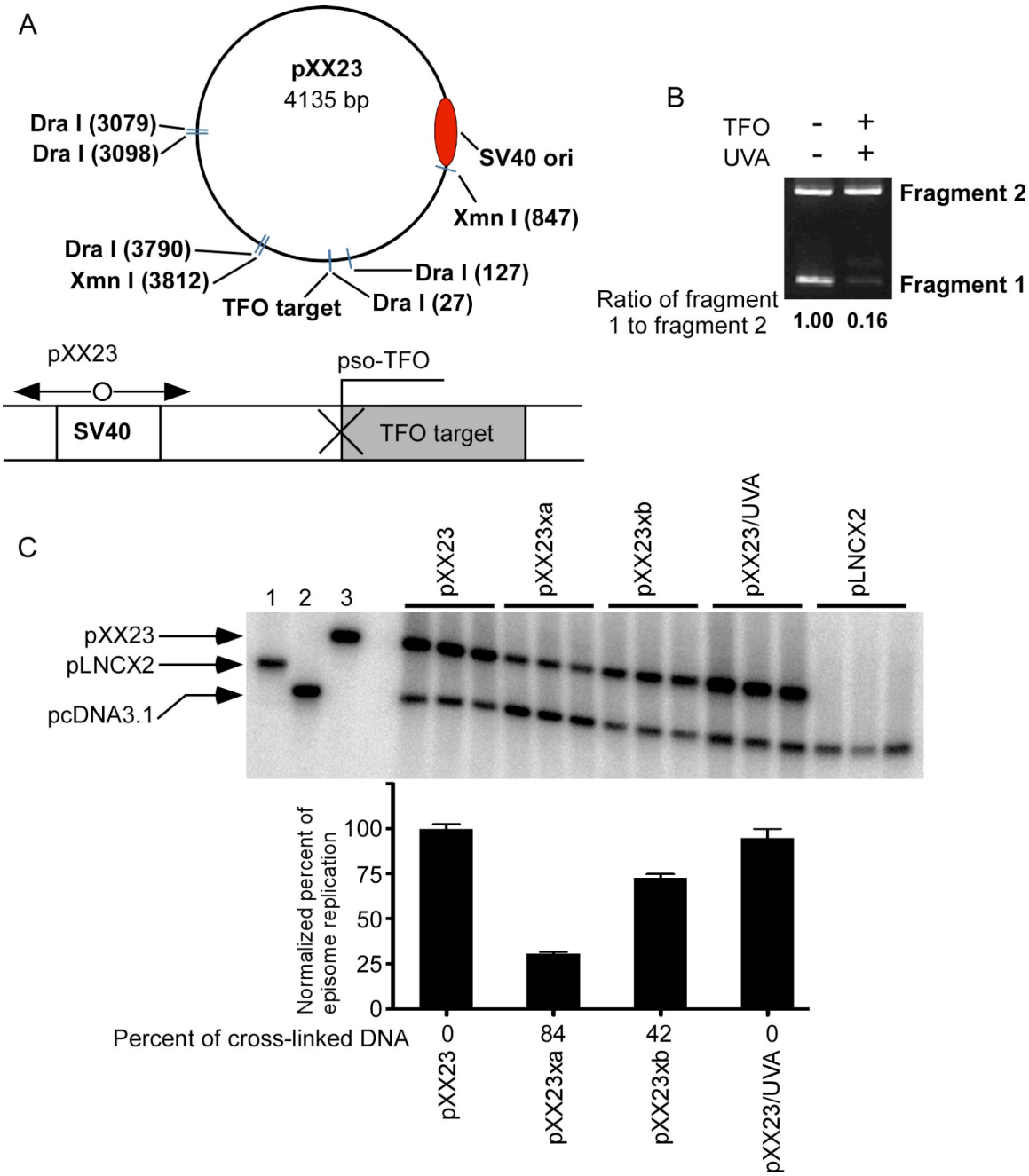

Figure 2.4. Inter-strand cross-link inhibits SV40 episome replication in COS-1 cells. (A) A diagram of SV40 episome used (pXX23). (B) Inter-strand cross-link was achieved on pXX23 as previously, and the cross-linking efficiency was determined by DraI protection assay. (C) PXX23, cross-linked pXX23 [pXX23xa (84% cross-linking efficiency) and pXX23xb (42% cross-linking efficiency by mixing 50% of pXX23 and pXX23a)], pXX23 treated with UVA 1.8 J/m^2, and pLNCX2 (no SV40 origin) were transfected into COS-1 cells with pcDNA3.1 (containing SV40 origin) as the internal control. 24 hours after transfection, the episome DNA was extracted and digested with *Hin*dIII and *Dpn*I followed by southern blot with the AMP gene fragment as probe (top panel). Lane 1, 2, and 3 are plasmid DNA linearized with *Hin*dIII only and served as control for DNA size. The replicated pXX23 DNA was quantitated and normalized to pXX23 without cross-link (bottom panel). Error Bars stand for SE from 3 experiments.

gel has been used to map DNA replication intermediates (260). In the first dimension, DNA is separated by size. In the second dimension, DNA is separated by complexity. Theoretically, the smallest and the largest DNA fragments migrate to point “a” and point “e” respectively (Figure 2.5A). The most complex DNA migrates to point “c” (Figure 2.5A). The fork movements from point “a” to point “e” were exhibited for the uncross-linked (pXX23) and the cross-linked (pXX23x) plasmid DNA (Figure 2.5B). In theory, the replication fork of pXX23 moves from point “a” to point “e” gradually, and replication intermediates are “Y” shaped DNA (Figure 2.5B, left panel). The replication fork of pXX23x moves from point “a” to point “d” and stops at point “d” where the cross-link occurs. The other fork from the opposite direction encounters this stalled fork at the cross-link site. Therefore, a unique “X” shaped DNA is generated (Figure 2.5B, right panel).

The pXX23 episome or cross-linked pXX23 (pXX23x, figure 2.5B) were transfected into COS-1 cells to allow DNA replication. Episomal DNA was digested to produce the DNA fragments from site “a” to site “e”. Two-dimension agarose gels were used to separate replication intermediates followed by southern blot to detect the replication intermediates. The result matches very well with the theoretic fork movements (Figure 2.5C). The dot at site “d” indicated that the replication fork of pXX23x is paused (Figure 2.5C, right panel). The dot at site “e” reflects that the “X” shaped DNA was formed when two replication forks encounter with the cross-link (Figure 2.5C, right panel). The data here indicates that the cross-link on DNA does not inhibit origin firing but stalls the replication fork.

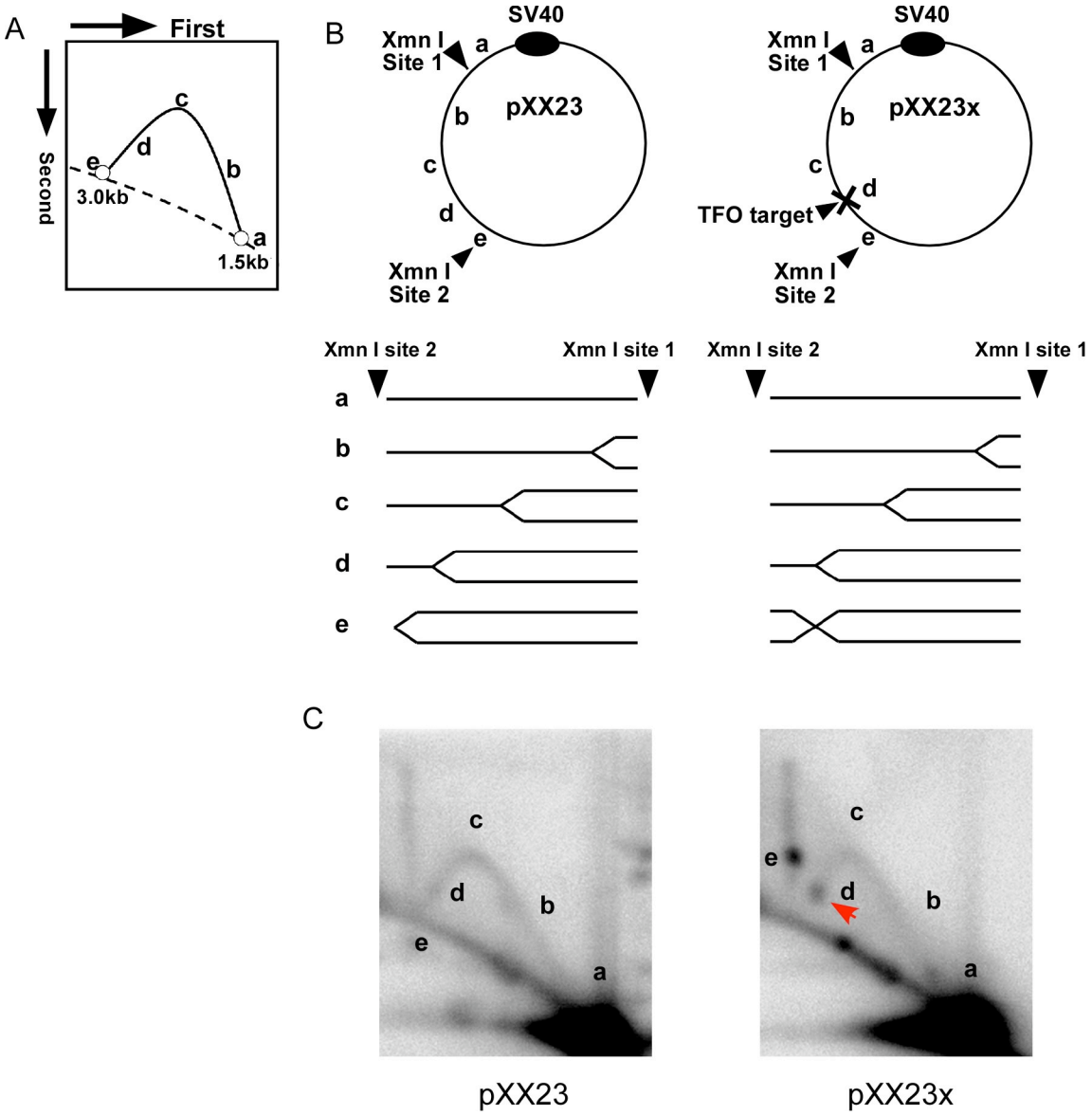

Figure 2.5. Inter-strand cross-link stalls DNA replication forks. (A) Demonstration of analyzing DNA replication intermediates by 2-D agarose gel. In the first dimension, DNA is separated by size (a indicates unreplicated DNA, and e indicates fully replicated DNA). In the second dimension, DNA is separated by complexity (c marks the most complex DNA). (B) Demonstration of pXX23 or cross-linked pXX23 (pXX23x) replication intermediates. a to e represent the locations of replication forks move to and correspondent DNA fragments generated after digestion with *Xmn*I. (C) PXX23 or pXX23x was transfected into COS-1 cells. 8 hours after transfection, episomal DNA was extracted and digested with *Xmn*I followed by separation on 2-D agarose gel. Southern blot was performed to detect the DNA replication intermediates.

An intra-strand DNA cross-link is formed at a specific site

We then tested whether the stalled replication forks activate the ATR dependent checkpoint. Chk1 is phosphorylated by ATR kinase after DNA damage and replication stress (133). There was no detectable Chk1 phosphorylation induced in cells transfected with inter-strand cross-linked DNA of oriP or SV40 episomes (data not shown). Not all stalled replication forks cause ATR activation. It is reported that the functional uncoupling of replication polymerases and helicases generates long stretches of single-stranded DNA (ss-DNA), and this ss-DNA is required to activate ATR (139, 266). It is possible that both polymerases and helicases are stalled at the inter-strand cross-link site on replicating episomes. This may inhibit the formation of long stretches of ss-DNA.

A cross-link on one strand of DNA (intra-strand cross-link) might allow DNA helicases to pass the cross-link site but prevent the DNA polymerase from passing. The 400nm wavelength light generated from a Xenon lamp can induce only the furan ring of psoralen cross-linked with thymidine [Figure 2.2B and reference (265)]. In the model system of SV40 episome, the other fork encounters with the stalled fork indicated by the "X" shaped DNA (Figure 2.5C). I thought that intra-strand cross-link on oriP episome would uncouple the DNA helicases and DNA polymerase for a longer time than on SV40 episome because oriP origin is a unidirectional (46). In addition, this characteristic of oriP episome allows us to distinguish the fork stalling by a lesion on the leading and the lagging strand.

The pXX27 and the pXX28 constructs were generated with two different orientated TFO targets similar to pXX2 and pXX3 (Figure 2.6A). To determine the specificity and efficiency of intra-strand cross-links, we performed primer extension with

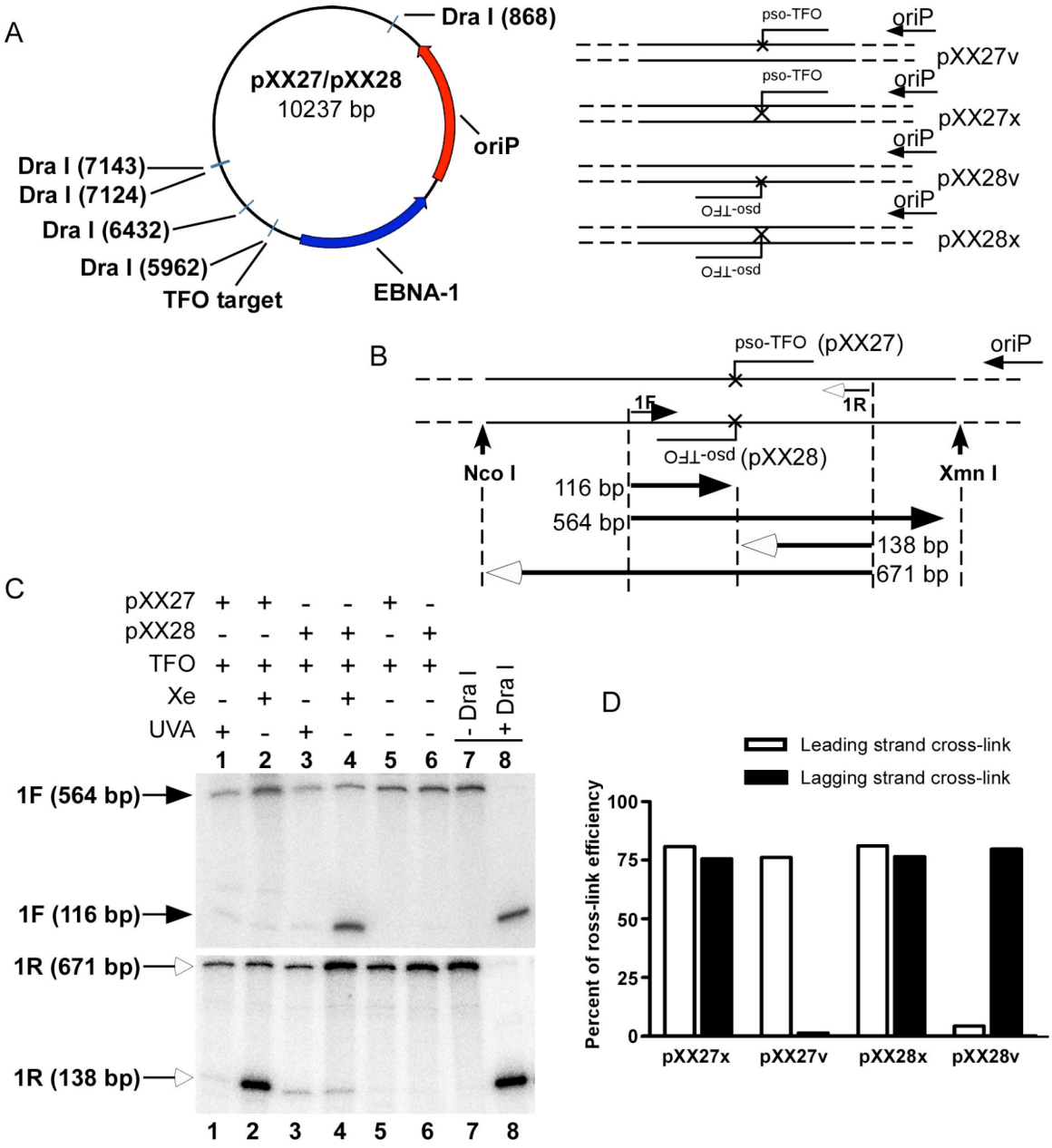

Figure 2.6. Intra-strand cross-links formation. (A) A diagram of oriP episomes used. Two oriP episomes containing different directions of the TFO target (pXX27 and pXX28) form inter- and intra-strand cross-links (right panel). (B) The schematic demonstration of analyzing the cross-link specificity on individual strands by primer extension. The pCEP4PPT-1F (1F) primer pairs to the lagging strand, and the pCEP4PPT-1R (1R) primer pairs to the leading strand. After inter- (pXX27x and pXX28x) or intra-strand cross-links (pXX27v and pXX28v) were formed on DNA, DNA was digested with *Nco*I and *Xmn*I to yield a fragment suitable as the template for primer extension with the p32 labeled primers. Theoretic products were marked with single strand DNA length (arrows indicate the directions of primer extension). (C) Primer extension was performed with both 1F and 1R primers for the intra- (lane 2 and 4) and inter-strand cross-linked DNA (lane 1 and 3). The products were separated on 6% DNA sequencing gel. Lane 7 is the control for no cross-link (pXX28 plasmid digested with *Xmn*I and *Nco*I). Lane 8 is the control for 100% cross-link (pXX28 plasmid digested with *Xmn*I, *Nco*I, and *Dra*I). D, Cross-link efficiencies were calculated on each strand and plotted.

two primers flanking the cross-link sites. Inter- and intra-strand cross-links were formed on pXX27 and pXX28. The cross-linked DNA was digested by restriction enzymes (*Nco*I and *Xmn*I) to generate a suitable template for primer extension. The primer extension products were separated on DNA sequencing gel followed by exposure to phosphor imager. The theoretic products are shown in Figure 2.6B.

The digested pXX28 serves as a negative control for 0% cross-linking efficiency (Figure 2.6C, lane 7). Because the cross-link site is also a cleavage site of *Dra*I, pXX28 was digested with *Nco*I, *Xmn*I, and *Dra*I to serves as a positive control for 100% cross-linking efficiency (Figure 2.6C, lane 8). While TFO forms a triplex with plasmid DNA, it does not block primer extension (Figure 2.6C, lanes 5 and 6). The cross-link will stop primer extension at the cross-link site due to DNA polymerase stalling. A shorter product is generated with the template of cross-linked DNA than the template without cross-links. For intra-strand cross-linked pXX27 (pXX27v), a 138 bp fragment is produced with the primer 1R, but not 1F (Figure 2.6C, lane 2). For intra-strand cross-linked pXX28v, a 116 bp fragment is produced with the primer 1F but not 1R (Figure 2.6C, lane 4). This proved that the cross-link occurred on the specific strand. The intra-strand cross-linking efficiency is determined by the percentage of shorter products in total products. About 76% and 80% strand-specific cross-link were achieved on pXX27v and pXX28v (Figure 2.6D).

The double strands of inter-strand cross-linked DNA can not be separated completely. This can cause two strand re-annealed during primer extension, which inhibits DNA polymerase moving. Therefore, the cross-linking efficiency of inter-strand cross-link can not determined by the above method. Instead, it was determined by the loss

of the larger fragment (564 bp for the primer 1F and 671 bp for the 1R primer; Figure 2.6C, lanes 1 and 3). About 81% and 76% of each strand were cross-linked on pXX27x (Figure 2.6D). Similar cross-link efficiencies were achieved on pXX28x. The inter-strand cross-linking efficiency was also determined with *Dra*I protection assay. The cross-link efficiencies determined by these two methods were consistent (data not shown).

Intra-strand cross-linked DNA induces Chk1 phosphorylation

There was no detectable Chk1 phosphorylation in cells transfected with the inter- and intra-strand cross-linked oriP plasmid. I was unable to prove that the cross-link on oriP plasmid can stall replication forks partially because the replication efficiency of oriP plasmid in cells is very low (once per cell cycle).

The *Xenopus* egg extract system has been used to study DNA replication as a model system (40). In this system, the concentrated S phase components support a robust DNA replication *in vitro*. In addition, any region on DNA can serve as a replication origin. In collaboration with Dr. Karlene Cimprich laboratory, we tested whether the cross-linked plasmid induces Chk1 phosphorylation in this system. Because origin fires in both directions, we were unable to distinguish the intra-strand cross-link on the leading strand and the lagging strand. The cross-linked pXX27 plasmid was used here (Figure 2.7). The addition of pXX27 causes Chk1 phosphorylation induced by aphidicolin (Figure 2.7, compare lanes 7 and 8). The addition of intra-strand cross-linked pXX27 (pXX27v) induces Chk1 phosphorylation but the control of Xenon light treated does not (Figure 2.7, compare lanes 11 and 12). In contrast, the inter-strand cross-linked pXX27 (pXX27x) did not induce detectable Chk1 phosphorylation. Moreover, inhibition of DNA

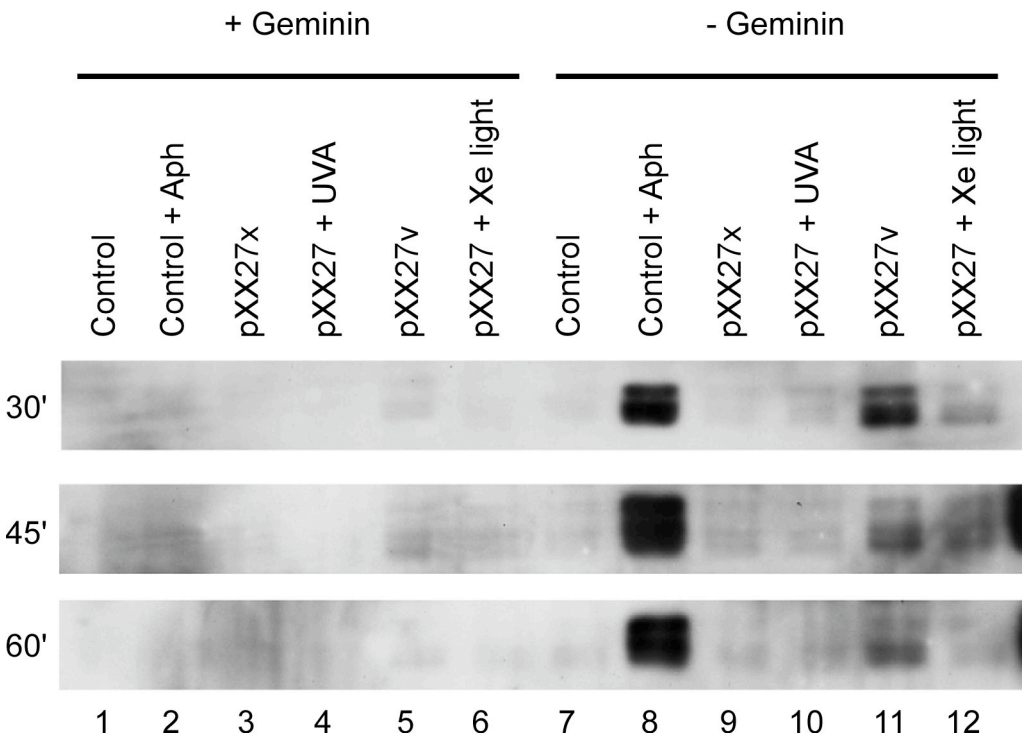

Figure 2.7. Intra-strand cross-linked DNA causes Chk1 phosphorylation in *Xenopus* egg extracts. Equal amount of untreated plasmid (Control), inter-strand cross-linked plasmid (pXX27x), inter-strand cross-link control plasmid (pXX27 + UVA), intra-strand cross-linked plasmid (pXX27v), and intra-strand cross-link control plasmid (pXX27 + Xe light) were incubated with Xenopus egg extract in the presence and absence of Geminin (30 minutes, 45 minutes and 60 minutes). Chk1 phosphorylation was examined by immunoblotting with an antibody to phospho-specific Chk1. The control plasmid also was incubated with the egg extract in the presence of aphidicolin to serve as a positive control. This experiment was performed by Dr. Karlene Cimprich laboratory.

replication by addition of Geminin abolishes the Chk1 phosphorylation induced by the intra-strand cross-link (Figure 2.7, compare lanes 5 and 11). This result suggests that the combination of the cross-linked episomes with *Xenopus* egg extract system is an ideal system to study replication fork stalling.

Distinguishing cross-links on the leading and lagging strand in the egg extract system

Any region on DNA can serve as a replication origin, and any origin fires in both directions in the egg extract system. Although the origin on DNA is not sequence specific, only one origin occurs per 10kb DNA in general (267). This characteristic provides a strategy to distinguish the cross-link on the leading and lagging strand. One origin per molecule was achieved by limiting the size of plasmid DNA to less than 10 kb. Since the inter-strand cross-link does not induce Chk1 phosphorylation, we can generate a psoralen-APRT-mediated inter-strand cross-link to block one direction of fork progression [Figure 2.8A and reference (258)]. The TFO target is 500 bp away from the APRT target (Figure 2.8B). Therefore, 95% of the forks will be initiated from the larger fragment between TFO target and APRT target. Thus, 95% of intra-strand cross-link generated by pso-TFO is specifically on leading or lagging strand dependent of orientation of TFO target.

Although the SV40 origin is not committeed to fire in the egg extract system, we used an SV40 episome as the vector to clone APRT and TFO targets because this episome can replicate robustly in COS-1 cells (Figure 2.8B). The pso-APRT-mediated inter-strand cross-link can block one direction of replication fork initiated from the SV40 origin (Figure 2.8B, bottom panel). This allows the DNA helicase from the other fork to

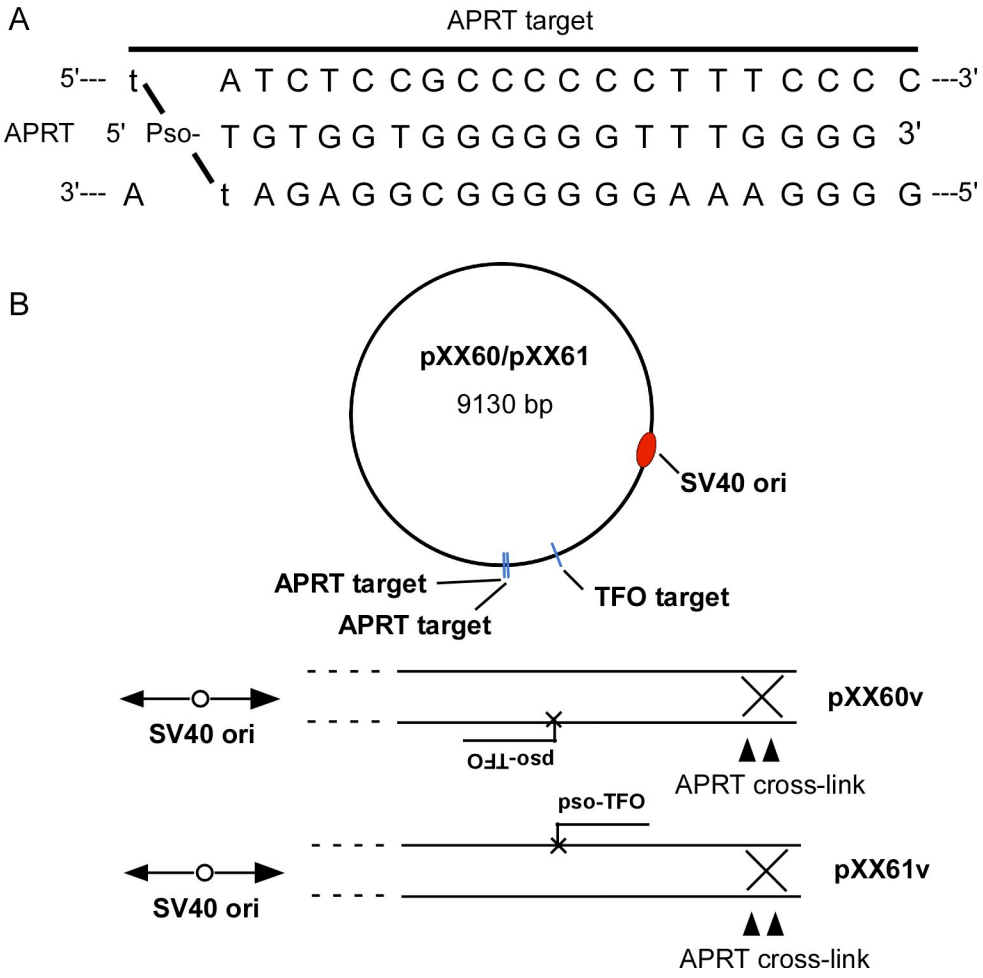

Figure 2.8. Modified SV40 constructs for studying leading and lagging strands replication stress. (A) APRT oligo forms a triplex with its target DNA. Psoralen-mediated cross-links can be induced by UVA through the thymidines on both strands (t). (B) A diagram of plasmid DNA with two adjacent APRT target sites and one TFO target site (top panel). Illustration of pXX60 and pXX61 forms intra-strand cross-links. The TFO target is 500 bp away from the APRT target.

unwind template DNA longer when the fork is stalled by the cross-link on the leading or lagging strand separately in COS-1 cells. The oligonucleotide APRT efficiently forms triple helix with the APRT target (258). The psoralen-APRT-mediated inter-strand cross-link was achieved about 95% upon UVA irradiation (data not shown). Then the DNA formed triple helix with pso-TFO followed by exposure to the light of 400 nm wavelength. The cross-links on APRT target was remained after this treatment. About 70% cross-link was achieved on the leading or lagging strand specifically determined by primer extension (data not shown). We will determine whether different levels of Chk1 phosphorylation are induced by the cross-link on the leading and lagging strand. Also this modified episome in combination with the egg extract system provides an ideal system to study protein recruitment to the stalled forks by CHIP.

Discussion

To understand how the stalled forks are stabilized, we need to identify what proteins are recruited to the stalled forks. Currently, protein foci formation co-localized with the replication fork is detected by immunofluorescence microscopy. Here we proposed to establish a system to study protein localization on stalled forks by CHIP, a higher resolution and more sensitive approach than immunofluorescence microscopy. CHIP requires the DNA sequence information for PCR. Therefore, a model system with stalled replication forks on the defined sites is needed. The combination of the cross-linked episomes with *Xenopus* egg extract system is an ideal system to detect protein localizations on the stalled replication fork by CHIP. This is supported by the evidence

that intra-strand cross-linked DNA causes Chk1 phosphorylation in the egg extract system (Figure 2.7).

A similar system was established to detect protein localization on replicating episomes by CHIP (33). In this system, plasmid replication is stalled by biotin-streptavidin complex. The biotin-streptavidin complex blocks DNA helicase and DNA polymerases. Replication proteins including Mcm2-7, Cdc45, and GINS are detected to be enriched on the site of stalled forks. The system I established is expected to differentiate the inter-strand cross-link and intra-strand cross-link. Also with the modified episome containing APRT and TFO targets, we will be able to differentiate the stalled forks on the leading strand and the lagging strand (Figure 2.8B).

We proposed to detect protein recruitment to the stalled forks by CHIP. This method requires a high quality of antibody to proteins known on the stalled forks. Our main targets are checkpoint proteins including RPA, ATR, and ATRIP. There is only one report about detecting these proteins on DNA by CHIP (268). I was unsuccessful to detect these proteins on stalled fork in cells by CHIP under the condition as described (268). Then I tried an alternative approach to detect protein localization on DNA in cells. A biotin group was conjugated to the 3' end of pso-TFO, and the proteins bound on the stalled forks can be pulled down by streptavidin beads. The proteins on the beads can be detected by western blot or proteomics approach. Compared with CHIP, the pull-down method is less sensitive because PCR is used to amplify signal in CHIP assay. Therefore, a lot more samples are needed to detect proteins by the pull-down assay. I was unsuccessful to detect ATR, ATRIP, or RPA on the stalled forks in cells by the pull-

down assay. However, it is worth to try both CHIP and streptavidin pull-down approaches in the egg extract system with the cross-linked plasmid DNA.

The functional uncoupling of replication polymerases and helicases generates long stretches of single-stranded DNA (ss-DNA), and this ss-DNA is required to activate ATR (139, 266). On a circled episome with a bidirectional origin, the DNA helicase of one fork is functionally uncoupled from the DNA polymerases when the fork encounters the intra-strand cross-link. The other moving fork will inhibit the activity of this DNA helicase by limiting the template. The functional uncoupling of DNA helicase and DNA polymerase generates ss-DNA, and longer stretches of ss-DNA can cause higher levels of ATR signaling (139). Therfore, the intra-strand cross-link on an episome with a unidirectional origin may cause higher levels of Chk1 phosphorylation than on an episome with a bidirectional origin. The intra-strand cross-link on oriP episome does not cause detectable Chk1 phosphorylation. This may due to the low replication efficiency of oriP episomes. The SV40 episome replicates robustly in COS-1 cells. The pso-APRT-mediated inter-strand cross-link on pXX60/61 can block one direction of replication fork initiated from the SV40 origin (Figure 2.8B, bottom panel). This will extend the duration time of the founctional uncoupling of DNA helicase and polymerase by pso-TFO-mediated intra-strand cross-link, which may increase the level of Chk1 phosphorylation to be detected.

The replications of the SV40 and the oriP episomes were inhibited by the inter-strand cross-link (Figures 2.3 and 2.4). The inhibition efficiency was proportional to the cross-linking efficiency for the SV40 episome. However, the inhibition efficiency was not matched with the cross-linking efficiency for the oriP episome. This is due to the

methodology used to detect replicated DNA, which is determined by the resistance to *Dpn*I. Two rounds of replication are required for replicated DNA to be *Dpn*I resistant. A minimum time of 48 hours is required for oriP DNA replication to be detected with this method. The cross-link on DNA possibly has been removed by the DNA repair proteins in 48 hours. SV40 episome replicates multiple rounds in one cell cycle. Therefore, DNA replication can be detected at earlier time point (Figure 2.4).

Although the fork stalling of SV40 episome by the inter-strand cross-link can be detected by 2-D agarose gel (Figure 2.5C), detecting the replication intermediates was unsuccessful for oriP episomes replicated for 24 hours. There were two possible reasons for this difficulty. One, the oriP origin only fires once per cell cycle (50), and SV40 plasmid replicates constantly in S phase (41). Two, less copy numbers of the oriP episome can be replicated than SV40 episomes (Figure 2.1). A lot more sample is required to detect the replication intermediates for oriP episome than SV40 episome.

Transfection of the inter-strand cross-linked oriP or SV40 episomes into cells does not activate Chk1 phosphorylation (data not shown). Functional uncoupling of the replication helicases with DNA polymerases activates ATR (139, 266). It is unclear whether the helicases can pass the inter-strand cross-link. I thought that the cross-link on one strand of the double stranded DNA template would provide a better chance to uncouple the replication helicases and DNA polymerases. The strand-specific cross-link was achieved on the oriP episome that targeted the leading strand and the lagging strand individually (Figure 2.6). Although the intra-strand cross-linked oriP episomes did not induce Chk1 phosphorylation in cells (data not shown), they are able to induce Chk1 phosphorylation in *Xenopus* egg extract system (Figure 2.7). The possible explanation is

that DNA is replicated more synchronized and robustly in the *Xenopus* egg extract system than in cells. Therefore, the combination of the cross-linked episomes with *Xenopus* egg extract system is an ideal system to detect protein localizations on the stalled replication fork.

In summary, we established a model system to study cellular responses to a stalled DNA replication fork. In this model system, one fork is stalled at the defined site. This model system with a single fork stalling provides a focused window to study protein recruitments to the stalled fork. Although we have not identified any checkpoint protein on the stalled fork in cells yet, the *Xenopus* egg extract system may provide better chance to identify protein recruitment to stalled forks. Also, this model system can be used to study how different DNA damages are repaired for the inter-strand cross-links, leading strand cross-links, and lagging strand cross-links.

CHAPTER III

REGULATION OF ATR SIGNALING BY ATRIP AND CINP[1]

Summary

ATR regulates cellular responses to DNA damage and replication stress. ATRIP is a constitutive interaction partner of ATR and critical for ATR activation. Post-translation modification and protein-protein interaction are common mechanisms for regulation of protein functions. Mass spectrometry was used to identify phosphorylation sites on the ATRIP-ATR complex. Two novel phosphorylation sites on ATRIP were identified, S224 and S239. S224 matches a consensus site for cyclin-dependent kinase (Cdk) phosphorylation and is phosphorylated by Cdk2-cyclin A *in vitro* and *in vivo*. Mutation of S224 to alanine causes a defect in maintaining the ATR-ATRIP dependent G2-M checkpoint response to ionizing and ultraviolet radiation. We also identified CINP as a novel regulator of ATR signaling. Furthermore, CINP interacts with ATRIP and regulates phosphorylation of ATRIP on S224. Thus, Cdk2 regulates ATR signaling in response to DNA damage through CINP and ATRIP S224 phosphorylation.

[1] A portion of this chapter has been previously published in ref 175. Myers, J.S., et al. (2007) Cyclin-dependent kinase 2 dependent phosphorylation of ATRIP regulates the G2-M checkpoint response to DNA damage. *Cancer Res*, **67**, 6685-90.

Introduction

The ATM (ataxia-telangiectasia mutated) and ATR (ATM and Rad3-related) kinases function at the apex of cell cycle checkpoint signaling pathways (92, 133, 269). ATM functions primarily in response to double strand breaks throughout the entire cell cycle. ATR activation occurs primarily in S-phase in response to long stretches of replication protein A (RPA) coated single strand DNA (hereafter RPA-ssDNA) (134, 266, 270). ATM and ATR share many biochemical and functional similarities. Both are large protein kinases with significant sequence homology and a strong preference to phosphorylate serine or threonine followed by glutamine (S/TQ) (61, 92-94). However, ATR is essential for cell proliferation in humans and mice, whereas ATM is not (163, 231, 232).

ATR, ATM, and DNA-PK are members of a phosphoinositide 3-kinase related kinases (PIKKs) family. Phosphorylation is a common regulatory mechanism of kinase activation. ATM is autophosphorylated on three different sites, S367, S1893, and S1981. These phosphorylation sites are important for ATM function (124, 125). ATM S1981 phosphorylation promotes a conformation change of ATM from inactive dimers to active monomers (124). DNA-PK contains two clusters of S/TQ phosphorylation required for its activity. These sites are phosphorylated by autophosphorylation, ATM, or ATR (271, 272). Therefore, we propose that ATR activity is also regulated by phosphorylation. This is supported by the evidence that both ATR and ATRIP can be phosphorylated by ATR in an *in vitro* kinase assay (163). However, no phosphorylation sites on ATR-ATRIP have been described.

Protein-protein interaction is another common mechanism to regulate protein functions. ATR has a constitutive interaction partner, ATRIP (163). This is a key difference between ATR and ATM. ATRIP regulates ATR activation in many aspects. ATRIP and ATR proteins mutually stabilize each other (163). The N-terminal region of ATRIP is required to localize the ATR-ATRIP complex to DNA damage sites through an interaction with RPA (137, 160). The ATRIP coiled-coil domain contributes to ATRIP oligomerization, stabilization of the ATR-ATRIP complex, and Chk1 phosphorylation after DNA damage (168). The ATRIP C-terminal region containing residues 658-684 is required for the formation of ATR-ATRIP complex (160). Both the formation of ATR-ATRIP complex and ATR kinase activity are required for the complex localization to DNA damage sites (119, 160, 172). Moreover, TopBP1 is an ATR kinase enhancer, and its interaction with the ATR depends on the formation of ATR-ATRIP (217, 218, 273).

Here we identified two phosphorylation sites on ATRIP, S224 and S239. Using phospho-peptide-specific antibodies and mutational analysis, we have determined that phosphorylation of ATRIP S224 is dependent on Cdk2 kinase activity and critical for ATR-dependent checkpoint responses after DNA damage. Furthermore, we identified Cdk2-interacting protein (CINP) as a novel ATRIP interacting protein. CINP is also a regulator of the ATR-ATRIP checkpoint kinase complex. Thus, in addition to being a target for ATR-dependent checkpoint responses, Cdk2 also regulates the ATR checkpoint kinase through ATRIP and CINP.

Materials and Methods

Antibodies

The following antibodies were purchased: γH2AX (Upstate Biotechnology), ATR and CHK1 (Santa Cruz Biotechnology), GAPDH (Chemicon), Flag (Sigma), MCM2 (BD) and HA.11 (Covance). The phosphopeptide-specific antibodies to pS345 of CHK1, pS317 of CHK1, and pS15 of p53 were obtained from Cell Signaling Technology. Antibodies against ATRIP and ATRIP pS224 were generated and described previously (163, 175). Mouse polyclonal antibodies to full-length recombinant CINP were generated by the Vanderbilt Monoclonal Antibody Core (VMAC).

Cell culture, cell lines, cell treatments, and transfections

HeLa, U2OS, and HEK293T cell lines were grown in DMEM (Invitrogen) supplemented with 7.5% fetal bovine serum at 37°C in 5% CO_2. RPE-hTERT cells were grown in DMEM/F12 (Invitrogen) supplemented with 10% fetal bovine serum and 0.2% sodium bicarbonate. U2OS cell lines expressing the pLPCX empty vector, HA-ATRIP, and HA-ATRIP S224A and RPE-hTERT cells expressing HA-ATRIP were established by retrovirus infection followed by puromycin selection. UV treatment was conducted with a Stratalinker (Stratagene). IR treatment was done with a ^{137}Cs irradiator with a dose rate of ~1.4 Gy/min. Plasmid DNA transfections were done with LipofectAMINE 2000 (Invitrogen), and siRNA transfections were done with OligofectAMINE (Invitrogen) according to manufacturer's instruction. For G2-M checkpoint assays with ATRIP and the ATRIP S224A mutant, cells were transfected twice in day one and day two.

RPE-hTERT cell synchronization

Twenty-four hours after siRNA transfection, RPE-hTERT cells were plated from one well in a 6-well plate to one well in a 12-well plate. The cells were incubated for 48 hours. This is considered time 0 when cells were arrested in G0 by contact inhibition. Cells were then plated from one well to one 100 mm dish, allowing cells to release from the arresting and re-enter the cell cycle. Cells were in S phase after incubation for 24 hours. DNA content was analyzed for asynchronized, arrested, and released cells by flow cytometry with propidium iodide staining.

DNA content analysis

Cells were harvested, washed with PBS, and fixed with 70% cold ethanol. After fixation, cells were pelleted and resuspended in PBS containing propidium iodide and RNase followed by incubation at 37°C for one hour. Cells were analyzed on a BD Biosciences FACSCalibur.

DNA constructs and siRNA targeting sequences

Site-directed mutagenesis was performed using QuickChange (Stratagene). All DNA constructs generated using PCR were confirmed by sequencing. DNA constructs for retrovirus infection were generated with the pLPCX vector (BD). DNA constructs for transient gene expression were generated with the pcDNA3.1 vector (Invitrogen). Non-specific siRNA (5'-ATGAACGTGAATTGCTCAA), siRNA targeting endogenous ATRIP (5'-GGTCCACAGATTATTAGAT), and siRNA targeting CINP [CINP-1 (5'-AAACCTGTCTTATCTGTCA), CINP-2 (5'-GCGGCTGATTGGCACAATT), CINP-4

(an ON-TARGETplus SMARTpool duplex including 5'-CAAGGGAATTTGTGAACTA, 5'-GAACTGTAACGCCCAGAAA, 5'-CGCATAAGCTCTTGGAGAT, and 5'-GAAAAGGTGTGTCTGGAAT), CINP-6 (5'-GCGGCTGATTGGCACAATTTA)] were purchased from Dharmacon, Inc. except CINP-2, which was from Invitrogen.

Total cell lysate and nuclear extracts preparation

Total cell lysates were prepared by lysing cell pellets with different lysis buffers on ice for 30 minutes followed by centrifugation according to the approaches of individual experiments. CHAPS lysis buffer (50 mM Tris, pH 7.5, 150 mM NaCl, 0.75% CHAPS, 0.1% triton x-100) was used for protein co-immunoprecipitation. For immunoblotting, NP-40 lysis buffer (50 mM Tris, pH 7.5, 200 mM NaCl, 1% Igepal) was used. Both lysis buffers were supplemented with protease inhibitors including 5 μg/ml aprotinin, 5 μg/ml leupeptin, 1 mM NaF, 20 mM β-glycerolphosphate, 1 mM sodium vanadate, 1 mM dithiothreitol, and 1 mM phenylmethylsulfonate (PMSF). For preparation of nuclear extracts, two 10cm dishes of 90-100% HEK293T cells were harvested. The cells were washed twice with PBS and resuspended in 1 ml cold hypotonic buffer (20 mM HEPES-KOH, pH 7.9, 1.5 mM $MgCl_2$, 10 mM KCl, 0.2 mM PMSF, 0.5 mM DTT). Cells were then spun at 2500xg for 3 min at 4^{o}C, and the supernatant was discarded. Cells were resuspended in 0.4 ml cold hypotonic buffer and allowed to swell on ice for 10 minutes. The suspension was homogenized in a small dounce homogenizer with ten up and down strokes and spun at 3300xg for 6 min at 4^{o}C. Then, 250 μl of high salt buffer (20 mM HEPES-KOH, pH 7.9, 25% glycerol, 1.5 mM $MgCl_2$, 350 mM NaCl, 0.2 mM PMSF, 0.5 mM DTT, 1 mM NaF, 10 mM Sodium

Vanadate, 10 mM β-glycerolphoshpate, 5 μg/ml aprotinin, 5 μg/ml leupeptin) was slowly added to the pellet in a drop wise with occasional flicking. The suspension was placed on an end-over-end rotator for 30 min at 4°C. The extract was spun at 16,000xg for 10 min at 4°C to get rid of the insoluble proteins. The supernatant was recovered, mixed with 200 μl no salt buffer (20 mM HEPES-KOH, pH 7.9, 20% glycerol, 0.2 mM PMSF, 0.1% Tween 20), and spun at 16,100xg for 5 min at 4°C. The supernatant (the nuclear extract) was recovered.

Co-immunoprecipitation

HEK293T cells were transiently transfected with constructs encoding tagged ATR, ATRIP, and CINP. Cells were harvested and lysed in CHAPS lysis buffer. Anti-Flag agarose beads (Sigma) were added to clarified cell lysates, and the mixture was incubated at 4°C for 3 hours. The beads were washed with lysis buffer twice and lysis buffer containing 0.5% triton x-100 once. Precipitated proteins were eluted and separated on SDS-PAGE gels followed by immunoblotting. For co-immunoprecipitations with endogenous protein, total cell lysates from HeLa cells or nuclear extracts from HEK293T cells were incubated with mouse anti-CINP antibodies and protein G agarose beads (Invitrogen) at 4°C for 3 hours. The beads were washed with TGN buffer (Tris, pH 8.0, 150 mM NaCl, 1.0% Tween 20, 10% glycerol) supplemented with protease inhibitors. Precipitated proteins were eluted and separated by SDS-PAGE followed by immunoblotting.

Cdk2-cyclin A Kinase assay

HA-ATRIP-Flag-ATR complexes were purified from transiently transfected HEK293T cells. Total cell lysates were prepared with TGN buffer supplemented with protease inhibitors. Anti-HA agarose beads (Sigma) were added to clarified cell lysates and incubated for 3 hours. The beads were washed with TGN buffer, TGN buffer containing 0.5 M LiCl, and 1xCdk2 kinase buffer (New England Biolabs). Kinase reactions were started by the addition of 28 units of Cdk2-cyclin A complexes (New England Biolabs) and 10 μCi γ^{32}P-ATP (3,000 Ci/mM) in kinase buffer supplemented with 20 μM ATP directly to the HA-ATRIP-Flag-ATR complexes on the beads. Reactions were incubated at 30°C for 20 minutes and stopped by the addition of SDS sample buffer and boiling. Reactions were separated on duplicate SDS-PAGE gels. One gel was stained with coomassie blue, dried, and exposed to X-ray film. Proteins from the duplicate gel were transferred to nitrocellulose followed by immunoblotting with antibodies for ATR and ATRIP.

G2-M checkpoint assay

U2OS cells were transfected with siRNA as described above. Three days after transfection cells were irradiated with IR or UV followed by incubation in the presence of 1 μM nocodazole to capture cells that entered mitosis. Cells were incubated for 16 hours after being treated with 5 Gy of IR or 8 hours after being treated with 25 J/m^2 of UV. All cells were harvested and fixed with Carnoy's fixative solution. Cells were stained with 4'6-diamidino-2-phenylindole (DAPI) and imaged with microscopy. Mitotic spreads were counted. At least 300 cells were counted for each sample. Alternatively, all cells

were harvested and fixed with 70% ethanol. Cells were permeabilized followed by staining with anti-phospho-histone H3 S10 antibody and propidium iodide. Mitotic cells were quantitated by flow cytometry analysis. 10,000 cells were analyzed for each sample.

Immunofluorescence

U2OS cells were cultured on cover slips for 24 hours, rinsed with PBS once, and fixed with 3% paraformaldehyde for 10 minutes at room temperature. After being washed with PBS, cells were permeabilized with 0.5% triton X-100 for 10 minutes on ice followed by washing with PBS. After being blocked at room temperature for 15 minutes with 5% BSA/PBS, cells were incubated with primary antibodies followed by washing with PBS. Then cells were incubated with fluorophore conjugated secondary antibody followed by washing with PBS. Cells were counterstained with DAPI, and cover slips were mounted on microscope slides. For γH2AX immunostaining, cells were cultured on cover slips two days after siRNA transfection. After 24 hours of culturing, cells were incubated with mouse anti-γH2AX (pS139) antibody as primary antibody and rhodamine conjugated goat anti-mouse antibody (Jackson ImmunoResearch) as secondary antibody. Cells were imaged with a Zeiss Axioplan microscope equipped with a Zeiss camera and software.

Immunoblotting

Proteins transferred onto nitrocellulose were incubated with primary antibodies and secondary antibodies. Secondary antibodies conjugated with horseradish peroxidase (HRP) were detected by an enhanced chemiluminescent lighting kit (ECL, GE

Healthcare), and the blots were exposed to X-ray film followed by development. Scanned images were quantitated with NIH image software. Secondary antibodies conjugated with IRDye (LI-COR Biosciences) were detected by an Odyssey scanner, and the images were quantitated with the equipped software.

Results

ATRIP S224 is phosphorylated by Cdk2

To identify post-translational modifications on the ATR-ATRIP complex, the complex was purified from HeLa cells using affinity chromatography with an anti-ATRIP antibody (175). ATR and ATRIP proteins were separated by SDS-PAGE and subjected to mass spectrometry by Jeremy Myers (175). Two phosphorylation sites on ATRIP were identified, S224 and S239. ATRIP S224 surrounding peptides contain a Cdk2 consensus site S/TPXR/K (274). This peptide is highly conserved across many species (Figure 3.1A). It suggests that ATRIP is a potential Cdk2 substrate. Detected with a phosphopeptide-specific antibody, phosphorylation of ATRIP on S224 occurs in cells, peaks in S phase, and correlates with Cdk2 kinase activity (175). In addition, phosphorylation of ATRIP on S224 is sensitive to Roscovitine, a Cdk2 inhibitor, but not to any other kinase inhibitor tested (Figure 3.1B).

To confirm that ATRIP S224 is a substrate of Cdk2, an *in vitro* kinase assay was performed with the purified Cdk2-cyclin A complex (Figure 3.1C). The ATRIP S224A mutant exhibits no phosphorylation while phosphorylation of wild type ATRIP is indicated by ^{32}P-ATP incorporation (Figure 3.1C, compare lanes 2 and 4). However, the ATRIP S239A mutant is phosphorylated to a comparable level to the wild type ATRIP.

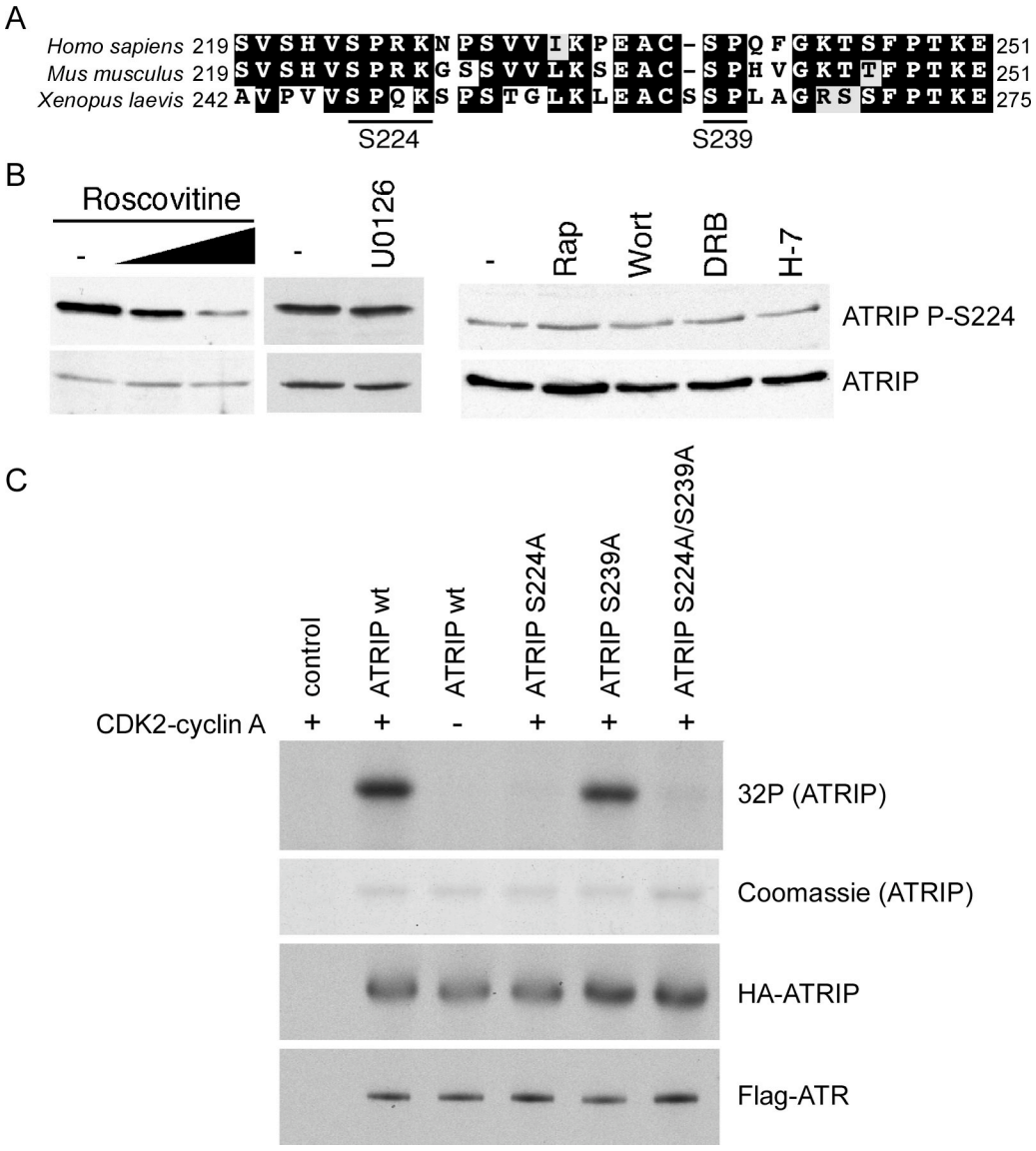

Figure 3.1. ATRIP S224 is a Cdk2 substrate. (A) Sequence alignment of the ATRIP region containing S224 and S239. (B) HeLa cells were treated with the following inhibitors for 14 h: roscovitine (25 and 50 μmol/L), U0126 (25 μmol/L), 10 nmol/L rapamycin (Rap), 20 μmol/L wortmannin (Wort), 10 μmol/L 5,6-dichlorobenzimidazole riboside (DRB), 10 μmol/L H-7 dihydrochloride (H-7). Cell lysates were separated by SDS-PAGE and immunoblotted with ATRIP P-S224 or ATRIP antibodies. (C) Wild type or mutant HA-ATRIP-Flag-ATR complexes were purified from transiently transfected HEK293T cells with HA-agarose beads. Kinase reactions were done with recombinant Cdk2-cyclin A. This experiment of panel B was done by Dr. Jeremy Myers.

This suggests that the S224 site is the major substrate of Cdk2-cyclinA while ATRIP S239 is phosphorylated in cells (175, 176). In addition, mutation of S224 and S239 to alanine does not alter ATRIP interaction with ATR (Figure 3.1C). Taken together, ATRIP S224 is phosphorylated by Cdk2 *in vitro* and *in vivo*.

The phosphorylation of ATRIP S224 is required for G2-M checkpoint maintenance

To examine the functional significance of ATRIP S224 phosphorylation, we established stable cell lines expressing either HA-ATRIP or the HA-ATRIP S224A mutant by retrovirus infection. Both cell lines express equal ATRIP as determined by western blot. The percentage of cells expressing ATRIP was determined to be equal by immunofluorescence. ATRIP forms DNA damage inducible foci (163). The ATRIP S224A mutant has the same ability to form foci in response to IR (data not shown). The ATRIP cDNA contains wobble base pair mutations. This property makes them insensitive to RNAi mediated depletion when using a specific ATRIP siRNA. Transfection of ATRIP siRNA decreases endogenous ATRIP expression at least 90% without affecting the expression of exogenous HA-ATRIP (Figure 3.2A).

When cells are irradiated with UV or IR, ATR is activated. ATR activation promotes cell cycle arrest at G2 before entering mitosis through inhibition of Cdk1 activity (133). ATRIP is required for maintaining the ATR-dependent G2-M checkpoint after DNA damage. All three cell lines expressing no cDNA, HA-ATRIP, or HA-ATRIP S224A exhibit indistinguishable growth curves, cell cycle profiles, and mitotic indices (about 1.7%; 45% after 12 hours incubation in the presence of nocodazole). Among the cells expressing wild type ATRIP, about 2.5% of cells enter mitosis after UV treatment in

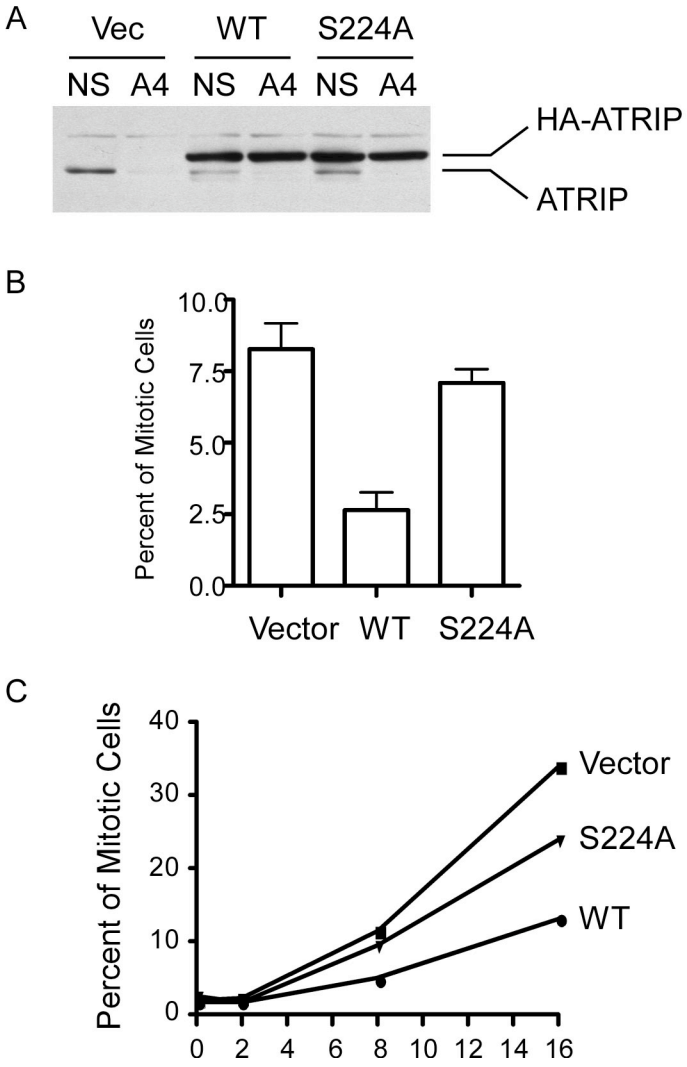

Figure 3.2. ATRIP S224 is required for ATR-ATRIP-dependent G2-M checkpoint responses to DNA damage. (A) U2OS cells expressing siRNA-resistant cDNA for HA-ATRIP (WT), HA-ATRIP S224A, or no cDNA (Vec) were transfected with non-specific (NS) or ATRIP (A4) siRNA. Cells were harvested 3 days after transfection and analyzed for ATRIP expression by immunoblotting. (B and C) 3 days after transfection with ATRIP siRNA, U2OS cells containing ATRIP (WT), ATRIP S224A, or vector were treated with 25 J /m^2 UV radiation (B) or 4 Gy of IR (C). Nocodazole was added to the culture media to trap cells in mitosis. In (B), cells were harvested and fixed with Carnoy's fixative, and mitotic spreads were analyzed 8 hours after exposure to UV. The percentage of mitotic cells was calculated based on counting at least 600 cells. *Bars*, SE. In (C), cells were harvested at the indicated time points following IR, fixed with ethanol, permeabilized, and stained with anti-phospho-histone H3 S10 antibody and propidium iodide. The percentage of mitotic cells was determined by flow cytometry. Runxiang Zhao contributed significant efforts in this figure.

8 hours (Figure 3.2B). However, among the cells without ATRIP, 8% of cells enter mitosis after UV treatment. In the cells expressing the ATRIP S224A mutant, about 7% of cells enter mitosis after UV treatment. This suggests that a G2-M checkpoint defect occurred in the ATRIP mutant cell line. The level of this defect is nearly the same as the ATRIP deficiency. In addition, the mutant cell line exhibits a G2-M checkpoint defect after IR treatment. In the early time point (2 hours after IR), there is no significant difference among the 3 cell lines. However, at the time point of 8 hours and 16 hours, there are more cells expressing the ATRIP mutant entered mitosis compared to the cells expressing wild type ATRIP (Figure 3.2C). It suggests a G2-M checkpoint maintenance defect with the ATRIP S224A mutant.

CINP is an ATRIP interacting protein

ATRIP is associated with ATR constitutively (163). We also tried another approach to study the mechanism of ATR activation regulated by ATRIP by identifying ATRIP interacting proteins. A yeast-two hybrid screen was performed by Gloria Glick with full length ATRIP as the bait and a B cell cDNA library was screened. ATRIP interacts with ATRIP in the yeast two hybrid screen. It suggests that ATRIP forms oligomers. This is consistent with our previous report (168).

CINP (gene accession number: NM_032630) was identified as a novel ATRIP interacting protein in yeast two hybrid screen. To validate the ATRIP interaction with CINP, co-immunoprecipitation was performed. After transient transfection of HEK293T cells with Flag-ATR and HA-CINP or Flag-ATRIP and HA-CINP, total cell lysates were used for immunoprecipitation with anti-Flag beads. HA-CINP can be co-precipitated with

Flag-ATR and Flag-ATRIP (Figure 3.3A, top and middle panels). Reciprocally, ATR and ATRIP can be co-precipitated with CINP as well (Figure 3.3A, bottom panel). The data here confirmed that ectopically expressed CINP can interact with the ATR-ATRIP complex. Furthermore, the interaction between CINP and ATR-ATRIP is not altered after cells are treated with DNA damage agents or replication inhibitors (Figure 3.3B).

In addition to detecting the exogenous level of protein interaction, Courtney Lovejoy and Gloria Glick performed co-immunoprecipitation with an anti-CINP antibody for endogenous CINP. Both ATR and ATRIP are co-precipitated with CINP (Figure 3.3C and 3.3D). These data verified that CINP interacts with ATRIP-ATR complex in a physiological condition.

CINP interacts with ATRIP coiled-coil domain

To map the specific regions of ATRIP involved in its interaction with CINP, we performed a yeast two-hybrid screen as described (168). We fused full length CINP to the GAL4 DNA binding domain to screen a library containing random ATRIP fragments fused to the GAL4 activation domain. The interaction positive fragments were recovered and sequenced. The protein sequences encoded by recovered ATRIP fragments are aligned (Figure 3.4A). Among these ATRIP fragments, the common region contains amino acids 118 to 156 of ATRIP, which is also the N-terminal half of the predicted ATRIP coiled-coil domain (Figure 3.4A).

I validated the yeast two hybrid results by co-immunoprecipitation. HA tagged ATRIP or the ATRIP fragments were co-expressed with Flag-CINP in HEK293T cells. Immunoprecipitation was performed with anti-Flag agarose beads. The ATRIP fragment

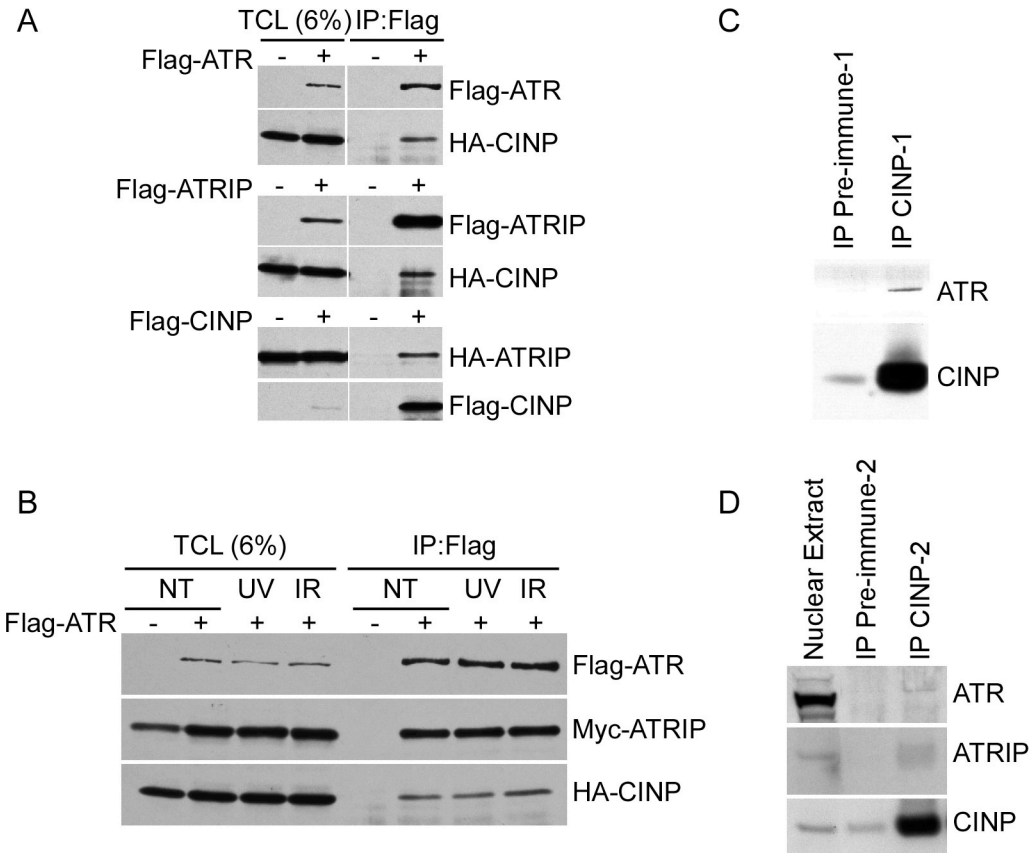

Figure 3.3. CINP interacts with ATRIP-ATR complex. (A) HA-CINP and Flag-ATR (top panel), or HA-CINP and Flag-ATRIP (middle panel), or Flag-CINP and HA-ATRIP (bottom panel) were co-expressed in HEK293T cells as indicated. Immunoprecipitation was performed with anti-Flag beads. Input (TCL) and precipitated proteins were detected by immunoblotting with anti-Flag and anti-HA antibodies. (B) Flag-ATR, Myc-ATRIP and HA-CINP were co-expressed in HEK293T cells. Cells were mock treated (NT), treated with UV 50 J/m^2 followed by 2 hours incubation, or IR 5 Gy followed by 1 hour incubation before harvesting. IP was performed with anti-Flag beads. Input (TCL) and precipitated proteins were detected by immunoblotting with anti-Flag, anti-Myc, and anti-HA antibodies. (C) Endogenous CINP was immnuoprecipitated with anti-CINP antibody from HeLa cell total cell lysate. Precipitated proteins were detected with anti-ATR and anti-CINP antibodies. (D) Endogenous ATRIP was immunoprecipitated from HEK293T cell nuclear extracts. Precipitated proteins were detected with anti-CINP, anti-ATR, and anti-ATRIP antibodies. The experiments for panels C and D were performed by Courtney Lovejoy and Gloria Glick.

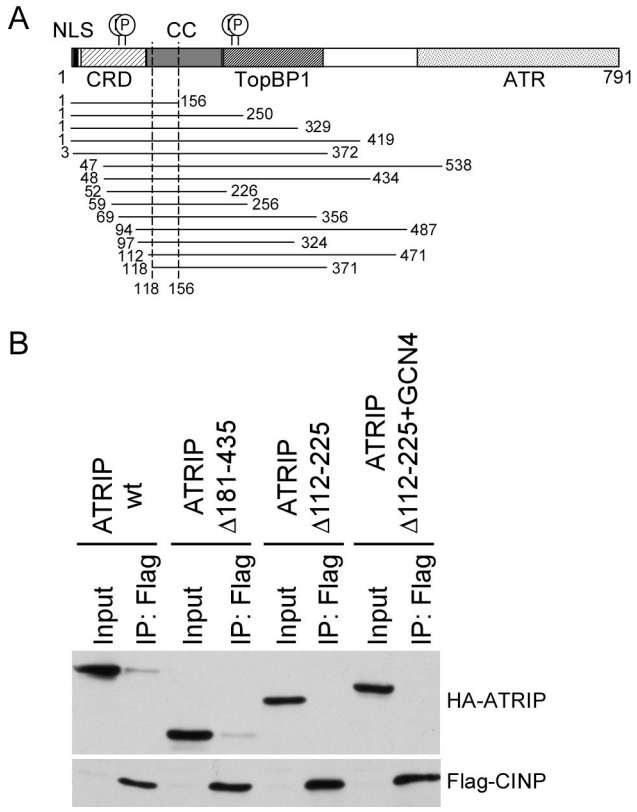

Figure 3.4. CINP interacts with the coiled-coil domain of ATRIP. (A) A schematic diagram of ATRIP indicating the known functional domains including the nuclear localization signal (NLS), checkpoint recruitment domain (CRD), coiled-coil domain (CC), TopBP1-binding domain (TopBP1), ATR-binding domain (ATR), and phosphorylation sites. ATRIP fragments found to interact with full-length CINP in a yeast two-hybrid screen were aligned with their starting and ending sites. (B) Flag-CINP was co-expressed with HA-ATRIP or HA-ATRIP mutants including 181-435 residues deletion, 112-225 residues deletion, and the coiled-coil domain (112-225) replaced with GCN4 coiled-coil domain in HEK293T cells. Immunoprecipitation was performed with anti-Flag beads. The precipitated proteins were detected by immunoblotting with anti-HA and anti-Flag antibodies. This experiment was performed by Dr. David Cortez.

lacking residues 181-435 co-precipitated with CINP efficiently as wild type ATRIP (Figure 3.4B). However, the ATRIP fragment lacking the coiled-coil domain (lacking residues 112-225) can not be detected in the Flag-CINP precipitates (Figure 3.4B). Although the ATRIP mutant with a GCN4 coiled-coil domain substitution has been shown able to oligomerize (168), this mutant was not detected in the CINP precipitates (Figure 3.4B).

CINP regulates ATR signaling

ATR functions in checkpoint maintenance in part through activating Chk1 (97, 219). Chk1 phosphorylation on S345 and S317 by ATR after DNA damage is required for Chk1 function in arresting the cell cycle (97, 219-221). ATRIP is required for ATR-dependent Chk1 phosphorylation and G2-M checkpoint maintenance (163). Therefore, I examined whether CINP functions in regulating Chk1 phosphorylation. CINP was depleted in cells by siRNA transfection. Chk1 phosphorylation was determined by immunoblotting with anti-phosphopeptide antibodies to Chk1, p-Chk1 S345 and p-Chk1 S317. After DNA damage treatments including UV and IR, the CINP depleted cells exhibit decreased Chk1 phosphorylation on S345 and S317 compared to the cells transfected with non-targeting siRNA (Figure 3.5A). Phosphorylation of Chk1 on S317 was reduced 30% and 50% in CINP depleted cells compared to non-specific siRNA transfected cells upon UV and IR treatment respectively (Figure 3.5A). ATR activation occurs in S after DNA damage or replication stress during the cell cycle. At the time point I assayed for Chk1 phosphorylation, the CINP depleted cells show indistinguishable cell cycle profile as non-specific siRNA transfected cells (data not shown).

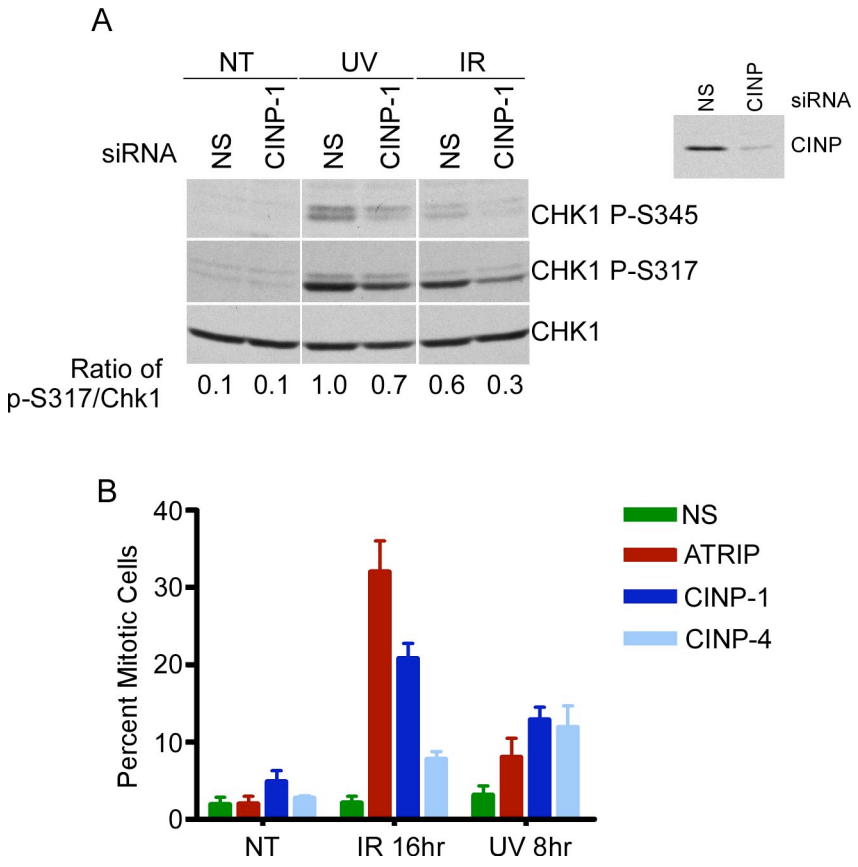

Figure 3.5. CINP functions in ATR signaling. (A) hTERT-RPE cells were transfected with non-specific siRNA (NS) or siRNA targeting CINP (CINP-1). 3 days after transfection, cells were untreated (NT), treated UV 50 J/m^2 followed by 2 hours incubation, or treated with IR 5 Gy followed by 1 hour incubation. Phosphorylation of Chk1 on S345 and S317 were examined (top panel). The ratio of phosphorylated Chk1 S317 to Chk1 were quantitated with NIH image and normalized to non-specific siRNA transfected cells with UV treatment. (B) U2OS cells were transfected with non-specific siRNA (NS), siRNA targeting CINP (CINP-1 and CINP-4), or siRNA targeting ATRIP. 3 days after transfection, cells were untreated (NT), treated with UV 25 J/m^2 followed by 8 hours incubation in the presence of 1 μg/ml Nocodazole, or treated with IR 4 Gy followed by 8 hours incubation in the presence of 1 μg/ml Nocodazole. Cells were harvested and fixed with Carnoy's fixative, and mitotic spreads were analyzed. The percentage of mitotic cells was calculated based on counting 300 cells. *Bars*, SE.

Furthermore, I examined whether CINP is required for ATR-dependent G2-M checkpoint maintenance. Cells were damaged with UV or IR and then incubated in the presence of nocodazole to trap cells in mitosis. The percentage of mitotic cells was determined. In cells with ATRIP depletion, more cells entered mitosis after DNA damage treatment than cells transfected with non-specific siRNA (Figure 3.5B). This indicates that the maintenance of the G2-M checkpoint is compromised when ATRIP is depleted. A comparable percentage of cells entered mitosis after DNA damage treatment in CINP depleted cells and ATRIP depleted cells. Thus, CINP functions in ATR signaling and maintaining the G2-M checkpoint.

CINP regulates ATRIP S224 phosphorylation

CINP was identified as a Cdk2 interacting protein (275). ATRIP S224 is phosphorylated by Cdk2. Both depletion of CINP or mutation of ATRIP S224 to alanine compromise ATR-dependent G2-M checkpoint maintenance. Therefore, I hypothesized that CINP functions in regulation of ATR signaling through regulating the phosphorylation of ATRIP S224. I examined phosphorylation of ATRIP S224 when CINP is depleted from cells (Figure 3.6A). ATRIP S224 phosphorylation is barely detected in RPE cells when they are arrested in G0 (Figure 3.6A). This is consistent with our previous report (175). Cells were released into S phase, and phosporylation of ATRIP S224 was elevated (Figure 3.6A). The level of phosphorylation on ATRIP S224 was decreased 51% and 58% in cells where CINP was depleted by transfection with two different siRNA oligos targeting CINP (Figure 3.6A). However, depletion of CINP leads to indistinguishable cell cycle profiles (Figure 3.6B).

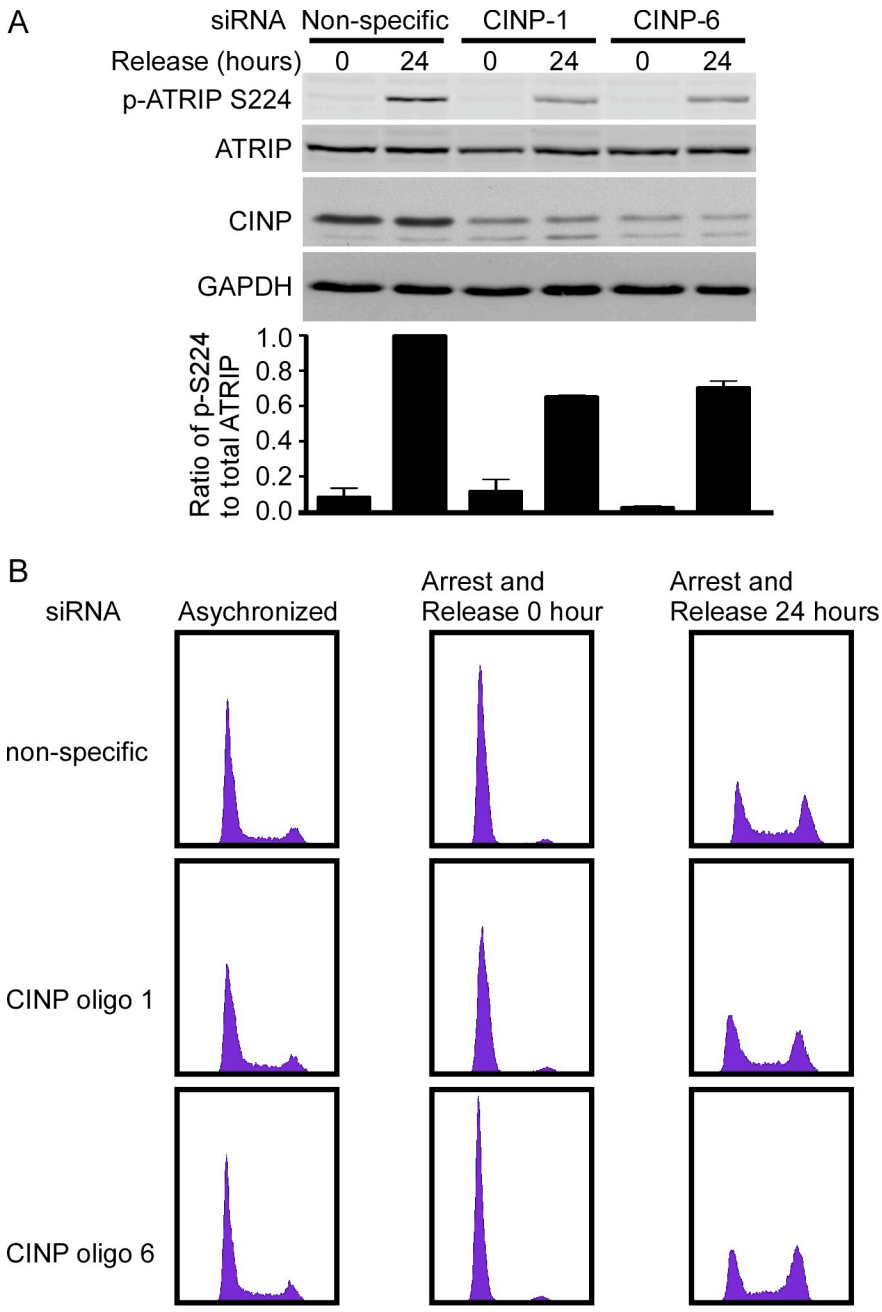

Figure 3.6. CINP regulates phosphorylation of ATRIP S224. hTERT-RPE cells stably expressing HA-ATRIP were established by retrovirus infection. Cells were transfected with non-specific siRNA or CINP siRNA (CINP-1 and CINP-6) followed by plating cells at high density to arrest in G0 for 24 hours. 3 days after siRNA transfection, cells were released by splitting to allow cells back to cell cycle for 24 hours. (A) ATRIP S224 phosphorylation and total ATRIP were examined (top panel) and quantitated by Odyssey system. The ratio of phosphorylated ATRIP S224 to total ATRIP were calculated and normalized to the released non-specific siRNA transfected cells (bottom panel). Error Bars stand for standard error. (B) cells in parallel with cells in (A) were fixed and analyzed for DNA content by flow-cytometry after PI staining.

Depletion of CINP induces DNA damage

While I characterized the function of CINP, a screen for loss of gene function inducing DNA damage responses was conducted by Courtney Lovejoy. The readout is phosphorylation of KAP-1 (KRAB domain association protein 1) on S824. KAP-1 S824 is a substrate of ATM, and phosphorylation of KAP-1 can be detected as a pan-nuclear staining by immunofluorescence when DNA double strand breaks occur (276, 277). Courtney Lovejoy found that depletion of CINP causes phosphorylation of KAP-1 in by immunofluorescence in the screen (data not shown). Histone proteins H2AX are phosphorylated and form foci when DNA damage occurs in cells (278, 279). CINP depletion also leads to γH2AX foci formation, which also suggests that DNA damage response is activated in CINP depleted cells (Figure 3.7A).

We further examined the DNA damage response induced by CINP depletion with other markers by immunoblotting. P53 is phosphorylated upon induction of DNA damage by PI-3 kinases including DNA-PK, ATM, and ATR (98, 99, 101, 102). While depletion of CINP does not cause detectable Chk1 or Chk2 phosphorylation (data not shown), depletion of CINP leads to a mild level of p53 phosphorylation compared to the level of p53 phosphorylation induced by DNA damage (Figure 3.7B). Thus, consistent with the result that depletion of CINP leads to phosphorylation of KAP-1 and γH2AX foci formation, CINP is required to maintain the genome integrity.

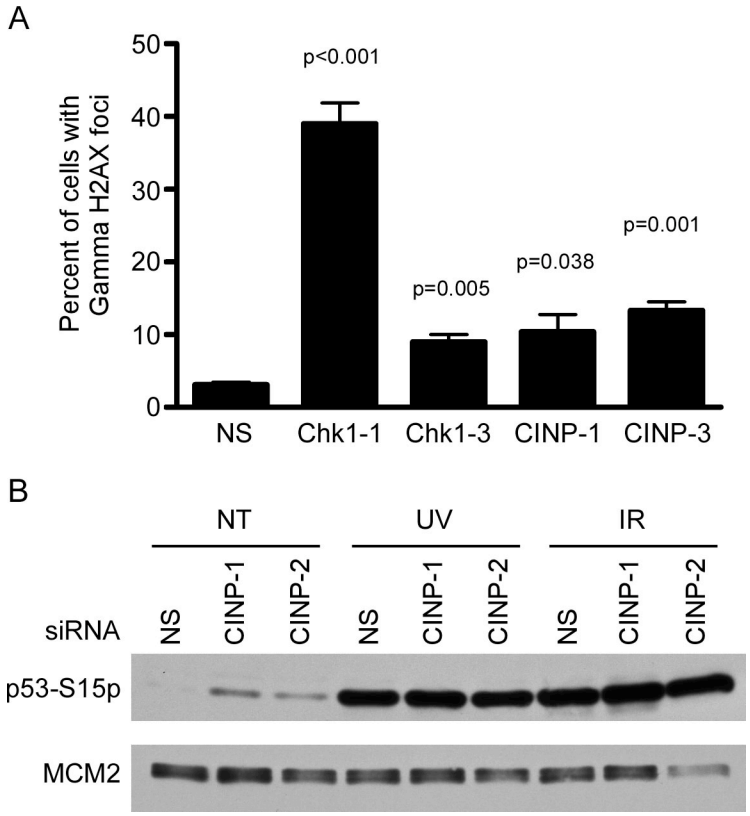

Figure 3.7. Depletion of CINP causes DNA damage response in cells. (A) U2OS cells were transfected with non-specific siRNA (NS), siRNA targeting Chk1 (Chk1-1 and Chk1-2), or siRNA targeting CINP (CINP-1 and CINP-3). 2 days after transfection, cells were cultured on cover slip for 24 hours. Cells on cover slip were analyzed by immunofluorescence microscopy with anti-phospho-H2AX antibody. γ-H2AX foci were counted for 100 cells and repeated for 3 times each sample. *Bars*, SE. Numbers on top of the bars are p values calculated with unpaired, two-tailed *t* test with the sample of NS. (B) hTERT-RPE cells were transfected with non-specific siRNA (NS) or siRNA targeting CINP (CINP-1 and CINP-3). 42 hours after transfection, cells were untreated (NT), treated UV 50 J/m^2 followed by 2 hours incubation, or treated with IR 5 Gy followed by 1 hour incubation. Phosphorylation of p53 on S15 was examined by immunoblotting. MCM2 levels were determined and served as loading control. The experiment of panel A was performed by Courtney Lovejoy.

Discussion

ATRIP interacts with ATR constitutively (163). The ATR-ATRIP complex is required for ATR function in many aspects including the localization of ATR to sites of DNA damage and enhancement of ATR kinase activity (137, 160). Here we reported that ATRIP regulates ATR function by additional mechanisms. First, phosphorylation of ATRIP on S224 is required for ATR-dependent G2-M checkpoint maintenance (Figure 3.2). Second, ATRIP interacting protein, CINP regulates ATR signaling and its function in G2-M checkpoint maintenance (Figure 3.5). Furthermore, CINP also regulates phosphorylation of ATRIP on S224 (Figure 3.6).

Phosphorylation is a common mechanism by which PIKKs regulate the DNA damage response in cells. We have identified two phosphorylation sites on ATRIP, S224 and S239. ATRIP S224 phosphorylation is not induced upon DNA damage or replication stress (175). Instead, it correlates with cyclin A level during the cell cycle. It suggests this phosphorylation is not a rapid regulation to turn on or off the ATR signaling pathway. The ATRIP S224 phosphorylation may be important to potentiate specific ATR activities.

We also found ATRIP S239 is phosphorylated in the mass spectrometry study. Consistent with our result, phosphorylation of ATRIP S239 was identified with anti-phospho-peptide antibodies and is required for G2-M checkpoint maintenance after DNA damage (176). Moreover, it is reported that phosphorylation of ATRIP S239 is required for interaction with the BRCT (BRCA1 COOH-terminal) repeats of BRCA1 (176). BRCA1 also functions in G2-M checkpoint maintenance (280). This suggests that phosphorylation of ATRIP S239 contributes to the G2-M checkpoint maintenance through interaction with BRCA1 (176). The ATRIP S224A mutant and the S239A

mutant form foci efficiently after DNA damage (175, 176). Consistent with this, these mutants have normal ATRIP functions in oligomerization, interaction with ATR, and supporting ATR kinase activity stimulated by TopBP1 *in vitro* (data not shown). It is possible that both ATRIP phosphorylation on S224 and S239 serve as protein interaction binding sites to facilitate the G2-M checkpoint maintenance. BRCTs domains of BRCA1 tend to bind phospho-peptides (281, 282). It is possible that both phosphorylation on S224 and S239 contribute to ATRIP interaction with other proteins including BRCA1. This could be the mechanism by which ATRIP S224 phosphorylation regulates ATR-dependent checkpoints.

While ATRIP S224 is the major substrate of the Cdk2-cyclin A complex in the *in vitro* kinase assay (Figure 3.1), ATRIP S239 could be a Cdk2 substrate *in vivo*. Plus Cdk2 can function as a kinase with either cyclin E or cyclin A. ATRIP S239 phosphorylation occurs in a later time point when cell cycle is arrested after DNA damage (176). Whether ATRIP S239 phosphorylation is sensitive to Cdk2 inhibitor is undetermined.

CINP is a novel ATRIP interacting protein identified by yeast-two hybrid screen. This interaction was confirmed by co-immunoprecipitation with endogenous and exogenous proteins (Figure 3.3). However, the interaction between CINP and ATRIP is much less efficient with endogenous levels of protein than the interaction with ectopically expressed level of proteins (compare Figure 3.3A and 3.3C). There are several possibilities. One, endogenous CINP abundance is very low in cells. Two, a better anti-CINP antibody is required to perform the co-immunoprecipitation. Three, the interaction between CINP and ATRIP is very dynamic. We were unsuccessful to detect CINP

localization by immunofluorescence with current antibodies. Therefore, we were not able to detect CINP co-localization with ATRIP by immunofluorescence.

CINP interacts with the ATRIP coiled-coil domain (Figure 3.4). It is unclear which region on CINP is involved in the interaction with ATRIP. The CINP protein sequence predicts a coiled-coil domain in the N-terminal region containing residues 25-125 by the coiled-coil domain prediction program. Coiled-coil domains are often involved in protein oligomerization (283). It is likely that ATRIP interacts with CINP through their coiled-coil domains. The ATRIP mutant forms oligomers but fails to facilitate Chk1 phosphorylation after DNA damage when the coiled-coil domain is replaced with the GCN4 coiled-coil domain (168). This ATRIP mutant interaction with CINP is compromised (Figure 3.8). This suggests that the CINP interaction with ATRIP is distinct from ATRIP oligomerization. Defected binding ability to CINP may in part explain why the ATRIP mutant with GCN4 coiled-coil domain replacement leads to a Chk1 phosphorylation defect.

CINP regulates phosphorylation of ATRIP S224 (Figure 3.6). It is not known whether this regulation is direct. CINP was identified as a Cdk2 interacting protein by a yeast two-hybrid assay (275). Because phosphorylation of ATRIP S224 is regulated by Cdk2-cyclin A directly, CINP may function as a bridge between Cdk2 and ATRIP (Figure 3.9). This can be tested by examining ATRIP interaction with Cdk2 in the absence and presence of CINP. Also it is possible that CINP plays a role to protect the phosphorylation of ATRIP S224 from phosphatases. In this case, the phosphatase remains to be identified.

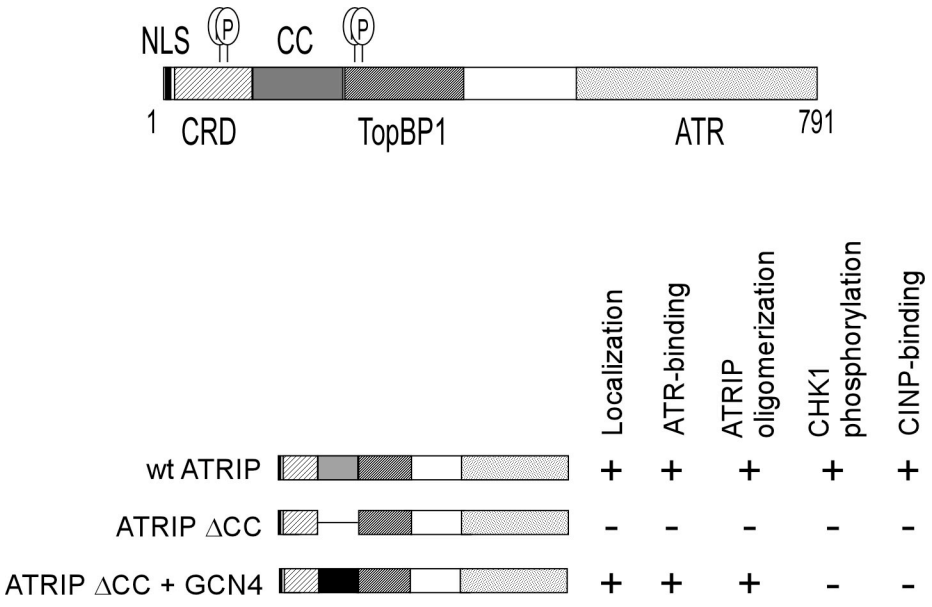

Figure 3.8. Summary of ATRIP functional domains. Top panel, full length ATRIP highlighted with nuclear localization signal (NLS), checkpoint recruit domain (CRD), phosphorylation sites (p, on S68, S72, S224, and S239), coiled-coil domain (CC), TopBP1 binding domain (TopBP1), and ATR binding domain (ATR). Bottom panel, summary of loss of function in ATRIP mutants including the coiled-coil domain deletion mutant and the coiled-coil domain replaced with GCN4 coiled-coil domain mutant [this study and reference (168)]. Localization means ATRIP foci formation after DNA damage.

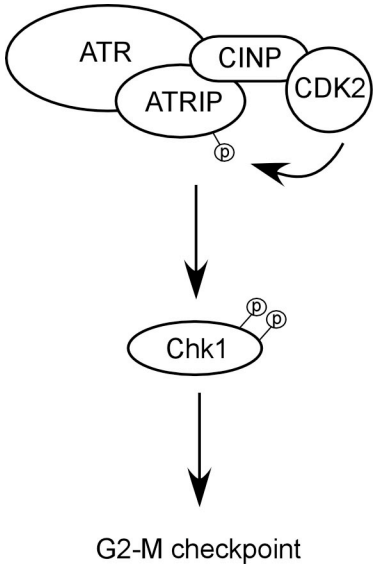

Figure 3.9. The current testing model of CINP dependent ATR-Chk1 signaling pathway. We hypothesize that CINP functions as a bridge between ATR-ATRIP complex and Cdk2. The ATRIP S224 is required for Chk1 phosphorylation and G2-M checkpoint maintenance after DNA damage.

Cyclin-dependent kinases are major targets of the ATR/ATM-dependent checkpoint response to DNA damage. Inhibition of Cdk activities promote cell cycle arrest and therefore provide time for cells to repair the damaged DNA. Meanwhile, more and more evidence suggests that the cell cycle and Cdk activity also regulate many aspects of cellular response to DNA damage (284, 285). First, ATR is activated primarily in S-phase. A long stretch of single-stranded DNA coated by RPA is the main upstream signal for ATR activation. This RPA-ssDNA structure can be generated during DNA lesion processing (233-236, 284, 286, 287) or the uncoupling of DNA helicase and polymerase activities at DNA replication forks (139, 266). Cdk2 activity is required for both situations. Second, ATR activation after double strand breaks requires the ends to be resected into single stranded DNA. This process depends on Cdk activity (233, 236, 286). Third, inhibition of Cdk2 activity leads to reduced Chk1 expression, and Chk1 is a substrate of ATR (287). Here we found that ATRIP S224 phosphorylation is Cdk2 dependent, and this phosphorylation is required for G2-M checkpoint maintenance after DNA damage (175). Thus, Cdk2 regulates checkpoint signaling and also is inhibited by cell cycle checkpoints.

CINP was identified as a Cdk2 interacting protein by a yeast two-hybrid assay. Moreover, CINP is phosphorylated by the Cdc7-Dbf4 complex but not the Cdk2-cyclin E complex *in vitro* (275). CINP is an *in vitro* substrate of Cdk2-cyclin A (data not shown). The CINP peptide TLGTV(p)TPR was detected to be phosphorylated in a mass spectrometry analysis (288). The responsible kinase for CINP in cells needs to be determined. The CINP T10 surrounding residues (TPRK) indicate a Cdk consensus site (274). Moreover, CINP contains the specific cyclin-binding motif (Cy motif) RXL (RAL,

210-212) (289). This is a property for proteins to interact with cyclins, which also suggests that CINP is a substrate candidate of Cdk2. While no CINP orthologue in yeast has been discovered, the TPRK peptide is conserved in mice, rats, and xenopus. Further experiments are required to confirm CINP phosphorylation and characterize its function.

I show here that CINP is required for ATR signaling after DNA damage. The checkpoint maintenance defect in cells where CINP is depleted is comparable to cells where ATRIP is depleted (Figure 3.5). In contrast, CINP depletion only reduces ATRIP phosphorylation on S224 about 45%. Thus, in addition to ATRIP S224 phosphorylation, other mechanisms by which CINP regulates G2-M checkpoint maintenance remain unclear. The CINP mutant lacking ATRIP interaction domain will suggest whether the regulation of checkpoint maintenance by CINP is ATRIP-dependent. We are in the process to identify proteins interacting with CINP. The results will lead us a direction to study how the checkpoint maintenance is regulated by CINP.

CINP has additional functions other than G2-M checkpoint maintenance. Depletion of CINP causes a DNA damage response but not as severe as depletion of Chk1 (Figure 3.7A). In the loss of function screen, Courtney Lovejoy also found that depletion of CINP affects cell proliferation and sensitizes cells to hydroxyurea (HU, a replication inhibitor by depletion of the dNTP pool). It suggests that CINP may function in regulation of DNA replication. ATR and ATM function in regulation of DNA replication by controlling DNA replication origin firing (138). CINP interaction with ATRIP may also contribute to the regulation of origin firing. Consistent with this, CINP is speculated to play a role in DNA replication based on reported interactions with Cdk2, CDC7, ORC and MCM complexes (275).

In summary, we characterized additional mechanisms by which ATRIP regulates ATR function. Phosphorylation of ATRIP S224 regulates ATR function in G2-M checkpoint maintenance. We found that CINP is a novel ATRIP interacting protein functioning in G2-M checkpoint maintenance after DNA damage and is required for genome stability. This is the first report for CINP function to my knowledge. Our data suggest that CINP functions in G2-M checkpoint maintenance partially through regulating ATRIP S224 phosphorylation. Thus, CINP functions in the maintenance of checkpoints and genome stability.

CHAPTER IV

THE BASIC CLEFT OF RPA70N BINDS MULTIPLE CHECKPOINT PROTEINS, INCLUDES RAD9, TO REGULATE ATR SIGNALING[2]

Summary

ATR kinase activation requires the recruitment of the ATR-ATRIP and RAD9-HUS1-RAD1 (9-1-1) checkpoint complexes to sites of DNA damage or replication stress. Replication Protein A (RPA) bound to single-stranded DNA is at least part of the molecular recognition element that recruits these checkpoint complexes. We have found that the basic cleft of the RPA70 N-terminal oligonucleotide-oligosaccharide fold (OB-fold) domain is a key determinant of checkpoint activation. This protein-protein interaction surface is able to bind several checkpoint proteins, including ATRIP, RAD9, and MRE11. RAD9 binding to RPA is mediated by an acidic peptide within the C-terminal RAD9 tail that has sequence similarity to the primary RPA-binding surface in the checkpoint recruitment domain (CRD) of ATRIP. Mutation of the RAD9 CRD impairs its localization to sites of DNA damage or replication stress without perturbing its ability to form the 9-1-1 complex or bind the ATR activator TopBP1. Disruption of the RAD9-RPA interaction also impairs ATR signaling to CHK1 and causes hypersensitivity to both DNA damage and replication stress. Thus, the basic cleft of the RPA70 N-terminal OB-fold domain binds multiple checkpoint proteins, including RAD9, to promote ATR signaling.

[2] This chapter has been previously published in ref 290. Xu, X., et al. (2008) The basic cleft of RPA70N binds multiple checkpoint proteins, including RAD9, to regulate ATR signaling. *Mol Cell Biol*, **28**, 7345-53.

Introduction

The DNA damage response (DDR) coordinates cell cycle transitions, DNA replication, DNA repair and apoptosis. The major regulators of the DDR are the phosphoinositide-3-kinase-related protein kinases ATM (ataxia-telangiectasia mutated) and ATR (ATM and Rad3 related). ATR is activated during every S-phase to regulate the firing of replication origins, the repair of damaged replication forks and to prevent the premature onset of mitosis (133).

ATR is activated in response to many types of DNA lesions including double strand breaks (DSB), base adducts, cross-links, as well as replication stress. In most cases these lesions activate ATR as a consequence of tracts of single-stranded DNA (ss-DNA) that are formed during lesion processing (233-236) or uncoupling of helicase and polymerase activities at replication forks that encounter the lesion (139). Most forms of ss-DNA in the cell, including the ss-DNA formed during DNA replication and DNA repair, are rapidly coated by replication protein A (RPA) (36). Depletion of RPA from *Xenopus* egg extracts reduces the association of ATR with chromatin (136), and RPA-coated ss-DNA (hereafter RPA-ssDNA) is important to localize ATR to sites of DNA damage in both human and budding yeast systems (137).

Although RPA-coated ssDNA may be sufficient for localizing the ATR-ATRIP complex, it is not sufficient for ATR activation (140, 291, 292). ATR signaling is dependent on co-localization of the ATR-ATRIP complex with the 9-1-1 complex, a hetero-trimeric ring-shaped molecule related in structure and sequence to the replicative sliding clamp, PCNA (244).

Like PCNA, the 9-1-1 complex is loaded onto primer-template junctions in an ATP-dependent reaction that involves the RAD17 damage-specific clamp loader (161, 190, 196). Loading of the 9-1-1 complex occurs at a DNA end that is adjacent to a stretch of RPA-coated ssDNA. The presence of RPA is critical for this reaction and imparts specificity in loading, creating a preference for a 5'- rather than a 3'-primer end (159, 161). The 9-1-1 complex concentrates an ATR-activator, TopBP1, at sites of DNA damage or replication stress. TopBP1 stimulates ATR kinase activity (217) by interacting with both a PIKK regulatory domain in ATR and the ATR-interacting protein ATRIP (163, 218).

ATR recognition of RPA-coated ssDNA depends upon ATRIP (137). Biochemical studies indicate that ATRIP binds RPA directly via evolutionarily conserved binding surfaces (151). The primary interaction involves an acidic alpha helix within a checkpoint recruitment domain (CRD) of ATRIP that binds in the basic cleft of the N-terminal OB-fold domain of the large RPA subunit, (RPA70N) (151). Deleting or mutating the ATRIP CRD abolishes its interaction with RPA70 and prevents ATR-ATRIP complexes from being efficiently retained at sites of DNA damage or stalled replication forks (160). Remarkably, mutations within the ATRIP CRD or even deletion of the entire CRD do not cause a large ATR-checkpoint signaling defect in human, *Xenopus* or budding yeast systems (151, 160, 293). This result is surprising given that the current model of ATR activation postulates that the ATRIP-RPA interaction should be essential for ATR signaling.

In this report, we further investigated the role of RPA in checkpoint signaling. First, the consequences of mutating the ATRIP binding surface on RPA70N were

analyzed. As expected, these mutations impair ATRIP binding. However, in contrast to the ATRIP CRD mutations, the RPA binding surface mutations cause a significant defect in ATR-dependent signaling to CHK1. To reconcile these data, we hypothesized that additional ATR regulatory proteins may bind to RPA using the same binding surface. We found that at least three checkpoint proteins bind to RPA using the same binding cleft within the RPA70N OB-fold domain. Notably, the C-terminal tail of RAD9 binds in the cleft. We show this interaction is important for RAD9 recruitment to sites of DNA damage and stalled replication forks, and is important for ATR signaling. Thus, RPA-ssDNA is a common signal within the DNA damage response to regulate multiple checkpoint complexes.

Materials and Methods

NMR analysis

Nuclear magnetic resonance (NMR) experiments were performed at 25 °C using Bruker AVANCE 500 MHz or 600 MHz NMR spectrometers equipped with a 5 mm single axis z-gradient Cryoprobe. Two-dimensional, gradient-enhanced ^{15}N-^{1}H heteronuclear single-quantum coherence (HSQC) spectra were recorded with 1,024 complex points in the ^{1}H dimension and 96 complex points in ^{15}N dimension. ^{1}H and ^{15}N backbone NMR assignments for RPA70N were kindly provided by Cheryl Arrowsmith (Ontario Cancer Institute, Toronto, Canada). ^{15}N-enriched RPA70N NMR samples were prepared in a buffer containing 5 mM DTT, 50 mM NaCl, 20 mM Tris-d_{11}, and 5% D_2O at pH 7.4 at a protein concentration of ~100 μM. ATRIP (DFTADDLEELDTLAD), MRE11 (AFSADDLMSIDLAEQ), and RAD9 (DFANDDIDSYMIAME) peptides were

purchased (Sigma) and purified by HPLC. Peptides were added at a four- to six-fold molar excess to maximize the population of peptide-bound RPA70N molecules. All spectra were processed with TOPSPIN v1.3 (Bruker, Billerica, MA) and analyzed with Sparky v3.1 (University of California, San Francisco, CA).

Cell culture

HEK293T, HeLa, and U2OS cells were cultured in Dulbecco modified Eagle medium (DMEM, Invitrogen) supplemented with 7.5% fetal bovine serum at 37°C in 5% CO_2. *RAD9*$^{+/+}$ and *RAD9*$^{-/-}$ mouse embryonic stem (ES) cells were kindly provided by Dr. Howard Lieberman and cultured as described (185). *RAD9*$^{-/-}$ ES cells were transfected with Lipofectamine2000 (Invitrogen), and stable clones were selected in medium containing G418 (0.2 mg/ml). U2OS cells expressing RAD9 or RAD9-crd were established by retroviral infection and puromycin selection. HeLa cells were transfected with Lipofectamine2000 (Invitrogen) according to the manufacture's instructions.

Nuclear extracts, in vitro translation, chromatin lysate, and cell lysate preparation

Nuclear extracts were prepared as described in Chapter III and reference (218). RAD9 and RAD9-crd proteins were *in vitro* translated with TNT Quick Coupled Transcription/Translation System (Promega). Chromatin lysates were prepared by sonicating nuclei resuspended in immunoprecipitation buffer (0.3% CHAPS {3-[(3-cholamidopropyl)-dimethylammonio]-1-propanesulfonate}, 20 mM HEPES, pH 7.9, and 150 mM NaCl supplemented with protease and phosphatase inhibitors [5 μg/ml aprotinin, 5 μg/ml leupeptin, 1 mM NaF, 20 mM β-glycerol phosphate, 1 mM sodium vanadate, 1

mM DTT, 1 mM PMSF]). Cell lysates were prepared using Igepal lysis buffer (1% Igepal CA-630, 50 mM Tris, pH 8.0, and 200 mM NaCl supplemented with protease and phosphatase inhibitors).

Antibodies

Antibodies were purchased from Covance (HA.11), Oncogene Research Products (RPA70), Cell Signaling Technology (CHK1 P-S345 and CHK1 P-S317), Santa Cruz Biotechnology (CHK1 and RAD1), Bethyl Laboratories (KAP1 P-S824, RAD17, and TopBP1), Chemicon/Millipore (GAPDH), and Abgent (RAD9 P-S272 and RAD9 P-S387).

GST pull down assays

Recombinant GST-tagged RPA70N proteins were purified from *E. coli* with glutathione sepharose 4B beads according to the manufacturers instructions (GE Healthcare). ATRIP1-217 and ATRIP-crd (D58K/D59K)1-217 proteins were also purified with glutathione sepharose 4B beads followed by cleavage with PreScission protease (GE Healthcare). Nuclear extracts were incubated with the GST-tagged proteins bound to beads overnight at 4°C. Beads were washed two times in wash buffer 1 (25 mM Tris, pH 8.0, 25 mM NaCl, 0.1 mM EDTA, 10% Glycerol, and 0.25% Trion x-100 supplemented with protease and phosphatase inhibitors) and once in wash buffer 2 (25 mM Tris, pH 8.0, 50 mM NaCl, 0.1 mM EDTA, 5% Glycerol, and 0.5% Trion X-100 supplemented with protease and phosphatase inhibitors). Proteins were eluted with SDS sample buffer and separated by SDS-PAGE prior to immunoblotting.

DNA constructs and siRNA oligo nucleotides

Site-directed mutagenesis was performed using QuickChange (Stratagene). All constructs generated using PCR were confirmed by sequencing. The siRNA targeting RPA70 (5'-AACACUCUAUCCUCUUUCAUG) was purchased from Dharmacon, Inc.

DNA content analysis

Harvested cells were fixed in ethanol, stained with propidium iodide, and analyzed on a BD Biosciences FACSCalibur.

Immunofluorescence

Cells were cultured on a glass cover slip, fixed with paraformaldehyde, and processed as described (294) except using anti-HA primary antibody and FITC-conjugated goat anti-mouse secondary antibody. Cells were imaged with a Zeiss Axioplan microscope equipped with a Zeiss camera and software.

Immunoprecipitation

Nuclear extracts or chromatin lysates expressing HA-RAD9 or HA-RAD9-crd were incubated with anti-HA agarose beads (Sigma). Immunoprecipitates were washed three times in TGN buffer (50 mM Tris, pH8.0, 150 mM NaCl, 10% glycerol, and 1% Tween 20 supplemented with protease inhibitors).

Cell survival assays

ES cells were plated on gelatinized 6-well dishes and treated with 10 mM hydroxyurea (HU) for 12 hours or UV-irradiated (10 J/m^2). Surviving cells were stained with methylene blue seven days later. Colonies were counted and survival was calculated as the percentage of colonies in the treated compared to untreated dishes.

Results

The RPA70N domain is a checkpoint signaling module

Previous studies did not identify an ATR signaling defect when the primary RPA binding surface within ATRIP is mutated (160). Yet, multiple lines of investigation indicate that RPA is a critical regulator of ATR signaling (133). In an attempt to understand this discrepancy, we mutated the primary ATRIP binding surface within the N-terminal OB-fold domain of RPA70. Based on a computational model of the interacting surfaces (151), we predicted that a double charge reversal mutation (R41E/R43E) within the basic cleft of the OB-fold would abolish the ATRIP interaction. As expected, the RPA70 R41E/R43E mutant no longer binds ATRIP (Figure 4.1A). Biophysical characterization of the RPA70N mutant was performed to verify that the structural integrity and stability of the domain was retained and therefore any observed effect in functional assays is due only to alterations in the binding surface.

To test the functional consequences of this RPA mutation, HeLa cells were co-transfected with siRNA targeting RPA70 and vectors encoding siRNA-resistant wild-type or mutant RPA70 proteins. Silencing RPA70 causes a reduction in the phosphorylation of the ATR-substrate CHK1 in response to ultraviolet (UV) radiation (Figure 4.1B, compare

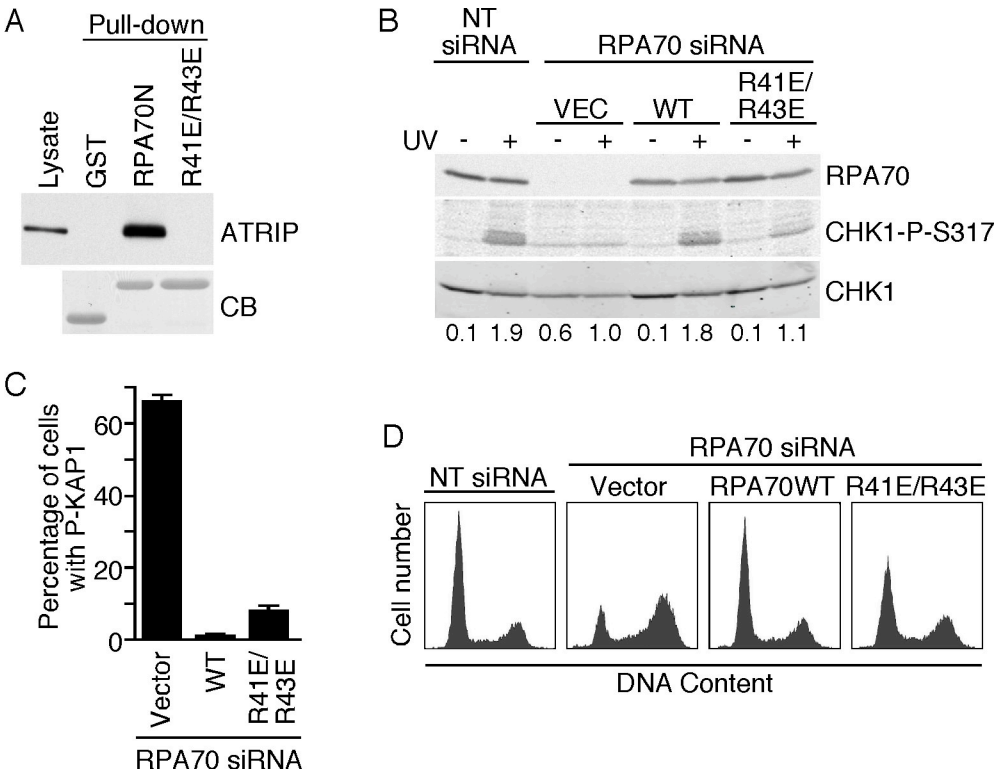

Figure 4.1. The basic cleft of RPA70N is required for ATR-Chk1 activation. (A) Nuclear extracts from HEK293 cells expressing HA-ATRIP were incubated with GST, GST-RPA70N, or GST-RPA70N R41E/R43E proteins bound to glutathione beads. Proteins bound to the beads were eluted, separated by SDS-PAGE and immunoblotted with anti-HA antibody to detect ATRIP or stained with coomassie blue to detect GST proteins (CB). (B-D) HeLa cells were transfected with RPA70 siRNA or non-targeting (NT) siRNA as indicated. In addition, cells were co-transfected with expression vectors encoding siRNA-resistant wild-type RPA70, RPA70 R41E/R43E, or an empty vector control. (B) Transfected cells were left untreated (-) or UV-irradiated (50J/m^2). Two hours after irradiation, cell lysates were separated by SDS-PAGE and immunoblotted with antibodies to RPA70, CHK1-P-S317, and total CHK1 antibodies. Quantitations of phospho-CHK1 and CHK1 were measured by infrared imaging system (Odyssey) and the ratios of phospho-CHK1 to CHK1 were normalized to the sample of cells transfected with empty vector and RPA70 siRNA after DNA damage. (C) The percentage of successfully transfected cells in the population with an activated DNA damage response (in the absence of an added genotoxic agent) was determined by staining with the phospho-peptide specific antibodies to the ATM substrate KAP1. At least 300 cells were scored. Error bars indicate standard error, n=3. (D) Transfected cells were stained with propidium iodide and analyzed by flow cytometry.

lanes 2 and 4) and also causes an increase in CHK1 phosphorylation in untreated cells compared to cells transfected with non-targeting siRNA (compare lanes 1 and 3). This increased CHK1 phosphorylation in untreated cells following RPA70 silencing is presumably due to the stalling and collapse of replication forks, which activate the DNA damage response. Indeed, RPA70 silencing causes activation of ATM (295) and phosphorylation of its substrates, including KAP1 (Figure 4.1C). It also causes the activation of a G2 DNA damage checkpoint and accumulation of cells with 4N DNA content (Figure 4.1D). Co-transfection of a vector encoding wild-type RPA complements all of these phenotypes including the UV-induced CHK1 phosphorylation. Co-transfection of the RPA R41E/R43E mutant also largely complements the spontaneous DNA damage defect, although there is evidence of a continued DNA damage response activation in a small percentage of successfully transfected cells (Figure 4.1C). However, the RPA70 R41E/R43E protein does not complement the defect in UV-induced CHK1 phosphorylation in the endogenous RPA70-silenced cells (Figure 4.1B, compare lanes 4, 6 and 8).

These data combined with previously published results, indicate that mutations in ATRIP or RPA that abolish their primary binding surfaces do not yield identical phenotypes. The mutation in RPA causes a significant defect in CHK1 phosphorylation following UV radiation (Figure 4.1B), whereas the mutation in ATRIP did not (160). A possible explanation for this result is that the RPA mutation may interfere with binding to proteins other than ATRIP that are important for ATR signaling to CHK1. Indeed, this surface of RPA is known to interact with p53 (149), suggesting that it may mediate interactions with multiple proteins. We searched other checkpoint proteins for sequence

similarity to the RPA binding surfaces in ATRIP and p53 and found homologous regions in both MRE11 and RAD9 (Figure 4.2A). To test whether these peptides were capable of binding to RPA, we employed the NMR-based chemical shift perturbation approach applied previously to investigate the interaction with ATRIP (151). A series of ^{15}N-^{1}H-HSQC NMR spectra were acquired for uniformly ^{15}N-labeled RPA70N protein as unlabeled ATRIP, RAD9, and MRE11 peptides were added into the solution. Significant chemical shift perturbations were observed upon the addition of increasing concentrations of all three peptides to RPA70N (Figure 4.2B to 4.2D). The chemical shift perturbations observed for the RAD9 and MRE11 peptides were remarkably similar to those of the ATRIP peptide (Figure 4.2B to 4.2D). Indeed, mapping of the perturbed residues onto the crystal structure of RPA70N reveals that all three peptides bind to the basic cleft of the OB-fold domain in similar manners (Figure 4.2E to 4.2G). The small differences observed between the spectra of the three complexes are consistent with minor differences in the positioning of each peptide within the binding site, which reflect the differences in the sequence of each protein.

The RAD9 C-terminal tail binds to RPA70N

While MRE11 is known to function upstream of ATR at sites of double strand breaks, this does not appear to be the case after UV radiation or replication stress (234). RAD9, in contrast, is critical for ATR activation because of its role in recruiting the ATR activator TopBP1 (203, 206). The NMR data suggested that RAD9 uses a similar checkpoint recruitment domain (CRD) to bind to RPA70N. Therefore, we tested whether

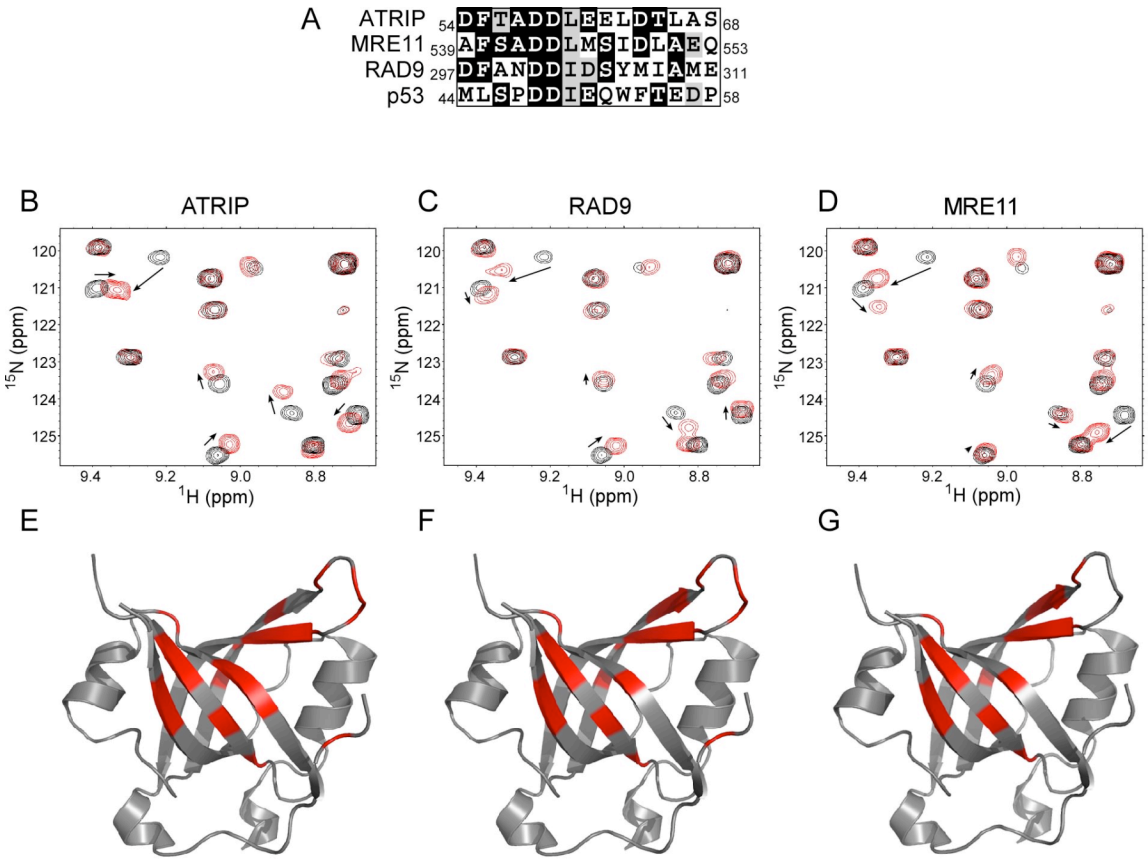

Figure 4.2. ATRIP, MRE11, and RAD9 interact with the same binding surface on RPA70N. (A) Sequence alignment of acidic peptides in RAD9, MRE11, ATRIP, and p53. (B-D) The ^{15}N-^{1}H HSQC NMR spectra of ^{15}N-labelled RPA70N were obtained in the absence (black) and presence (red) of ATRIP (B), RAD9 (C), or MRE11 (D) peptides. (E-G) The RPA70N residues perturbed upon addition of ATRIP (E), RAD9 (F), and MRE11 peptide (G) were mapped (in red) onto the crystal structure of RPA70N (PDB accession 2B3G). The NMR experiment was collaborated with Dr. Walter Chazin laboratory and was performed by Dr. Sivaraja Vaithiyalingam.

full-length RAD9 indeed binds RPA70N, and whether this interaction could explain the CHK1 phosphorylation defect we observed in RPA70 R41E/R43E-expressing cells.

Purified GST-RPA70N binds RAD9 (Figure 4.3A). In contrast, neither GST nor the GST-RPA70N R41E/R43E mutant interacts with RAD9. We confirmed that both RAD9 and ATRIP compete for the same binding surface on RPA70N by doing a competition binding assay. When purified ATRIP1-217 containing its CRD was added to the pull-down experiment, it bound to RPA70N and blocked the ability of RPA70N to bind HA-RAD9 (Figure 4.3B).

To determine whether the RPA binding surface on RAD9 contains the acidic C-terminal peptide, mutations were engineered into the putative RAD9 CRD (Figure 4.4A). This RAD9 mutant (RAD9-crd) was epitope tagged and expressed either in HEK293 cells or in rabbit reticulocyte lysates. The RAD9-crd mutant made in both systems migrates consistently faster than wild-type RAD9 on SDS-PAGE gels (Figure 4.4B). Wild-type RAD9 migrates as multiple bands due to its extensive phosphorylation (203, 204). We initially considered whether the crd mutation might perturb RAD9 phosphorylation. However, both the DNA damage-induced S272 phosphorylation and damage-independent S387 phosphorylation are retained (Figure 4.4C). Furthermore, the RAD9 and RAD9-crd proteins both form complexes with RAD1, RAD17, and TopBP1 as expected (Figure 4.4D). The interaction with TopBP1 is mediated by S387 phosphorylation (203), while the interaction with RAD1 is mediated by the PCNA-homology region within the rest of the protein (244). Thus, the RAD9-crd protein is stable, phosphorylated, and retains its known protein-protein interactions. Its aberrant migration on SDS-PAGE gels is possibly due to an increase in its ability to bind SDS

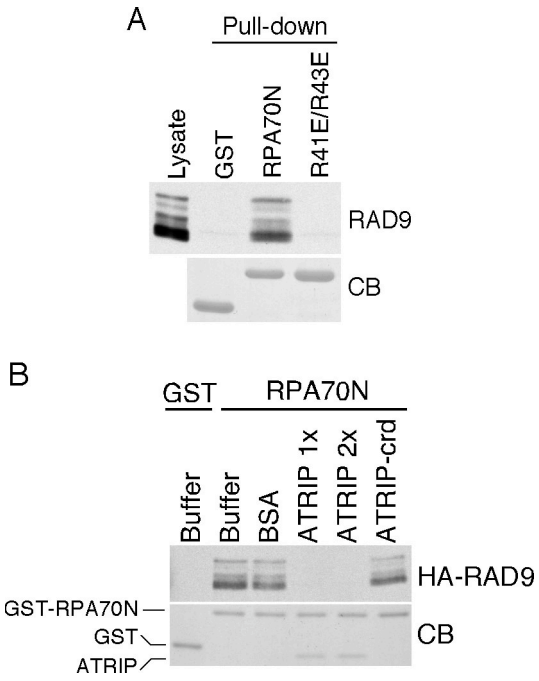

Figure 4.3. RAD9 and ATRIP compete for the same binding surface on RPA70N. (A) Nuclear extracts from HEK293 cells expressing HA-RAD9 were incubated with GST, GST-RPA70N, or GST-RPA70N R41E/R43E proteins bound to glutathione beads. Proteins bound to the beads were eluted, separated by SDS-PAGE and immunoblotted with anti-HA antibody to detect RAD9 or stained with coomassie blue to detect GST proteins (CB). (B) BSA (1.6 nmols), purified ATRIP1-217 (0.8 nmols-1X or 1.6 nmols-2X), or purified ATRIP-crd (D58K/D59K) 1-217 (1.6 nmols) was added as indicated to nuclear extracts from HEK293 cells expressing HA-RAD9. The nuclear extracts were incubated with 0.8 nmols of GST-RPA70N or GST proteins bound to glutathione beads. Proteins bound to the beads were eluted, separated by SDS-PAGE and immunoblotted with anti-HA antibody to detect RAD9 or stained with coomassie blue to detect GST proteins (CB).

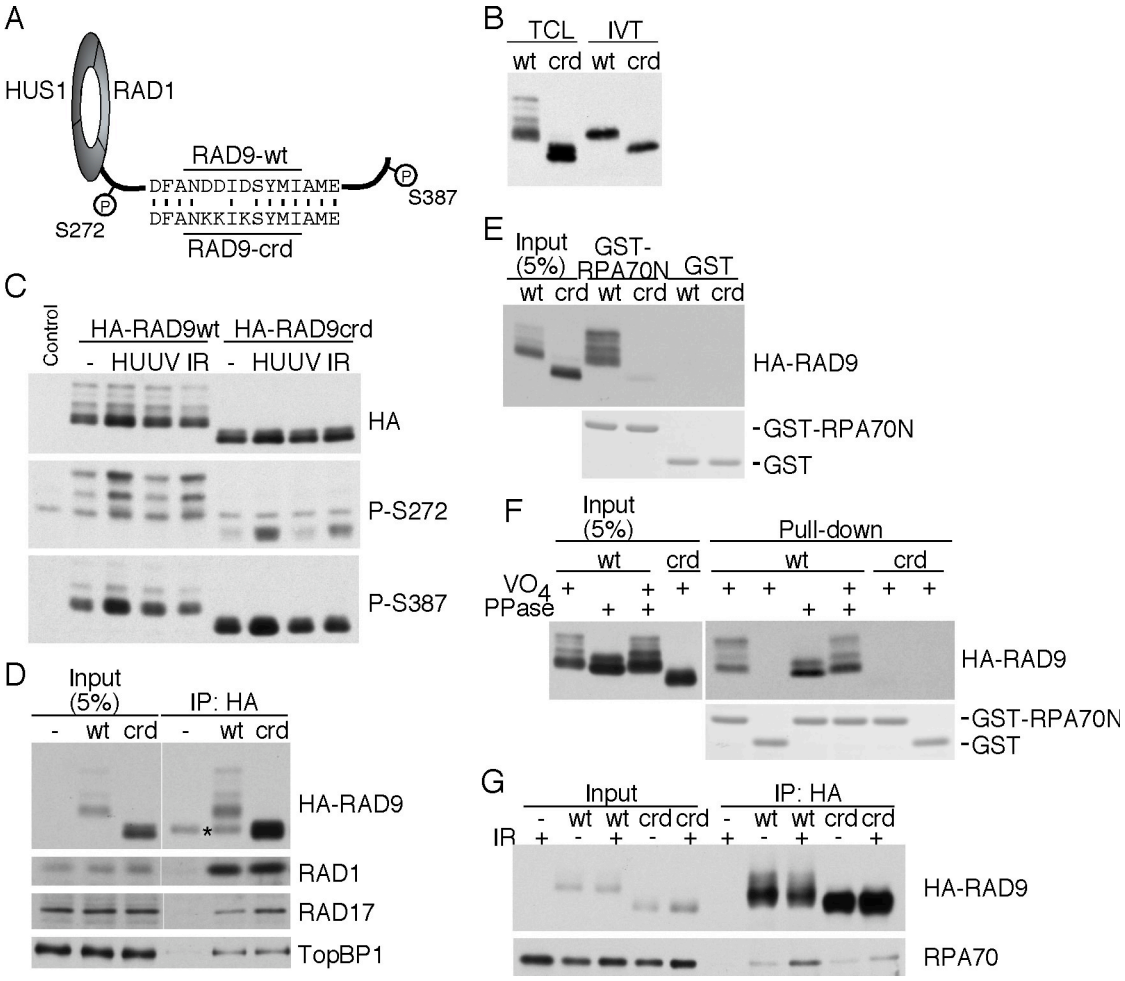

Figure 4.4. The RAD9 checkpoint recruitment domain interacts with RPA70N. (A) Diagram of the RAD9-crd protein illustrating the positions of the engineered mutations and two of the phosphorylated residues. (B) Wild-type HA-RAD9 (wt) or mutant HA-RAD9-crd (crd) was expressed in HEK293 cells or rabbit reticulocyte lysates. Total cell lysates (TCL) or the *in vitro* transcription/translation reactions (IVT) were resolved by SDS-PAGE and immunoblotted with HA antibodies. (C) Wild-type HA-RAD9 or the RAD9-crd mutant was expressed in HEK293 cells. Cells were left untreated (-), or treated with HU (10 mM), UV (50 J/m^2), or IR (20Gy). One hour after treatment, cells were harvested, lysates were resolved by SDS-PAGE, and immunoblots were probed with antibodies to RAD9 P-S272, RAD9 P-S387, or HA. Control is the lysate from untransfected cells. (D) Nuclear extracts from HEK293 cells expressing HA-RAD9 (wt), HA-RAD9-crd (crd), or untransfected (-) cells were incubated with anti-HA agarose beads. The immunoprecipitated proteins were separated on SDS-PAGE followed by immunoblotting with antibodies to RAD1, RAD17, TopBP1, and HA. The asterisk (*) marks the position of IgG heavy-chain background band. (E and F) Nuclear extracts from HEK293 cells expressing HA-RAD9 (wt) or HA-RAD9-crd were incubated with GST-RPA70N or GST. Proteins bound to the beads were eluted, separated by SDS-PAGE, and detected by immunoblotting with anti-HA antibody or staining with coomassie blue to detect GST-RPA70N and GST. In (F) the extracts were treated with lambda phosphatase (PPase) in the absence or presence of sodium vanadate (VO_4) as indicated prior to incubation with GST proteins. (G) HEK293 cells expressing HA-RAD9 (wt) or HA-RAD9-crd (crd) were treated with IR 20Gy as indicated followed by 2 hours incubation. Chromatin lysates were prepared and incubated with anti-HA agarose beads. The immunoprecipitated proteins were separated on SDS-PAGE followed by immunoblotting with antibodies to HA and RPA70.

because of the replacement of three negative charges with three positively charged residues. We observed a similar change in SDS-PAGE mobility of ATRIP when we made mutations in the ATRIP CRD (data not shown) further supporting this interpretation.

We next tested whether the RAD9-crd mutation impairs RPA binding. In contrast to wild-type RAD9, the interaction between RAD9-crd and RPA70N is reduced while not abolished (Figure 4.4E and 4.4F). The lack of interaction is not due to a change in RAD9-crd phosphorylation since the wild-type RAD9-RPA70N interaction is insensitive to phosphatase treatment (Figure 4.4F). Moreover, the RAD9-crd mutant has significantly reduced binding to endogenous RPA70 compared to wild-type RAD9 when measured by co-immunoprecipitation from solubilized chromatin fractions (Figure 4.4G). The residual co-immunoprecipitation may be due to an interaction between RAD9 and RPA32 (296). Combined with the NMR data, these results indicate that RAD9 binds to RPA70 through an acidic peptide within its C-terminal tail and the basic cleft of the RPA70N OB-fold domain, largely the same way as ATRIP binds RPA70 (151).

The RAD9-RPA interaction regulates RAD9 localization

Mutation of the ATRIP CRD prevents ATRIP from efficiently localizing to sites of DNA damage or replication stress (160). To determine whether the RAD9 CRD performs a similar function we created U2OS cells that express HA-RAD9 or HA-RAD9-crd. Both proteins were localized throughout the nucleus in untreated cells. Treatment with hydroxyurea (HU), UV, or ionizing radiation (IR) causes relocalization of both proteins to intra-nuclear foci; however, the RAD9-crd mutant consistently relocalized less efficiently (Figure 4.5A and 4.5B). To examine this more closely, the numbers of

foci in each cell were counted. This analysis revealed that following a low dose of IR, there were significantly fewer RAD9-crd nuclear foci than wild-type RAD9 foci (Figure 4.5C). The RAD9 wild-type and crd mutants are expressed at equal levels (Figure 4.5D). Thus, although the RAD9 CRD-RPA70N interaction is not absolutely required to recruit RAD9 to sites of DNA damage, it does contribute to the efficiency of its localization.

The RAD9-RPA interaction regulates ATR signaling

We examined whether the RAD9-crd mutant could functionally complement *RAD9*$^{-/-}$ embryonic stem (ES) cells. CHK1 is not phosphorylated in response to DNA damage in *RAD9*$^{-/-}$ ES cells because of a defect in activating ATR (185). We created *RAD9*$^{-/-}$ ES cell clones stably expressing either wild-type RAD9 or the RAD9-crd mutant. Two cell clones expressing each protein were analyzed to ensure the results were not due to clonal selection. These cell clones expressed similar amounts of RAD9 protein (Figure 4.6A). Immunofluorescence analysis indicated detectable expression of exogenous RAD9 proteins in approximately 90% of all cells in all the four cell lines. While the wild-type RAD9 protein efficiently complemented the checkpoint signaling defect in the *RAD9*$^{-/-}$ cells, the RAD9-crd mutant was consistently less capable of supporting checkpoint signaling (Figure 4.6B and 4.6C). Following UV radiation, CHK1 phosphorylation in the RAD9-crd expressing cells was reduced by 33% compared to wild-type expressing cells (Figure 4.6B, compare lanes 4 and 6). Following HU exposure, the difference was approximately 60% (Figure 4.6C, compare lanes 9 and 10 and lanes 11 and 12).

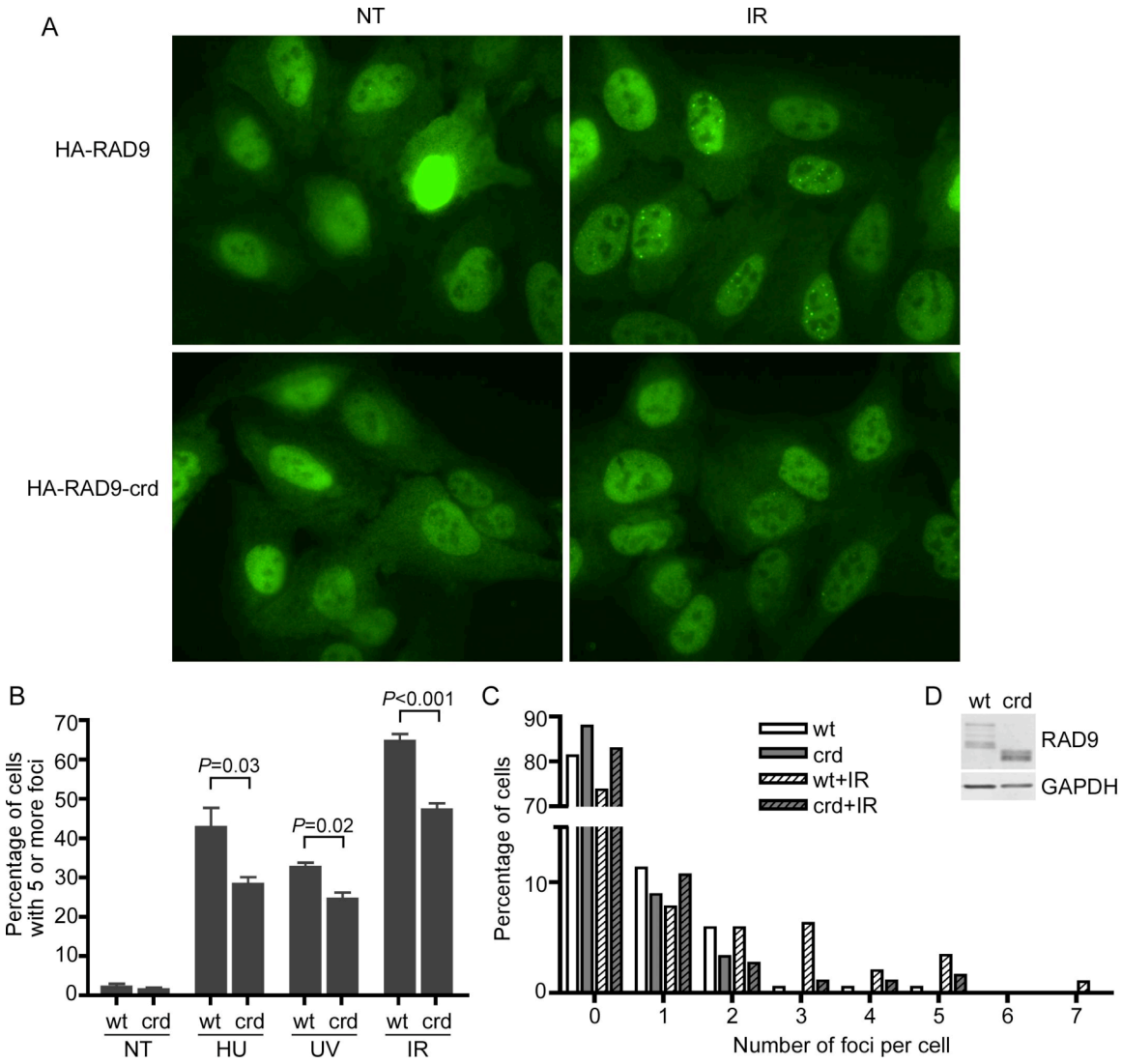

Figure 4.5. The RAD9-RPA interaction promotes RAD9 localization to sites of DNA damage. (A and B) U2OS cells stably expressing HA-RAD9 or HA-RAD9-crd were left untreated (NT) or treated with HU (10 mM) for 4 hours, UV (50 J/m^2) followed by one hour recovery, or IR (10Gy) followed by 6 hours recovery. Fixed cells were stained with anti-HA antibody and FITC–conjugated secondary antibody. (A) Representative images are shown. (B) Cells were scored for RAD9 localization to DNA damage foci. 300 cells were scored per experiment. Error bars indicate standard error (n=3). *P* values were calculated using an unpaired, two-tailed t-test. (C) HA-RAD9 or HA-RAD9-crd expressing U2OS cells were treated with low dose IR (1Gy) or left untreated followed by 6 hours incubation. The number of RAD9 foci in each cell was scored. (D) The expression level of HA-RAD9 and HA-RAD9-crd in the U2OS cells was analyzed by immunoblotting with anti-HA or anti-GAPDH antibody.

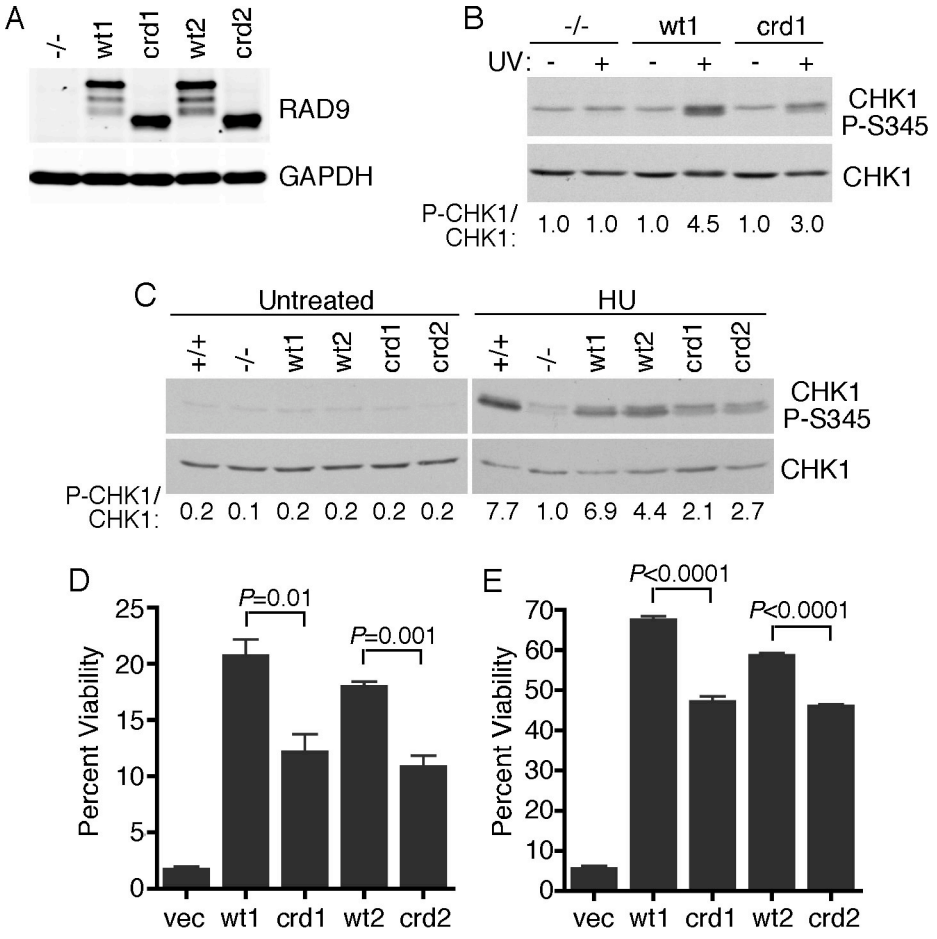

Figure 4.6. The RAD9-RPA interaction regulates DNA damage and replication stress responses. (A) Protein expression levels in two independent clones of RAD9$^{-/-}$ embryonic stem cells stably expressing HA-RAD9 or HA-RAD9-crd were analyzed by immunoblotting total cell lysates. (B and C) RAD9$^{+/+}$ and RAD9$^{-/-}$ cells complemented with vector (-/-), HA-RAD9 (wt1 and wt2), or HA-RAD9-crd (crd1 and crd2) were treated with UV (50J/m^2), HU (10mM), or left untreated as indicated. Following incubation for one hour, lysates were prepared, resolved by SDS-PAGE and immunoblotted with antibodies to CHK1 P-S345 or total CHK1. The phospho-CHK1 and CHK1 levels were quantitated with NIH Image software. The numbers are the ratio of phospho-CHK1 to CHK1 normalized to the sample from cells complemented with vector (-/-) after damage. (D) ES cell clones were treated with HU (10 mM for 12 hours) or (E) UV (10 J/m^2), and grown for 7 days prior to staining and scoring surviving colonies. Percent viability was calculated as compared to untreated cell populations. Error bars indicate standard error (n=3). *P* values were calculated using an unpaired, two-tailed t-test.

The defective DNA damage response activation in the RAD9-crd expressing cells correlated with a hyper-sensitivity of these cells to HU and UV compared to wild-type RAD9 expressing cells (Figure 4.6D and 4.6E). In both cases, the RAD9-crd expressing cells exhibited an intermediate sensitivity to these agents compared to the *RAD9*$^{-/-}$ cells expressing wild-type RAD9 or transfected with an empty vector.

Discussion

RPA functions as a single-stranded DNA binding protein in most nucleic acid metabolic processes. Its interactions with other proteins facilitate replication, repair, and checkpoint signaling (36, 156). RPA-ssDNA is thought to be the common intermediate in activating the ATR checkpoint pathway in response to a diversity of genome integrity challenges (133). ATR activation requires co-localization of the ATR-ATRIP and 9-1-1 complexes. RPA-ssDNA and a 5' primer-template junction are critical ligands to recruit these protein complexes (137, 159-161, 190, 196). We now show that a common protein-interaction surface on the N-terminal OB-fold domain of RPA70 binds to both ATRIP and RAD9. Both ATRIP and RAD9 contain an acidic patch that is predicted to fold into an alpha-helical structure capable of binding into the basic cleft of RPA70N. Given its similarity to the ATRIP checkpoint recruitment domain (CRD) we have named this region the RAD9 CRD.

Mutations in ATRIP, RAD9, or RPA that disrupt the ATRIP-RPA70 or RAD9-RPA70 interactions cause defects in checkpoint protein localization [this study and references (151, 160)]. Both the RAD9-crd and the RPA70 R41E/R43E mutant proteins cause similar deficiencies in ATR-dependent signaling to CHK1. The ATRIP-crd mutant

does not cause a detectable ATR signaling defect, at least as assayed by RNAi complementation analysis (160). However, it is possible that there are other contact points between RPA and ATRIP (169), and there are RPA-independent means of localizing the ATR-ATRIP complex (174, 268, 297). RPA frequently binds proteins using multiple subunits (298), and both RPA70 and RPA32 have been implicated in RAD9 interactions (296).

Our data on the role of human RPA in checkpoint signaling are consistent with the function of *S. cerevisiae* RPA (Rfa). The *rfa1-t11* mutant in budding yeast supports DNA replication but is compromised in DNA damage responses including a defect in loading the yeast 9-1-1 complex (157, 158, 211, 299). This mutation is a charge reversal in Rfa1 at residue K45 (analogous to the R41 site of human RPA70). Our data are also consistent with a recent analysis of a human RPA70 R41E/Y42F mutant which was reported to cause a G2/M checkpoint defect without causing a defect in ssDNA binding or DNA replication (300).

The RPA70N OB-fold domain is attached to the rest of RPA70 through a flexible linker (301). This flexibility may be important to allow RPA to recruit different checkpoint proteins and position them correctly for ATR kinase activation. In addition, since RPA binds ssDNA with a defined 5'-3' polarity (143, 144), the RPA70N OB-fold is positioned near the 5'-end of a primer-template junction (Figure 4.7). This position places it in an ideal location to mediate the 5'-junction specificity of 9-1-1 complex loading (159, 161). The RPA-RAD9 interaction may also help position the RAD9 tail such that it can present TopBP1 to ATR-ATRIP complexes in an optimal orientation.

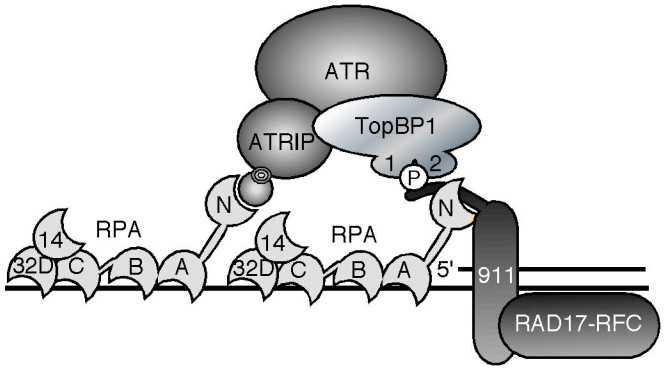

Figure 4.7. Simplified model of the RPA protein and DNA interactions that promote ATR signaling. RPA is a heterotrimer of three subunits, RPA70, RPA32, and RPA14 that contain six OB-folds. Four of these OB-fold domains can bind single-stranded DNA in a specific orientation such that the amino-terminal RPA70 OB-fold (70N) is positioned near the 5' primer-template junction. The RPA70N OB-fold binds checkpoint proteins including ATRIP and RAD9. These interactions help to concentrate ATR-ATRIP and 9-1-1-TopBP1 complexes to promote TopBP1 activation of ATR. Many additional protein-protein and protein-nucleic acid interactions also participate but are not shown in this simplified diagram.

Since ATRIP and RAD9 bind to the same surface of RPA, they are unlikely to be capable of binding at the same time. Indeed, ATRIP and RAD9 compete for binding to RPA70N (Figure 4.3B). This raises an interesting question of what is the timing of these interactions. Competitive binding to the same RPA surface may indicate that at least two molecules of RPA need to be present to efficiently activate ATR. Such a scenario would ensure that the ATR checkpoint is only activated when longer stretches of ssDNA are available. This hypothesis is consistent with the ssDNA length dependency for ATR activation which was observed using defined DNA templates to activate ATR in *X. laevis* egg extracts (140). It is also possible that another protein retains the ATR-ATRIP or 9-1-1 complexes at the site of DNA damage or replication stress. Once loaded, the 9-1-1 checkpoint clamp is topologically linked to the DNA. The RPA interaction may serve to decrease its ability to slide away from the ssDNA gap.

While we did not pursue our observation that MRE11 contains a peptide that binds RPA70N (Figure 4.2), a recent publication mapped an RPA binding surface on MRE11 to amino acids 521-569 (302). Notably, this region contains the acidic peptide we used in the NMR experiment. Furthermore, double mutation of D543 and D544 in MRE11 abolished the RPA interaction, impaired localization of MRE11 to replication centers, and caused a defect in the S-phase checkpoint (302). Our data suggest that this mutant disrupts an MRE11 CRD that interacts with the basic cleft of RPA70N. These data further support our conclusions that RPA70N provides a common checkpoint protein binding surface, and RPA-ssDNA is a signal for recruitment of multiple DNA damage response proteins.

The ATR signaling pathway is a potential target for cancer therapy (303, 304). ATR signaling inhibitors are expected to sensitize cells to DNA damaging agents. Cancer cells are also known to have higher levels of replicative stress than adjacent normal cells (88, 89). Thus, cancer cells may be more dependent on replication stress responses than normal cells to complete replication and retain viability. Thus, targeting the replication stress response could be a useful therapy. Our results suggest the basic cleft in RPA70N may be a useful target for the development of a protein-protein interaction inhibitor. Inhibiting RPA from binding multiple checkpoint proteins (at least ATRIP, RAD9, MRE11 and p53) should significantly impair the replication stress response. We are currently investigating whether our understanding of the structural basis for binding specificity can enable development of a selective DNA damage checkpoint inhibitor that suppresses the DNA damage response without eliminating the essential replication function of RPA.

CHAPTER V

CONCLUSIONS AND FUTURE DIRECTIONS

Conclusions

Establishing a model system with a site-specific stalled replication fork

I established an episome-based system in which a replication fork is stalled at a defined site (Chapter II). In this system, the inter-strand cross-link is achieved on DNA at a specific site, and the replication forks initiated from the SV40 origin can be paused at the cross-linked site in COS-cells. Also intra-strand cross-links on the leading strand and the lagging strand are achieved separately at the specific site. When added into *Xenopus* egg extracts, the intra-strand cross-link on DNA induces a higher level of Chk1 phosphorylation than the inter-strand cross-link. This suggests that the combination of cross-linked episomes and *Xenopus* egg extracts is a useful model system for studying protein recruitment to a stalled replication fork.

ATRIP S224 phosphorylation by Cdk2 is required for G2-M checkpoint maintenance

ATRIP interacts with ATR and is an essential partner for ATR function (163). ATR functions to delay cells from entering mitosis when cells are challenged by DNA damage (133). Phosphorylation of ATRIP S224 correlates with S phase in the cell cycle and is not induced by DNA damage or replication stress (Chapter III). Instead, phosphorylation of ATRIP on S224 is regulated by Cdk2. Phosphorylation of ATRIP S224 is inhibited when cells are treated with a Cdk2 inhibitor. ATRIP S224 is a substrate

of Cdk2-cyclin A *in vitro*. The mutation of ATRIP S224 to alanine compromises G2-M checkpoint maintenance induced by UV and IR. Thus, in addition to being a target for ATR-dependent checkpoint responses, Cdk2 is also a direct regulator of the ATR-ATRIP checkpoint kinase complex.

CINP regulates ATR signaling

We identified CINP as a novel ATRIP interacting protein (Chapter III). CINP interacts with the first coiled-coil domain of ATRIP. Depletion of CINP compromises phosphorylation of Chk1 on S345 and S317 when cells are treated with UV or IR. Furthermore, depletion of CINP compromises the G2-M checkpoint maintenance induced by UV or IR. Depletion of CINP also causes a decreased level of ATRIP phosphorylation on S224. Therefore, ATR signaling is regulated by CINP partially through regulating phosphorylation of ATRIP S224.

RPA70N is a checkpoint signaling module

The N terminal OB fold domain of RPA70 (RPA70N) forms a pocket structure with multiple positively charged residues on its surface (149, 151). The acidic regions of P53 and ATRIP interact with RPA70N (252). Both Mre11 and Rad9 contain homologous regions of the acidic regions on P53 and ATRIP. We determined that the acidic regions of ATRIP, Mre11, and Rad9 interact with RPA70N in similar manners (Chapter IV). A double charge reversal mutation of RPA70N (R41E/R43E) abolishes RPA70N interaction with ATRIP and Rad9. The RPA70 R41E/R43E mutant causes a defect in

Chk1 phosphorylation following UV radiation. Thus, the RPA70N domain is a checkpoint signaling module.

Rad9-RPA70N interaction regulates ATR signaling

The acidic region on the C-terminal tail of Rad9 interacts with the RPA70N domain. The Rad9-crd mutant disrupts Rad9 interaction with RPA70N while its interactions with Rad17 and TopBP1 remain (Chapter IV). The Rad9-crd mutant exhibits less efficient foci formation after DNA damage and replication stress compared to wild type Rad9. Cells expressing the Rad9-crd mutant exhibit compromised Chk1 phosphorylation after DNA damage and replication stress treatment. Furthermore, cells expressing the Rad9-crd mutant are hypersensitive to DNA damage and replication stress treatment. Thus, ATR signaling is regulated by an RPA70N interaction with Rad9.

Further Discussion and Future Directions

Stabilizing a stalled replication fork

How are stalled replication forks stabilized in cells? Evidence in yeast suggests that the ATR signaling pathway plays a role for cells to recover from replication stress or MMS treatment (248, 249). We hypothesized that the ATR-mediated checkpoint functions in stabilizing stalled forks in mammalian cells as in yeast and proposed to study checkpoint protein recruitment to stalled forks by CHIP. Establishing a stalled fork on DNA at a defined site is an initial step to test this hypothesis. The episome-based system, which can replicate in cells and *Xenopus* egg extracts, allows us to detect protein

recruitment to a stalled fork by CHIP. Therefore, the next step is to detect proteins involved in ATR signaling on the stalled fork by CHIP.

The attempt to detect three proteins, ATRIP, ATR, and RPA on the stalled fork by CHIP was unsuccessful when cross-linked episomes were transfected into cells. Checkpoint activation upon transfection of cross-linked episomes will encourage our hypothesis. However, Chk1 phosphorylation was not detectable when the cross-linked episomes were transfected into mammalian cells. Although it is not clear whether the intra-strand cross-link can stall the fork progression in cells, it does induce detectable Chk1 phosphorylation in the egg extract. Therefore, the combination of cross-linked episomes and *Xenopus* egg extracts is the model system we should use to detect checkpoint protein recruitments to the stalled replication fork by CHIP.

CHIP requires a high quality of antibody to enrich for the proteins to be detected. The antibodies I used here may not be suitable for CHIP. Different antibodies may yield positive results. Alternatively, we can perform streptavidin pull-down as described in Chapter II to detect RPA, ATRIP, and ATR in the egg extract system after cross-linked episome is added.

Why does the intra-strand cross-link induce Chk1 phosphorylation in the egg extract but not in mammalian cells? One possible reason is that the egg extract provides a robust replication environment. In cells, the intra-strand cross-link could be bypassed or repaired before the replisome encounters it. At earlier time points, episome replication has not been maximally initiated. If this is the case, using cells deficient for translesion synthesis and DNA repair may yield Chk1 phosphorylation upon addition of the cross-linked episomes. Consistently, the intra-strand cross-link induces Chk1 phosphorylation

at 30 minutes when added into the egg extract, and the level of Chk1 phosphorylation decreases at 45 minutes and 60 minutes. Depletion of proteins for translesion synthesis and DNA repair from the egg extract will extend the duration of Chk1 phosphorylation.

Why does the intra-strand cross-linked episome induce Chk1 phosphorylation while the inter-strand cross-linked episome does not? It has been shown that inhibition of DNA helicase activity suppresses ATR signaling in response to replication stress (139). We propose that the inter-strand cross-link stalls DNA helicases and polymerases while the intra-strand cross-link only stalls the DNA polymerases (Figure 5.1). Therefore, the intra-strand cross-link generates the ATR activation structure by functional uncoupling DNA helicases and polymerases. Localization of DNA helicases and polymerases on stalled forks induced by different cross-links can be detected by CHIP.

How do cells repair different lesions on DNA? Inter-strand cross-links and cross-links on the leading strand and lagging strand can be generated separately in the episome-based system as described in Chapter II. Products of DNA repair can be examined by PCR followed by DNA sequencing. Moreover, whether DNA replication alters the repair pathway and efficiency can be determined by deletion of the episome origins.

How phosphorylation of ATRIP regulates ATR signaling

ATRIP is phosphorylated on S68 and S72 by ATR upon DNA damage treatment (173). The functional significance of ATRIP phosphorylation on S68 and S72 is unclear (140). S68 and S72 sites fall in the region of the RPA interaction domain of ATRIP. They may contribute to the interaction between ATRIP and the basic cleft of RPA70N domain.

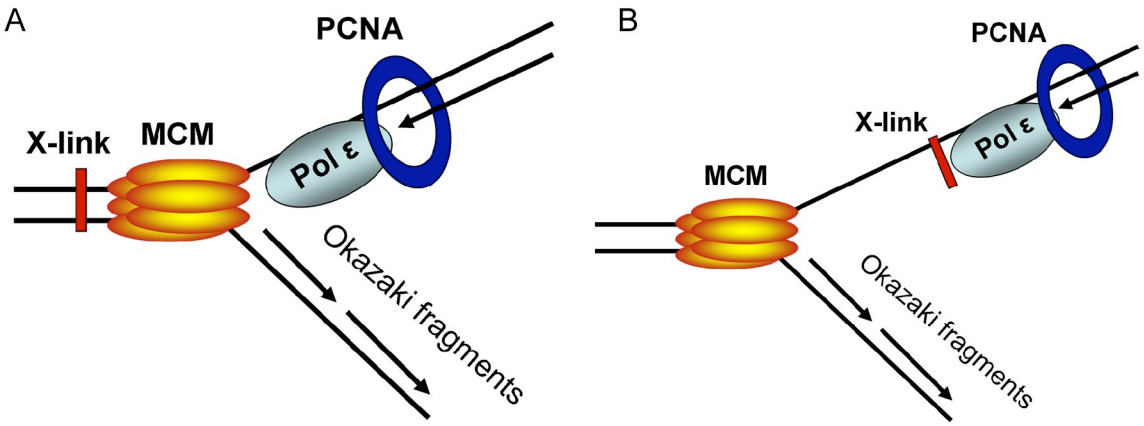

Figure 5.1. Illustration of DNA helicase and polymerase localization on the stalled fork. (A) A replication fork is stalled by inter-strand cross-link. Both DNA helicase and polymerase are stalled before the cross-link site. (B) A replication fork is stalled by intra-strand cross-link on the leading strand (the lagging strand polymerase is not shown for simplicity). DNA polymerase is stalled before the cross-link site, but the helicase is not. Although the uncoupling of polymerase and helicase is drawn here, DNA polymerase may not physically uncouple from the helicase.

An ATRIP phosphor peptide with S68 and S72 phosphorylation can be used to detect its direct interaction with the purified RPA70N protein *in vitro*.

Phosphorylation of ATRIP on S224 and S239 is required for G2-M checkpoint maintenance (176). ATRIP S224 is a substrate of Cdk2. The kinase responsible for phosphorylation of ATRIP S239 has not been determined. With a panel of specific kinase inhibitors, we can identify the kinase responsible for ATRIP S239 phosphorylation. It is unclear how phosphorylation of ATRIP S224 regulates the activation of ATR-ATRIP checkpoint responses. Phosphorylation of ATRIP S224 is not required for ATRIP binding to RPA, localization to sites of DNA damage, or binding to ATR. In addition, ATR-ATRIP complexes containing the ATRIP S224A mutant have similar kinase activities *in vitro* as wild type complexes in the presence and absence of TopBP1. One possibility is phosphorylation of S224 creates a binding site for another protein involved in the maintenance of G2-M checkpoint.

An ATRIP peptide containing phosphorylation of S239 interacts with BRCT repeats of BRCA-1 (175). This suggests that S239 phosphorylation dependent ATRIP interaction with BRCA-1 may be a mechanism of ATR activation. The BRCT domains often function in tandem as phospho-protein binding domains (282). ATRIP S224 phosphorylation may also contribute to ATRIP interaction with BRCA-1.

How CINP regulates ATR signaling

Depletion of CINP decreases the phosphorylation level of ATRIP on S224. Therefore, ATRIP S224 phosphorylation may be one of the mechanisms by which CINP regulates ATR signaling. CINP was identified as a Cdk2 interacting protein by a yeast

two-hybrid assay (275). Because phosphorylation of ATRIP S224 is regulated by Cdk2-cyclin A directly, CINP may function as a bridge between Cdk2 and ATRIP. This can be tested by examining ATRIP interaction with Cdk2 in the absence and presence of CINP. Also it is possible that CINP plays a role to protect the phosphorylation of ATRIP S224 from phosphatases. In this case, the phosphatase remains to be identified.

Depletion of CINP causes comparable defects as ATRIP depletion in G2-M checkpoint maintenance. However, depletion of CINP only decreases ATRIP S224 phosphorylation about 45%. This suggests that CINP also regulates ATR signaling through other mechanisms in addition to ATRIP S224 phosphorylation. Identifying CINP interacting proteins will reveal other mechanisms by which CINP regulates ATR signaling.

CINP is identified as a novel ATRIP interacting protein and is required for ATR signaling. Whether CINP interaction with ATRIP regulates ATR activation remains to be determined. CINP has a predicted coiled-coil domain. Coiled-coil domains often mediate protein-protein interaction (283). Moreover, CINP interacts with the first coiled-coil domain of ATRIP. It is likely that the coiled-coil domain of CINP mediates CINP interaction with ATRIP. CINP interaction with ATRIP can be disrupted by a CINP mutant that lacks the coiled-coil domain. Functional characterization for this CINP mutant will reveal whether CINP interaction with ATRIP regulates ATR signaling.

The roles of RPA70N in ATR signaling

RPA functions as an ss-DNA binding protein in most nucleic acid metabolic processes (36). Its interactions with other proteins facilitate DNA replication, DNA repair,

and checkpoint signaling (36, 156). ATR activation requires co-localization of the ATR-ATRIP and 9-1-1 complexes. RPA-ss-DNA and a 5′-DNA junction are critical for recruiting these proteins (137, 159-161, 190, 196). Localization of the ATR-ATRIP complex to sites of DNA damage is primarily regulated by the interaction of RPA70N with the N terminal region of ATRIP (137, 151, 160). A conserved checkpoint recruitment domain (CRD) in ATRIP orthologs is critical for ATRIP localization to sites of DNA damage in humans and yeast [Figure 5.2A and reference (151)]. Here we identified a similar acidic region on Rad9 and Mre11 (Figure 5.2B and 5.2C).

All the crd mutants of ATRIP, Mre11, and Rad9 exhibit dramatically reduced interaction with RPA70N [this study and references (151, 160, 302)]. Although the ATRIP-crd and Mre11-crd mutants exhibit strong defects in foci formation in response to DNA damage (151, 160, 302), the Rad9-crd mutant only causes a mild defect in Rad9 localization (Chapter IV). This suggests that Rad9 can be recruited to sites of DNA damage by alternative mechanisms. Consistent with this hypothesis, both RPA70 and RPA32 have been implicated in Rad9 interaction (296). The approach of immunofluorescence microscopy can not differentiate between loading and retention of proteins. Compared to ATRIP and Mre11, the 9-1-1 checkpoint clamp forms a ring structure to circle DNA and is topologically linked to the DNA once loaded. Therefore, the retention of Rad9 at sites of DNA damage may not require the interaction of Rad9 and RPA70N while the retention of ATRIP and Mre11 at sites of DNA damage requires RPA70N.

The Rad9-crd mutant exhibits defective ATR signaling (chapter IV). The Mre11-crd mutant causes a defect in S-phase checkpoint (302). However, the ATRIP-crd mutant exhibits wild type ATR signaling (160). This could be due to the different approaches

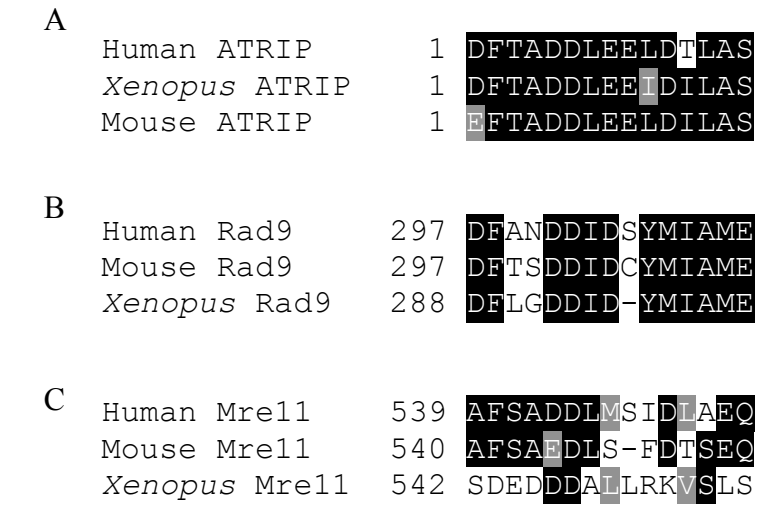

Figure 5.2. Evolutionarily conserved acidic regions on ATRIP, Rad9, and Mre11. (A) Sequence alignment of the conserved acidic region in the N terminal of ATRIP orthologues. (B) Sequence alignment of the acidic region in Rad9 orthologues. (C) Sequence alignment of the acidic region in Mre11 orthologues.

used to study functional complementation. The Rad9-crd and Mre11-crd mutants were used to reconstitute Rad9 and Mre11 deficient cells respectively while the ATRIP-crd mutant was examined by siRNA complementation. Consistent with this possibility, the $Ddc2^{ATRIP}$-crd mutant causes a defect in Rad53 phosphorylation after DNA damage (151). It is also possible that ATRIP-crd can be loaded to sites of DNA damage by other mechanisms although the retention of ATRIP is defective (169, 174, 268, 297), and this alternative loading of ATRIP-crd is efficient as wild type ATRIP to activate ATR.

Since ATRIP and Rad9 bind to the same surface of RPA70, they are unlikely to be capable of binding at the same time. A purified ATRIP-CRD fragment competes with Rad9 for the RPA70N domain (Chapter IV). What is the timing of these interactions when an ATR activation structure is generated? Competitive binding to the same RPA surface may indicate that at least two molecules of RPA need to be present to efficiently activate ATR. Such a scenario would ensure that the ATR checkpoint is only activated when long stretches of ssDNA are available. This hypothesis is consistent with the ssDNA length dependency of ATR activation which was observed using defined DNA templates to activate ATR in *Xenopus* egg extracts (140). It is also possible that another protein retains the ATR-ATRIP or 9-1-1 complexes at the site of DNA damage. RPA binds to ssDNA with a defined 5′→3′ polarity (190). Therefore, the RPA70N faces the 5′-DNA junction at the ATR activation structure. The 9-1-1 checkpoint clamp is preferentially loaded to a 5′-DNA junction and can slide on DNA once loaded (159, 161). These discoveries suggest that the RPA70N-Rad9 interaction may serve to decrease the ability of Rad9 to slide away from the ssDNA gap (Figure 5.3). Reconstitution of the

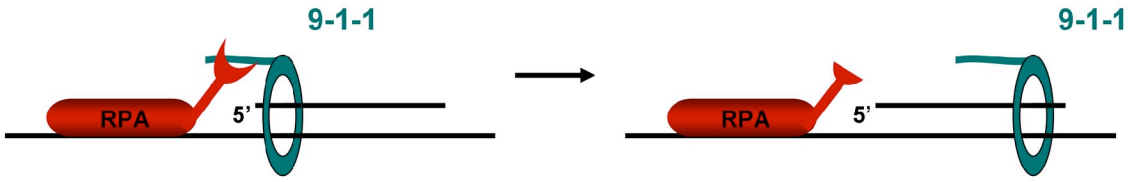

Figure 5.3. RPA70N retains 9-1-1 complex at the 5'-DNA junction from sliding away.

Rad9-crd-Hus1-Rad1 complex loading to 5'-DNA junction *in vitro* in the presence of Rad17-RFC complex and RPA will directly test this hypothesis.

Our data show that the RPA70 R41E/R43E mutant causes a defect in ATR signaling without causing a defect in DNA replication. This is consistent with the analysis of the RPA70 R41E/Y42F mutant, which exhibits a G2-M checkpoint defect without a defect in ss-DNA binding or DNA replication (300). Our data on the role of RPA70N in checkpoint signaling is also consistent with the function of $Rfa1^{RPA70}$ in S. cerevisiae.

The 9-1-1 complex recruits TopBP1 to stalled forks through Rad9 interaction with TopBP1 (217, 218). TopBP1 enhances ATR kinase activity (159). Therefore, TopBP1 is concentrated at stalled replication forks by the 9-1-1 complex to stimulate the kinase activity of ATR. Although Rad9 interaction with RPA70N regulates ATR signaling *in vivo*, this regulation is not essential for ATR signaling because Chk1 phosphorylation is reduced but not abolished with the Rad9-crd mutant (Chapter IV). Consistently, this regulation can be bypassed by fusing the ATR activation domain of TopBP1 to PCNA or 9-1-1 complex lacking the C-tail of Rad9 for ATR signaling (203).

RPA70N functions in other processes

RPA70N regulates Mre11 localization to replication centers in the absence of exogenous DNA damage or replication stress (302). This suggests that RPA70N may have some other roles in addition to checkpoint signaling. RPA70 interacts with many proteins for DNA replication, checkpoint signaling, and DNA repair (36, 156). Although an acidic region with a predicted alpha-helical structure is a common feature of CRD

domains on Rad9, ATRIP, Mre11, and p53, it is difficult to predict what other proteins may interact with RPA70N by sequence. GST-RPA70N can be used as bait to enrich candidate proteins on beads by a pull-down method and the RPA70 R41E/R43E mutant will be a good negative control. Mass spectrometry can be performed to identify the enriched candidate proteins.

RPA70N is a potential target for cancer therapy

Cancer cells are known to have higher levels of replicative stress than adjacent normal cells (88, 89). The ATR signaling pathway is the primary cellular response to replication stress (133). Thus, cancer cells may be more dependent on ATR signaling than normal cells to survive. Chk1, Claspin, ATR-ATRIP, and 9-1-1 complexes function in ATR signaling and also are essential for cellular viability (163, 185, 231). This suggests that ATR signaling is essential for viability. Eliminating all ATR signaling would be cytotoxic to normal and malignant cells. Pharmacological agents usually yield partial loss of function phenotypes. Thus, partial inhibition of ATR signaling could be a useful therapy to selectively kill cancer cells.

Traditionally, targeting protein kinases has relied on the development of ATP analogs that act as competitive inhibitors for the binding of ATP to the catalytic domain of kinases. This strategy raises an issue about the specificity of the inhibitors to kinases. For example, the ATR inhibitors, caffeine and wortmannin, are not specific for ATR. The Chk1 inhibitor, UCN-01 is not specific for Chk1 (305).

Our data suggests that the basic cleft of RPA70N binds multiple checkpoint proteins, ATRIP, Rad9, Mre11, and p53. Mutation and deletion of RPA70N does not

cause a defect in DNA replication [Chapter IV and reference (300)]. ATRIP, Rad9, and Mre11 all function in response to replication stress. Inhibiting RPA70N from binding these proteins should significantly impair the replication stress response, which will decrease the viability of cancer cells. The specificity of this inhibition is expected to be better than kinase inhibitors. We currently are investigating whether our understanding of the structural basis for binding specificity can enable the development of a selective DNA damage checkpoint inhibitor that suppresses the DNA damage response.

REFERENCES

1. Maton, A. (1997) *Cells : building blocks of life*. Prentice-Hall, Upper Saddle River, N.J.

2. Watson, J.D. and F.H. Crick. (1953) Molecular structure of nucleic acids; a structure for deoxyribose nucleic acid. *Nature*, **171**, 737-8.

3. Alberts, B. (2002) *Molecular biology of the cell*. Garland Science, New York.

4. Meselson, M. and F.W. Stahl. (1958) The Replication of DNA in Escherichia Coli. *Proc Natl Acad Sci U S A*, **44**, 671-82.

5. Murray, A.W. and T. Hunt. (1993) *The cell cycle : an introduction*. W.H. Freeman, New York.

6. Evans, T., et al. (1983) Cyclin: a protein specified by maternal mRNA in sea urchin eggs that is destroyed at each cleavage division. *Cell*, **33**, 389-96.

7. Murray, A.W. and M.W. Kirschner. (1989) Cyclin synthesis drives the early embryonic cell cycle. *Nature*, **339**, 275-80.

8. Sherr, C.J. (1993) Mammalian G1 cyclins. *Cell*, **73**, 1059-65.

9. Matsushime, H., et al. (1994) D-type cyclin-dependent kinase activity in mammalian cells. *Mol Cell Biol*, **14**, 2066-76.

10. Meyerson, M. and E. Harlow. (1994) Identification of G1 kinase activity for cdk6, a novel cyclin D partner. *Mol Cell Biol*, **14**, 2077-86.

11. Weinberg, R.A. (1995) The retinoblastoma protein and cell cycle control. *Cell*, **81**, 323-30.

12. Muller, H., et al. (2001) E2Fs regulate the expression of genes involved in differentiation, development, proliferation, and apoptosis. *Genes Dev*, **15**, 267-85.

13. Nigg, E.A. (1995) Cyclin-dependent protein kinases: key regulators of the eukaryotic cell cycle. *Bioessays*, **17**, 471-80.

14. Clurman, B.E., et al. (1996) Turnover of cyclin E by the ubiquitin-proteasome pathway is regulated by cdk2 binding and cyclin phosphorylation. *Genes Dev*, **10**, 1979-90.

15. Won, K.A. and S.I. Reed. (1996) Activation of cyclin E/CDK2 is coupled to site-specific autophosphorylation and ubiquitin-dependent degradation of cyclin E. *Embo J*, **15**, 4182-93.

16. Kelly, T.J. and G.W. Brown. (2000) Regulation of chromosome replication. *Annu Rev Biochem*, **69**, 829-80.

17. Pines, J. and T. Hunter. (1991) Human cyclins A and B1 are differentially located in the cell and undergo cell cycle-dependent nuclear transport. *J Cell Biol*, **115**, 1-17.

18. Sherr, C.J. and J.M. Roberts. (1999) CDK inhibitors: positive and negative regulators of G1-phase progression. *Genes Dev*, **13**, 1501-12.

19. Morgan, D.O. (1995) Principles of CDK regulation. *Nature*, **374**, 131-4.

20. Gu, Y., J. Rosenblatt, and D.O. Morgan. (1992) Cell cycle regulation of CDK2 activity by phosphorylation of Thr160 and Tyr15. *Embo J*, **11**, 3995-4005.

21. Poon, R.Y., et al. (1993) The cdc2-related protein p40MO15 is the catalytic subunit of a protein kinase that can activate p33cdk2 and p34cdc2. *Embo J*, **12**, 3123-32.

22. Fesquet, D., et al. (1993) The MO15 gene encodes the catalytic subunit of a protein kinase that activates cdc2 and other cyclin-dependent kinases (CDKs) through phosphorylation of Thr161 and its homologues. *Embo J*, **12**, 3111-21.

23. Gautier, J., et al. (1991) cdc25 is a specific tyrosine phosphatase that directly activates p34cdc2. *Cell*, **67**, 197-211.

24. Dunphy, W.G. (1994) The decision to enter mitosis. *Trends Cell Biol*, **4**, 202-7.

25. Bell, S.P. and A. Dutta. (2002) DNA replication in eukaryotic cells. *Annu Rev Biochem*, **71**, 333-74.

26. Aladjem, M.I. (2004) The mammalian beta globin origin of DNA replication. *Front Biosci*, **9**, 2540-7.

27. Labib, K., J.A. Tercero, and J.F. Diffley. (2000) Uninterrupted MCM2-7 function required for DNA replication fork progression. *Science*, **288**, 1643-7.

28. Lemaitre, J.M., S. Bocquet, and M. Mechali. (2002) Competence to replicate in the unfertilized egg is conferred by Cdc6 during meiotic maturation. *Nature*, **419**, 718-22.

29. Randell, J.C., et al. (2006) Sequential ATP hydrolysis by Cdc6 and ORC directs loading of the Mcm2-7 helicase. *Mol Cell*, **21**, 29-39.

30. Whitmire, E., B. Khan, and M. Coue. (2002) Cdc6 synthesis regulates replication competence in Xenopus oocytes. *Nature*, **419**, 722-5.

31. Kanemaki, M. and K. Labib. (2006) Distinct roles for Sld3 and GINS during establishment and progression of eukaryotic DNA replication forks. *Embo J*, **25**, 1753-63.

32. Labib, K. and A. Gambus. (2007) A key role for the GINS complex at DNA replication forks. *Trends Cell Biol*, **17**, 271-8.

33. Pacek, M., et al. (2006) Localization of MCM2-7, Cdc45, and GINS to the site of DNA unwinding during eukaryotic DNA replication. *Mol Cell*, **21**, 581-7.

34. Pacek, M. and J.C. Walter. (2004) A requirement for MCM7 and Cdc45 in chromosome unwinding during eukaryotic DNA replication. *EMBO J.*, **23**, 3667-3676.

35. Berg, J.M., et al. (2002) *Biochemistry*. W.H. Freeman, New York.

36. Fanning, E., V. Klimovich, and A.R. Nager. (2006) A dynamic model for replication protein A (RPA) function in DNA processing pathways. *Nucleic Acids Res*, **34**, 4126-37.

37. Walter, J. and J. Newport. (2000) Initiation of eukaryotic DNA replication: origin unwinding and sequential chromatin association of Cdc45, RPA, and DNA polymerase alpha. *Mol Cell*, **5**, 617-27.

38. Nick McElhinny, S.A., et al. (2008) Division of labor at the eukaryotic replication fork. *Mol Cell*, **30**, 137-44.

39. Pursell, Z.F., et al. (2007) Yeast DNA polymerase epsilon participates in leading-strand DNA replication. *Science*, **317**, 127-30.

40. Walter, J., L. Sun, and J. Newport. (1998) Regulated chromosomal DNA replication in the absence of a nucleus. *Mol Cell*, **1**, 519-29.

41. Fanning, E. and K. Zhao. (2009) SV40 DNA replication: from the A gene to a nanomachine. *Virology*, **384**, 352-9.

42. Dean, F.B., et al. (1987) Simian virus 40 (SV40) DNA replication: SV40 large T antigen unwinds DNA containing the SV40 origin of replication. *Proc Natl Acad Sci U S A*, **84**, 16-20.

43. Mastrangelo, I.A., et al. (1989) ATP-dependent assembly of double hexamers of SV40 T antigen at the viral origin of DNA replication. *Nature*, **338**, 658-62.

44. Li, J.J. and T.J. Kelly. (1984) Simian virus 40 DNA replication in vitro. *Proc Natl Acad Sci U S A*, **81**, 6973-7.

45. Wold, M.S., J.J. Li, and T.J. Kelly. (1987) Initiation of simian virus 40 DNA replication in vitro: large-tumor-antigen- and origin-dependent unwinding of the template. *Proc Natl Acad Sci U S A*, **84**, 3643-7.

46. Gahn, T.A. and C.L. Schildkraut. (1989) The Epstein-Barr virus origin of plasmid replication, oriP, contains both the initiation and termination sites of DNA replication. *Cell*, **58**, 527-35.

47. Yates, J.L., N. Warren, and B. Sugden. (1985) Stable replication of plasmids derived from Epstein-Barr virus in various mammalian cells. *Nature*, **313**, 812-5.

48. Chaudhuri, B., et al. (2001) Human DNA replication initiation factors, ORC and MCM, associate with oriP of Epstein-Barr virus. *Proc Natl Acad Sci U S A*, **98**, 10085-9.

49. Dhar, S.K., et al. (2001) Replication from oriP of Epstein-Barr virus requires human ORC and is inhibited by geminin. *Cell*, **106**, 287-96.

50. Yates, J.L. and N. Guan. (1991) Epstein-Barr virus-derived plasmids replicate only once per cell cycle and are not amplified after entry into cells. *J Virol*, **65**, 483-8.

51. Wood, R.D. (1996) DNA repair in eukaryotes. *Annu Rev Biochem*, **65**, 135-67.

52. Memisoglu, A. and L. Samson. (2000) Base excision repair in yeast and mammals. *Mutat Res*, **451**, 39-51.

53. Hess, M.T., et al. (1997) Bipartite substrate discrimination by human nucleotide excision repair. *Proc Natl Acad Sci U S A*, **94**, 6664-9.

54. Cadet, J., E. Sage, and T. Douki. (2005) Ultraviolet radiation-mediated damage to cellular DNA. *Mutat Res*, **571**, 3-17.

55. Pfeifer, G.P., Y.H. You, and A. Besaratinia. (2005) Mutations induced by ultraviolet light. *Mutat Res*, **571**, 19-31.

56. de Laat, W.L., N.G. Jaspers, and J.H. Hoeijmakers. (1999) Molecular mechanism of nucleotide excision repair. *Genes Dev*, **13**, 768-85.

57. Kraemer, K.H., et al. (1994) The role of sunlight and DNA repair in melanoma and nonmelanoma skin cancer. The xeroderma pigmentosum paradigm. *Arch Dermatol*, **130**, 1018-21.

58. Khanna, K.K. and S.P. Jackson. (2001) DNA double-strand breaks: signaling, repair and the cancer connection. *Nat Genet*, **27**, 247-54.

59. Hoeijmakers, J.H. (2001) Genome maintenance mechanisms for preventing cancer. *Nature*, **411**, 366-74.

60. Van Dyck, E., et al. (2001) Visualization of recombination intermediates produced by RAD52-mediated single-strand annealing. *EMBO Rep*, **2**, 905-9.

61. Gottlieb, T.M. and S.P. Jackson. (1993) The DNA-dependent protein kinase: requirement for DNA ends and association with Ku antigen. *Cell*, **72**, 131-42.

62. Smith, G.C. and S.P. Jackson. (1999) The DNA-dependent protein kinase. *Genes Dev*, **13**, 916-34.

63. Jackson, S.P. (2002) Sensing and repairing DNA double-strand breaks. *Carcinogenesis*, **23**, 687-96.

64. Stark, J.M. and M. Jasin. (2003) Extensive loss of heterozygosity is suppressed during homologous repair of chromosomal breaks. *Mol Cell Biol*, **23**, 733-43.

65. McHugh, P.J., V.J. Spanswick, and J.A. Hartley. (2001) Repair of DNA interstrand crosslinks: molecular mechanisms and clinical relevance. *Lancet Oncol*, **2**, 483-90.

66. Bergstralh, D.T. and J. Sekelsky. (2008) Interstrand crosslink repair: can XPF-ERCC1 be let off the hook? *Trends Genet*, **24**, 70-6.

67. Shiloh, Y. (2003) ATM and related protein kinases: safeguarding genome integrity. *Nat Rev Cancer*, **3**, 155-68.

68. Zhou, B.B. and S.J. Elledge. (2000) The DNA damage response: putting checkpoints in perspective. *Nature*, **408**, 433-9.

69. Vogelstein, B., D. Lane, and A.J. Levine. (2000) Surfing the p53 network. *Nature*, **408**, 307-10.

70. Bartek, J. and J. Lukas. (2001) Mammalian G1- and S-phase checkpoints in response to DNA damage. *Curr Opin Cell Biol*, **13**, 738-47.

71. Ryan, K.M., A.C. Phillips, and K.H. Vousden. (2001) Regulation and function of the p53 tumor suppressor protein. *Curr Opin Cell Biol*, **13**, 332-7.

72. Nyberg, K.A., et al. (2002) TOWARD MAINTAINING THE GENOME: DNA Damage and Replication Checkpoints. *Annual Review of Genetics*, **36**, 617-656.

73. Desany, B.A., et al. (1998) Recovery from DNA replicational stress is the essential function of the S-phase checkpoint pathway. *Genes Dev.*, **12**, 2956-2970.

74. Tercero, J.A., M.P. Longhese, and J.F. Diffley. (2003) A central role for DNA replication forks in checkpoint activation and response. *Mol Cell*, **11**, 1323-36.

75. Falck, J., et al. (2001) The ATM-Chk2-Cdc25A checkpoint pathway guards against radioresistant DNA synthesis. *Nature*, **410**, 842.

76. Mailand, N., et al. (2000) Rapid destruction of human Cdc25A in response to DNA damage. *Science*, **288**, 1425-9.

77. Donzelli, M. and G.F. Draetta. (2003) Regulating mammalian checkpoints through Cdc25 inactivation. *EMBO Rep*, **4**, 671-7.

78. Bulavin, D.V., S.A. Amundson, and A.J. Fornace. (2002) p38 and Chk1 kinases: different conductors for the G(2)/M checkpoint symphony. *Curr. Opin. Genet. Dev.*, **12**, 92.

79. Matsuoka, S., M. Huang, and S.J. Elledge. (1998) Linkage of ATM to Cell Cycle Regulation by the Chk2 Protein Kinase. *Science*, **282**, 1893-1897.

80. Sanchez, Y., et al. (1997) Conservation of the Chk1 checkpoint pathway in mammals: linkage of DNA damage to Cdk regulation through Cdc25. *Science*, **277**, 1497-501.

81. Bulavin, D.V., et al. (2001) Initiation of a G2/M checkpoint after ultraviolet radiation requires p38 kinase. *Nature*, **411**, 102-7.

82. Peng, C.Y. (1997) Mitotic and G2 checkpoint control: regulation of 14-3-3 protein binding by phosphorylation of Cdc25C on serine-216. *Science*, **277**, 1501-1505.

83. May, K.M. and K.G. Hardwick. (2006) The spindle checkpoint. *J Cell Sci*, **119**, 4139-42.

84. Collado, M., M.A. Blasco, and M. Serrano. (2007) Cellular senescence in cancer and aging. *Cell*, **130**, 223-33.

85. Hanahan, D. and R.A. Weinberg. (2000) The hallmarks of cancer. *Cell*, **100**, 57-70.

86. Campisi, J. (2005) Suppressing cancer: the importance of being senescent. *Science*, **309**, 886-7.

87. Finkel, T., M. Serrano, and M.A. Blasco. (2007) The common biology of cancer and ageing. *Nature*, **448**, 767-74.

88. Bartkova, J. (2005) DNA damage response as a candidate anti-cancer barrier in early human tumorigenesis. *Nature*, **434**, 864-870.

89. Gorgoulis, V.G., et al. (2005) Activation of the DNA damage checkpoint and genomic instability in human precancerous lesions. *Nature*, **434**, 907-13.

90. Bartkova, J., et al. (2006) Oncogene-induced senescence is part of the tumorigenesis barrier imposed by DNA damage checkpoints. *Nature*, **444**, 633-7.

91. Di Micco, R., et al. (2006) Oncogene-induced senescence is a DNA damage response triggered by DNA hyper-replication. *Nature*, **444**, 638-42.

92. Abraham, R.T. (2001) Cell cycle checkpoint signaling through the ATM and ATR kinases. *Genes Dev*, **15**, 2177-96.

93. Kim, S.T., et al. (1999) Substrate specificities and identification of putative substrates of ATM kinase family members. *J Biol Chem*, **274**, 37538-43.

94. O'Neill, T., et al. (2000) Utilization of oriented peptide libraries to identify substrate motifs selected by ATM. *J Biol Chem*, **275**, 22719-27.

95. Brown, A.L., et al. (1999) A human Cds1-related kinase that functions downstream of ATM protein in the cellular response to DNA damage. *Proc Natl Acad Sci U S A*, **96**, 3745-50.

96. Guo, Z., et al. (2000) Requirement for Atr in phosphorylation of Chk1 and cell cycle regulation in response to DNA replication blocks and UV-damaged DNA in Xenopus egg extracts. *Genes Dev*, **14**, 2745-56.

97. Liu, Q., et al. (2000) Chk1 is an essential kinase that is regulated by Atr and required for the G(2)/M DNA damage checkpoint. *Genes Dev*, **14**, 1448-59.

98. Banin, S., et al. (1998) Enhanced phosphorylation of p53 by ATM in response to DNA damage. *Science*, **281**, 1674-7.

99. Canman, C.E., et al. (1998) Activation of the ATM kinase by ionizing radiation and phosphorylation of p53. *Science*, **281**, 1677-9.

100. Cortez, D., et al. (1999) Requirement of ATM-dependent phosphorylation of brca1 in the DNA damage response to double-strand breaks. *Science*, **286**, 1162-6.

101. Siliciano, J.D., et al. (1997) DNA damage induces phosphorylation of the amino terminus of p53. *Genes Dev*, **11**, 3471-81.

102. Tibbetts, R.S., et al. (1999) A role for ATR in the DNA damage-induced phosphorylation of p53. *Genes Dev.*, **13**, 152-157.

103. Tibbetts, R.S., et al. (2000) Functional interactions between BRCA1 and the checkpoint kinase ATR during genotoxic stress. *Genes Dev*, **14**, 2989-3002.

104. Chehab, N.H., et al. (2000) Chk2/hCds1 functions as a DNA damage checkpoint in G(1) by stabilizing p53. *Genes Dev.*, **14**, 278.

105. Lee, J.S., et al. (2000) hCds1-mediated phosphorylation of BRCA1 regulates the DNA damage response. *Nature*, **404**, 201-4.

106. Shieh, S.Y., et al. (2000) The human homologs of checkpoint kinases Chk1 and Cds1 (Chk2) phosphorylate p53 at multiple DNA damage-inducible sites. *Genes Dev.*, **14**, 289.

107. Andegeko, Y. (2001) Nuclear retention of ATM at sites of DNA double strand breaks. *J. Biol. Chem.*, **276**, 38224-38230.

108. Mirzoeva, O.K. and J.H. Petrini. (2001) DNA damage-dependent nuclear dynamics of the Mre11 complex. *Mol Cell Biol*, **21**, 281-8.

109. Nelms, B.E., et al. (1998) In situ visualization of DNA double-strand break repair in human fibroblasts. *Science*, **280**, 590-2.

110. Suzuki, K., S. Kodama, and M. Watanabe. (1999) Recruitment of ATM protein to double strand DNA irradiated with ionizing radiation. *J Biol Chem*, **274**, 25571-5.

111. Celeste, A., et al. (2003) H2AX haploinsufficiency modifies genomic stability and tumor susceptibility. *Cell*, **114**, 371-83.

112. Rogakou, E.P., et al. (1999) Megabase chromatin domains involved in DNA double-strand breaks in vivo. *J Cell Biol*, **146**, 905-16.

113. Downs, J.A., N.F. Lowndes, and S.P. Jackson. (2000) A role for Saccharomyces cerevisiae histone H2A in DNA repair. *Nature*, **408**, 1001-4.

114. Paull, T.T., et al. (2000) A critical role for histone H2AX in recruitment of repair factors to nuclear foci after DNA damage. *Curr Biol*, **10**, 886-95.

115. Williams, R.S., et al. (2008) Mre11 dimers coordinate DNA end bridging and nuclease processing in double-strand-break repair. *Cell*, **135**, 97-109.

116. Hopfner, K.P., et al. (2002) The Rad50 zinc-hook is a structure joining Mre11 complexes in DNA recombination and repair. *Nature*, **418**, 562-6.

117. Lisby, M., et al. (2004) Choreography of the DNA damage response: spatiotemporal relationships among checkpoint and repair proteins. *Cell*, **118**, 699-713.

118. Nakada, D., K. Matsumoto, and K. Sugimoto. (2003) ATM-related Tel1 associates with double-strand breaks through an Xrs2-dependent mechanism. *Genes Dev*, **17**, 1957-62.

119. Falck, J., J. Coates, and S.P. Jackson. (2005) Conserved modes of recruitment of ATM, ATR and DNA-PKcs to sites of DNA damage. *Nature*, **434**, 605-11.

120. Uziel, T., et al. (2003) Requirement of the MRN complex for ATM activation by DNA damage. *Embo J*, **22**, 5612-21.

121. Wu, X., et al. (2000) ATM phosphorylation of Nijmegen breakage syndrome protein is required in a DNA damage response. *Nature*, **405**, 477-82.

122. D'Amours, D. and S.P. Jackson. (2002) The mre11 complex: at the crossroads of DNA repair and checkpoint signalling. *Nat. Rev. Mol. Cell. Biol.*, **3**, 317.

123. Buis, J., et al. (2008) Mre11 nuclease activity has essential roles in DNA repair and genomic stability distinct from ATM activation. *Cell*, **135**, 85-96.

124. Bakkenist, C.J. and M.B. Kastan. (2003) DNA damage activates ATM through intermolecular autophosphorylation and dimer dissociation. *Nature*, **421**, 499-506.

125. Kozlov, S.V., et al. (2006) Involvement of novel autophosphorylation sites in ATM activation. *Embo J*, **25**, 3504-14.

126. Hirao, A., et al. (2000) DNA damage-induced activation of p53 by the checkpoint kinase Chk2. *Science*, **287**, 1824-7.

127. Khosravi, R., et al. (1999) Rapid ATM-dependent phosphorylation of MDM2 precedes p53 accumulation in response to DNA damage. *Proc. Natl. Acad. Sci. USA*, **96**, 14973.

128. Dumaz, N. and D.W. Meek. (1999) Serine15 phosphorylation stimulates p53 transactivation but does not directly influence interaction with HDM2. *Embo J*, **18**, 7002-10.

129. Khanna, K.K., et al. (1998) ATM associates with and phosphorylates p53: mapping the region of interaction. *Nat Genet*, **20**, 398-400.

130. Cao, L., et al. (2006) ATM-Chk2-p53 activation prevents tumorigenesis at an expense of organ homeostasis upon Brca1 deficiency. *Embo J*, **25**, 2167-77.

131. Berkovich, E., R.J. Monnat, Jr., and M.B. Kastan. (2007) Roles of ATM and NBS1 in chromatin structure modulation and DNA double-strand break repair. *Nat Cell Biol*, **9**, 683-90.

132. Shroff, R., et al. (2004) Distribution and dynamics of chromatin modification induced by a defined DNA double-strand break. *Curr Biol*, **14**, 1703-11.

133. Cimprich, K.A. and D. Cortez. (2008) ATR: an essential regulator of genome integrity. *Nat Rev Mol Cell Biol*,

134. Shechter, D., V. Costanzo, and J. Gautier. (2004) Regulation of DNA replication by ATR: signaling in response to DNA intermediates. *DNA Repair (Amst)*, **3**, 901-8.

135. Bonilla, C.Y., J.A. Melo, and D.P. Toczyski. (2008) Colocalization of sensors is sufficient to activate the DNA damage checkpoint in the absence of damage. *Mol Cell*, **30**, 267-76.

136. Costanzo, V., et al. (2003) An ATR- and Cdc7-dependent DNA damage checkpoint that inhibits initiation of DNA replication. *Mol Cell*, **11**, 203-13.

137. Zou, L. and S.J. Elledge. (2003) Sensing DNA damage through ATRIP recognition of RPA-ssDNA complexes. *Science*, **300**, 1542-8.

138. Shechter, D., V. Costanzo, and J. Gautier. (2004) ATR and ATM regulate the timing of DNA replication origin firing. *Nat Cell Biol*, **6**, 648-55.

139. Byun, T.S., et al. (2005) Functional uncoupling of MCM helicase and DNA polymerase activities activates the ATR-dependent checkpoint. *Genes Dev*, **19**, 1040-52.

140. MacDougall, C.A., et al. (2007) The structural determinants of checkpoint activation. *Genes Dev*, **21**, 898-903.

141. Lopes, M., M. Foiani, and J.M. Sogo. (2006) Multiple mechanisms control chromosome integrity after replication fork uncoupling and restart at irreparable UV lesions. *Mol Cell*, **21**, 15-27.

142. Wold, M.S. (1997) Replication protein A: a heterotrimeric, single-stranded DNA-binding protein required for eukaryotic DNA metabolism. *Annu Rev Biochem*, **66**, 61-92.

143. de Laat, W.L., et al. (1998) DNA-binding polarity of human replication protein A positions nucleases in nucleotide excision repair. *Genes Dev*, **12**, 2598-609.

144. Iftode, C. and J.A. Borowiec. (2000) 5' --> 3' molecular polarity of human replication protein A (hRPA) binding to pseudo-origin DNA substrates. *Biochemistry*, **39**, 11970-81.

145. Kolpashchikov, D.M., et al. (2001) Polarity of human replication protein A binding to DNA. *Nucleic Acids Res*, **29**, 373-9.

146. Kim, C., B.F. Paulus, and M.S. Wold. (1994) Interactions of human replication protein A with oligonucleotides. *Biochemistry*, **33**, 14197-206.

147. Arunkumar, A.I., et al. (2003) Independent and coordinated functions of replication protein A tandem high affinity single-stranded DNA binding domains. *J Biol Chem*, **278**, 41077-82.

148. Bochkareva, E., et al. (2002) Structure of the RPA trimerization core and its role in the multistep DNA-binding mechanism of RPA. *Embo J*, **21**, 1855-63.

149. Bochkareva, E., et al. (2005) Single-stranded DNA mimicry in the p53 transactivation domain interaction with replication protein A. *Proc Natl Acad Sci U S A*, **102**, 15412-7.

150. Daughdrill, G.W., et al. (2001) The weak interdomain coupling observed in the 70 kDa subunit of human replication protein A is unaffected by ssDNA binding. *Nucleic Acids Res*, **29**, 3270-6.

151. Ball, H.L., et al. (2007) Function of a conserved checkpoint recruitment domain in ATRIP proteins. *Mol Cell Biol*, **27**, 3367-77.

152. Din, S., et al. (1990) Cell-cycle-regulated phosphorylation of DNA replication factor A from human and yeast cells. *Genes Dev*, **4**, 968-77.

153. Nuss, J.E., et al. (2005) DNA damage induced hyperphosphorylation of replication protein A. 1. Identification of novel sites of phosphorylation in response to DNA damage. *Biochemistry*, **44**, 8428-37.

154. Liu, J.S., S.R. Kuo, and T. Melendy. (2006) Phosphorylation of replication protein A by S-phase checkpoint kinases. *DNA Repair (Amst)*, **5**, 369-80.

155. Blackwell, L.J., J.A. Borowiec, and I.A. Mastrangelo. (1996) Single-stranded-DNA binding alters human replication protein A structure and facilitates interaction with DNA-dependent protein kinase. *Mol Cell Biol*, **16**, 4798-807.

156. Binz, S.K., A.M. Sheehan, and M.S. Wold. (2004) Replication protein A phosphorylation and the cellular response to DNA damage. *DNA Repair (Amst)*, **3**, 1015-24.

157. Umezu, K., et al. (1998) Genetic analysis of yeast RPA1 reveals its multiple functions in DNA metabolism. *Genetics*, **148**, 989-1005.

158. Kanoh, Y., K. Tamai, and K. Shirahige. (2006) Different requirements for the association of ATR-ATRIP and 9-1-1 to the stalled replication forks. *Gene*, **377**, 88-95.

159. Majka, J., et al. (2006) Replication protein A directs loading of the DNA damage checkpoint clamp to 5'-DNA junctions. *J Biol Chem*, **281**, 27855-61.

160. Ball, H.L., J.S. Myers, and D. Cortez. (2005) ATRIP binding to replication protein A-single-stranded DNA promotes ATR-ATRIP localization but is dispensable for Chk1 phosphorylation. *Mol Biol Cell*, **16**, 2372-81.

161. Ellison, V. and B. Stillman. (2003) Biochemical characterization of DNA damage checkpoint complexes: clamp loader and clamp complexes with specificity for 5' recessed DNA. *PLoS Biol*, **1**, E33.

162. Longhese, M.P. (2008) DNA damage response at functional and dysfunctional telomeres. *Genes Dev*, **22**, 125-40.

163. Cortez, D., et al. (2001) ATR and ATRIP: partners in checkpoint signaling. *Science*, **294**, 1713-6.

164. Edwards, R.J., N.J. Bentley, and A.M. Carr. (1999) A Rad3-Rad26 complex responds to DNA damage independently of other checkpoint proteins. *Nat. Cell Biol.*, **1**, 393.

165. Paciotti, V., et al. (2000) The checkpoint protein Ddc2, functionally related to S. pombe Rad26, interacts with Mec1 and is regulated by Mec1-dependent phosphorylation in budding yeast. *Genes Dev.*, **14**, 2046.

166. Rouse, J. and S.P. Jackson. (2000) LCD1: an essential gene involved in checkpoint control and regulation of the MEC1 signalling pathway in Saccharomyces cerevisiae. *EMBO J.*, **19**, 5801.

167. Wakayama, T., et al. (2001) Pie1, a protein interacting with Mec1, controls cell growth and checkpoint responses in Saccharomyces cerevisiae. *Mol. Cell. Biol.*, **21**, 755.

168. Ball, H.L. and D. Cortez. (2005) ATRIP oligomerization is required for ATR-dependent checkpoint signaling. *J Biol Chem*, **280**, 31390-6.

169. Namiki, Y. and L. Zou. (2006) ATRIP associates with replication protein A-coated ssDNA through multiple interactions. *Proc Natl Acad Sci U S A*, **103**, 580-5.

170. Rouse, J. and S.P. Jackson. (2002) Lcd1p recruits Mec1p to DNA lesions in vitro and in vivo. *Mol Cell*, **9**, 857-69.

171. Unsal-Kacmaz, K., et al. (2002) Preferential binding of ATR protein to UV-damaged DNA. *Proc Natl Acad Sci U S A*, **99**, 6673-8.

172. Barr, S.M., et al. (2003) ATR kinase activity regulates the intranuclear translocation of ATR and RPA following ionizing radiation. *Curr Biol*, **13**, 1047-51.

173. Itakura, E., et al. (2004) ATR-dependent phosphorylation of ATRIP in response to genotoxic stress. *Biochem Biophys Res Commun*, **323**, 1197-202.

174. Hermand, D. and P. Nurse. (2007) Cdc18 enforces long-term maintenance of the S phase checkpoint by anchoring the Rad3-Rad26 complex to chromatin. *Mol. Cell*, **26**, 553-563.

175. Myers, J.S., et al. (2007) Cyclin-dependent kinase 2 dependent phosphorylation of ATRIP regulates the G2-M checkpoint response to DNA damage. *Cancer Res*, **67**, 6685-90.

176. Venere, M., et al. (2007) Phosphorylation of ATR-interacting protein on Ser239 mediates an interaction with breast-ovarian cancer susceptibility 1 and checkpoint function. *Cancer Res*, **67**, 6100-5.

177. St Onge, R.P., et al. (1999) The human G2 checkpoint control protein hRAD9 is a nuclear phosphoprotein that forms complexes with hRAD1 and hHUS1. *Mol Biol Cell*, **10**, 1985-95.

178. Volkmer, E. and L.M. Karnitz. (1999) Human homologs of Schizosaccharomyces pombe rad1, hus1, and rad9 form a DNA damage-responsive protein complex. *J. Biol. Chem.*, **274**, 567.

179. Kaur, R., C.F. Kostrub, and T. Enoch. (2001) Structure-function analysis of fission yeast Hus1-Rad1-Rad9 checkpoint complex. *Mol Biol Cell*, **12**, 3744-58.

180. Caspari, T., et al. (2000) Characterization of Schizosaccharomyces pombe Hus1: a PCNA-related protein that associates with Rad1 and Rad9. *Mol Cell Biol*, **20**, 1254-62.

181. Thelen, M.P., C. Venclovas, and K. Fidelis. (1999) A sliding clamp model for the Rad1 family of cell cycle checkpoint proteins. *Cell*, **96**, 769-70.

182. Venclovas, C. and M.P. Thelen. (2000) Structure-based predictions of Rad1, Rad9, Hus1 and Rad17 participation in sliding clamp and clamp-loading complexes. *Nucleic Acids Res*, **28**, 2481-93.

183. Krishna, T.S., et al. (1994) Crystal structure of the eukaryotic DNA polymerase processivity factor PCNA. *Cell*, **79**, 1233-43.

184. Bao, S., et al. (2004) Disruption of the Rad9/Rad1/Hus1 (9-1-1) complex leads to checkpoint signaling and replication defects. *Oncogene*, **23**, 5586-93.

185. Hopkins, K.M. (2004) Deletion of mouse rad9 causes abnormal cellular responses to DNA damage, genomic instability, and embryonic lethality. *Mol. Cell. Biol.*, **24**, 7235-7248.

186. Weiss, R.S., T. Enoch, and P. Leder. (2000) Inactivation of mouse Hus1 results in genomic instability and impaired responses to genotoxic stress. *Genes Dev.*, **14**, 1886-1898.

187. Weiss, R.S., et al. (2002) Hus1 acts upstream of chk1 in a mammalian DNA damage response pathway. *Curr Biol*, **12**, 73-7.

188. Bowman, G.D., et al. (2005) DNA polymerase clamp loaders and DNA recognition. *FEBS Lett*, **579**, 863-7.

189. Rauen, M., et al. (2000) The human checkpoint protein hRad17 interacts with the PCNA-like proteins hRad1, hHus1, and hRad9. *J Biol Chem*, **275**, 29767-71.

190. Bermudez, V.P., et al. (2003) Loading of the human 9-1-1 checkpoint complex onto DNA by the checkpoint clamp loader hRad17-replication factor C complex in vitro. *Proc Natl Acad Sci U S A*, **100**, 1633-8.

191. Green, C.M., et al. (2000) A novel Rad24 checkpoint protein complex closely related to replication factor C. *Curr Biol*, **10**, 39-42.

192. Griffith, J.D., L.A. Lindsey-Boltz, and A. Sancar. (2002) Structures of the human Rad17-replication factor C and checkpoint Rad 9-1-1 complexes visualized by glycerol spray/low voltage microscopy. *J Biol Chem*, **277**, 15233-6.

193. Lindsey-Boltz, L.A., et al. (2001) Purification and characterization of human DNA damage checkpoint Rad complexes. *Proc Natl Acad Sci U S A*, **98**, 11236-41.

194. Majka, J. and P.M. Burgers. (2003) Yeast Rad17/Mec3/Ddc1: a sliding clamp for the DNA damage checkpoint. *Proc Natl Acad Sci U S A*, **100**, 2249-54.

195. Kim, H.S. and S.J. Brill. (2001) Rfc4 interacts with Rpa1 and is required for both DNA replication and DNA damage checkpoints in Saccharomyces cerevisiae. *Mol Cell Biol*, **21**, 3725-37.

196. Zou, L., D. Liu, and S.J. Elledge. (2003) Replication protein A-mediated recruitment and activation of Rad17 complexes. *Proc Natl Acad Sci U S A*, **100**, 13827-32.

197. Yan, S. and W.M. Michael, *TopBP1 and DNA polymerase-{alpha} directly recruit the 9-1-1 complex to stalled DNA replication forks*. 2009. p. jcb.200810185.

198. Hashimoto, Y. and H. Takisawa. (2003) Xenopus Cut5 is essential for a CDK-dependent process in the initiation of DNA replication. *Embo J*, **22**, 2526-35.

199. Parrilla-Castellar, E.R. and L.M. Karnitz. (2003) Cut5 is required for the binding of Atr and DNA polymerase alpha to genotoxin-damaged chromatin. *J Biol Chem*, **278**, 45507-11.

200. Van Hatten, R.A., et al. (2002) The Xenopus Xmus101 protein is required for the recruitment of Cdc45 to origins of DNA replication. *J Cell Biol*, **159**, 541-7.

201. Wang, W., et al. (2004) The human Rad9-Rad1-Hus1 checkpoint complex stimulates flap endonuclease 1. *Proc Natl Acad Sci U S A*, **101**, 16762-7.

202. Lupardus, P.J. and K.A. Cimprich. (2006) Phosphorylation of Xenopus Rad1 and Hus1 defines a readout for ATR activation that is independent of Claspin and the Rad9 carboxy terminus. *Mol Biol Cell*, **17**, 1559-69.

203. Delacroix, S., et al. (2007) The Rad9-Hus1-Rad1 (9-1-1) clamp activates checkpoint signaling via TopBP1. *Genes Dev*, **21**, 1472-7.

204. St Onge, R.P., et al. (2003) A role for the phosphorylation of hRad9 in checkpoint signaling. *J Biol Chem*, **278**, 26620-8.

205. Roos-Mattjus, P., et al. (2003) Phosphorylation of human Rad9 is required for genotoxin-activated checkpoint signaling. *J Biol Chem*, **278**, 24428-37.

206. Lee, J., A. Kumagai, and W.G. Dunphy. (2007) The Rad9-Hus1-Rad1 checkpoint clamp regulates interaction of TopBP1 with ATR. *J Biol Chem*, **282**, 28036-44.

207. Hirai, I. and H.G. Wang. (2002) A role of the C-terminal region of human Rad9 (hRad9) in nuclear transport of the hRad9 checkpoint complex. *J Biol Chem*, **277**, 25722-7.

208. Komatsu, K., et al. (2000) Human homologue of S. pombe Rad9 interacts with BCL-2/BCL-xL and promotes apoptosis. *Nat Cell Biol*, **2**, 1-6.

209. Bessho, T. and A. Sancar. (2000) Human DNA damage checkpoint protein hRAD9 is a 3' to 5' exonuclease. *J Biol Chem*, **275**, 7451-4.

210. Parker, A.E., et al. (1998) A human homologue of the Schizosaccharomyces pombe rad1+ checkpoint gene encodes an exonuclease. *J Biol Chem*, **273**, 18332-9.

211. Barlow, J.H., M. Lisby, and R. Rothstein. (2008) Differential regulation of the cellular response to DNA double-strand breaks in G1. *Mol Cell*, **30**, 73-85.

212. Guan, X., et al. (2007) The human checkpoint sensor Rad9-Rad1-Hus1 interacts with and stimulates DNA repair enzyme TDG glycosylase. *Nucleic Acids Res*, **35**, 6207-18.

213. Toueille, M., et al. (2004) The human Rad9/Rad1/Hus1 damage sensor clamp interacts with DNA polymerase beta and increases its DNA substrate utilisation efficiency: implications for DNA repair. *Nucleic Acids Res*, **32**, 3316-24.

214. Paulovich, A.G., C.D. Armour, and L.H. Hartwell. (1998) The Saccharomyces cerevisiae RAD9, RAD17, RAD24 and MEC3 genes are required for tolerating irreparable, ultraviolet-induced DNA damage. *Genetics*, **150**, 75-93.

215. Kai, M., et al. (2007) Rad3-dependent phosphorylation of the checkpoint clamp regulates repair-pathway choice. *Nat Cell Biol*, **9**, 691-7.

216. He, W., et al. (2008) Rad9 plays an important role in DNA mismatch repair through physical interaction with MLH1. *Nucleic Acids Res*, **36**, 6406-17.

217. Kumagai, A., et al. (2006) TopBP1 activates the ATR-ATRIP complex. *Cell*, **124**, 943-55.

218. Mordes, D.A., et al. (2008) TopBP1 activates ATR through ATRIP and a PIKK regulatory domain. *Genes Dev*, **22**, 1478-89.

219. Walworth, N.C. and R. Bernards. (1996) rad-dependent response of the chk1-encoded protein kinase at the DNA damage checkpoint. *Science*, **271**, 353-356.

220. Lopez-Girona, A., et al. (2001) Serine-345 is required for Rad3-dependent phosphorylation and function of checkpoint kinase Chk1 in fission yeast. *Proc Natl Acad Sci U S A*, **98**, 11289-94.

221. Zhao, H. and H. Piwnica-Worms. (2001) ATR-mediated checkpoint pathways regulate phosphorylation and activation of human Chk1. *Mol Cell Biol*, **21**, 4129-39.

222. Smits, V.A., P.M. Reaper, and S.P. Jackson. (2006) Rapid PIKK-dependent release of Chk1 from chromatin promotes the DNA-damage checkpoint response. *Curr. Biol.*, **16**, 150-159.

223. Kumagai, A. and W.G. Dunphy. (2000) Claspin, a novel protein required for the activation of Chk1 during a DNA replication checkpoint response in Xenopus egg extracts. *Mol Cell*, **6**, 839-49.

224. Liu, S., et al. (2006) Claspin operates downstream of TopBP1 to direct ATR signaling towards Chk1 activation. *Mol Cell Biol*, **26**, 6056-64.

225. Chini, C.C. and J. Chen. (2006) Repeated phosphopeptide motifs in human Claspin are phosphorylated by Chk1 and mediate Claspin function. *J Biol Chem*, **281**, 33276-82.

226. Kumagai, A. and W.G. Dunphy. (2003) Repeated phosphopeptide motifs in Claspin mediate the regulated binding of Chk1. *Nat Cell Biol*, **5**, 161-5.

227. Wang, X., et al. (2006) Rad17 phosphorylation is required for claspin recruitment and Chk1 activation in response to replication stress. *Mol Cell*, **23**, 331-41.

228. Bao, S., et al. (2001) ATR/ATM-mediated phosphorylation of human Rad17 is required for genotoxic stress responses. *Nature*, **411**, 969-74.

229. Unsal-Kacmaz, K., et al. (2007) The human Tim/Tipin complex coordinates an Intra-S checkpoint response to UV that slows replication fork displacement. *Mol Cell Biol*, **27**, 3131-42.

230. Thompson, D., et al. (2005) Cancer risks and mortality in heterozygous ATM mutation carriers. *J Natl Cancer Inst*, **97**, 813-22.

231. Brown, E.J. and D. Baltimore. (2000) ATR disruption leads to chromosomal fragmentation and early embryonic lethality. *Genes Dev*, **14**, 397-402.

232. de Klein, A. (2000) Targeted disruption of the cell-cycle checkpoint gene ATR leads to early embryonic lethality in mice. *Curr. Biol.*, **10**, 479-482.

233. Jazayeri, A., et al. (2006) ATM- and cell cycle-dependent regulation of ATR in response to DNA double-strand breaks. *Nat Cell Biol*, **8**, 37-45.

234. Myers, J.S. and D. Cortez. (2006) Rapid activation of ATR by ionizing radiation requires ATM and Mre11. *J Biol Chem*, **281**, 9346-50.

235. Adams, K.E., et al. (2006) Recruitment of ATR to sites of ionising radiation-induced DNA damage requires ATM and components of the MRN protein complex. *Oncogene*, **25**, 3894-904.

236. Cuadrado, M., et al. (2006) ATM regulates ATR chromatin loading in response to DNA double-strand breaks. *J Exp Med*, **203**, 297-303.

237. Lisby, M. and R. Rothstein. (2004) DNA damage checkpoint and repair centers. *Curr Opin Cell Biol*, **16**, 328-34.

238. Wyman, C. and R. Kanaar. (2006) DNA double-strand break repair: all's well that ends well. *Annu Rev Genet*, **40**, 363-83.

239. Gravel, S., et al. (2008) DNA helicases Sgs1 and BLM promote DNA double-strand break resection. *Genes Dev*, **22**, 2767-72.

240. Nakada, D., Y. Hirano, and K. Sugimoto. (2004) Requirement of the Mre11 complex and exonuclease 1 for activation of the Mec1 signaling pathway. *Mol Cell Biol*, **24**, 10016-25.

241. Yoo, H.Y., et al. (2007) Ataxia-telangiectasia mutated (ATM)-dependent activation of ATR occurs through phosphorylation of TopBP1 by ATM. *J. Biol. Chem.*, **282**, 17501-17506.

242. Stiff, T., et al. (2006) ATR-dependent phosphorylation and activation of ATM in response to UV treatment or replication fork stalling. *Embo J*, **25**, 5775-82.

243. Nghiem, P., et al. (2001) ATR inhibition selectively sensitizes G1 checkpoint-deficient cells to lethal premature chromatin condensation. *Proc Natl Acad Sci U S A*, **98**, 9092-7.

244. Parrilla-Castellar, E.R., S.J. Arlander, and L. Karnitz. (2004) Dial 9-1-1 for DNA damage: the Rad9-Hus1-Rad1 (9-1-1) clamp complex. *DNA Repair (Amst)*, **3**, 1009-14.

245. Zhu, A., C.X. Zhang, and H.B. Lieberman. (2008) Rad9 has a functional role in human prostate carcinogenesis. *Cancer Res*, **68**, 1267-74.

246. Parker, A.E., et al. (1998) Identification of a human homologue of the Schizosaccharomyces pombe rad17+ checkpoint gene. *J Biol Chem*, **273**, 18340-6.

247. Kinzel, B., et al. (2002) Downregulation of Hus1 by antisense oligonucleotides enhances the sensitivity of human lung carcinoma cells to cisplatin. *Cancer*, **94**, 1808-14.

248. Lopes, M., et al. (2001) The DNA replication checkpoint response stabilizes stalled replication forks. *Nature*, **412**, 557-561.

249. Tercero, J.A. and J.F. Diffley. (2001) Regulation of DNA replication fork progression through damaged DNA by the Mec1/Rad53 checkpoint. *Nature*, **412**, 553-7.

250. Carr, A.M. (2002) Checking That Replication Breakdown Is Not Terminal. *Science*, **297**, 557-558.

251. Kolodner, R.D., C.D. Putnam, and K. Myung. (2002) Maintenance of Genome Stability in Saccharomyces cerevisiae. *Science*, **297**, 552-557.

252. Casper, A.M., et al. (2002) ATR regulates fragile site stability. *Cell*, **111**, 779-89.

253. Rudin, N. and J.E. Haber. (1988) Efficient repair of HO-induced chromosomal breaks in Saccharomyces cerevisiae by recombination between flanking homologous sequences. *Mol Cell Biol*, **8**, 3918-28.

254. Richardson, C. and M. Jasin. (2000) Frequent chromosomal translocations induced by DNA double-strand breaks. *Nature*, **405**, 697-700.

255. White, C.I. and J.E. Haber. (1990) Intermediates of recombination during mating type switching in Saccharomyces cerevisiae. *Embo J*, **9**, 663-73.

256. Dodson, M., et al. (1987) Unwinding of duplex DNA from the SV40 origin of replication by T antigen. *Science*, **238**, 964-7.

257. Diviacco, S., et al. (2001) Site-directed inhibition of DNA replication by triple helix formation. *Faseb J*, **15**, 2660-8.

258. Vasquez, K.M., et al. (2002) Human XPA and RPA DNA repair proteins participate in specific recognition of triplex-induced helical distortions. *Proc Natl Acad Sci U S A*, **99**, 5848-53.

259. Arad, U. (1998) Modified Hirt procedure for rapid purification of extrachromosomal DNA from mammalian cells. *Biotechniques*, **24**, 760-2.

260. Friedman, K.L. and B.J. Brewer. (1995) Analysis of replication intermediates by two-dimensional agarose gel electrophoresis. *Methods Enzymol*, **262**, 613-27.

261. Mecsas, J. and B. Sugden. (1987) Replication of plasmids derived from bovine papilloma virus type 1 and Epstein-Barr virus in cells in culture. *Annu Rev Cell Biol*, **3**, 87-108.

262. Faria, M., et al. (2000) Targeted inhibition of transcription elongation in cells mediated by triplex-forming oligonucleotides. *Proc Natl Acad Sci U S A*, **97**, 3862-7.

263. Giovannangeli, C., et al. (1992) Triple-helix formation by oligonucleotides containing the three bases thymine, cytosine, and guanine. *Proc Natl Acad Sci U S A*, **89**, 8631-5.

264. Hearst, J.E., et al. (1984) The reaction of the psoralens with deoxyribonucleic acid. *Q Rev Biophys*, **17**, 1-44.

265. Barre, F.X., U. Asseline, and A. Harel-Bellan. (1999) Asymmetric recognition of psoralen interstrand crosslinks by the nucleotide excision repair and the error-prone repair pathways. *J Mol Biol*, **286**, 1379-87.

266. Cortez, D. (2005) Unwind and slow down: checkpoint activation by helicase and polymerase uncoupling. *Genes Dev*, **19**, 1007-12.

267. Gillespie, P.J. and J.J. Blow. (2000) Nucleoplasmin-mediated chromatin remodelling is required for Xenopus sperm nuclei to become licensed for DNA replication. *Nucleic Acids Res*, **28**, 472-80.

268. Jiang, G. and A. Sancar. (2006) Recruitment of DNA damage checkpoint proteins to damage in transcribed and nontranscribed sequences. *Mol Cell Biol*, **26**, 39-49.

269. Shiloh, Y. (2001) ATM and ATR: networking cellular responses to DNA damage. *Current Opinion in Genetics & Development*, **11**, 71-77.

270. Lukas, J., C. Lukas, and J. Bartek. (2004) Mammalian cell cycle checkpoints: signalling pathways and their organization in space and time. *DNA Repair (Amst)*, **3**, 997-1007.

271. Chen, B.P., et al. (2007) Ataxia telangiectasia mutated (ATM) is essential for DNA-PKcs phosphorylations at the Thr-2609 cluster upon DNA double strand break. *J Biol Chem*, **282**, 6582-7.

272. Yajima, H., K.J. Lee, and B.P. Chen. (2006) ATR-dependent phosphorylation of DNA-dependent protein kinase catalytic subunit in response to UV-induced replication stress. *Mol Cell Biol*, **26**, 7520-8.

273. Mordes, D.A. and D. Cortez. (2008) Activation of ATR and related PIKKs. *Cell Cycle*, **7**, 2809-12.

274. Shenoy, S., et al. (1989) Purified maturation promoting factor phosphorylates pp60c-src at the sites phosphorylated during fibroblast mitosis. *Cell*, **57**, 763-74.

275. Grishina, I. and B. Lattes. (2005) A novel Cdk2 interactor is phosphorylated by Cdc7 and associates with components of the replication complexes. *Cell Cycle*, **4**, 1120-6.

276. Friedman, J.R., et al. (1996) KAP-1, a novel corepressor for the highly conserved KRAB repression domain. *Genes Dev*, **10**, 2067-78.

277. Ziv, Y., et al. (2006) Chromatin relaxation in response to DNA double-strand breaks is modulated by a novel ATM- and KAP-1 dependent pathway. *Nat Cell Biol*, **8**, 870-6.

278. Fernandez-Capetillo, O., et al. (2004) H2AX: the histone guardian of the genome. *DNA Repair (Amst)*, **3**, 959-67.

279. Sedelnikova, O.A., et al. (2003) Histone H2AX in DNA damage and repair. *Cancer Biol Ther*, **2**, 233-5.

280. Deng, C.X. (2006) BRCA1: cell cycle checkpoint, genetic instability, DNA damage response and cancer evolution. *Nucleic Acids Res*, **34**, 1416-26.

281. Manke, I.A., et al. (2003) BRCT repeats as phosphopeptide-binding modules involved in protein targeting. *Science*, **302**, 636-9.

282. Yu, X., et al. (2003) The BRCT domain is a phospho-protein binding domain. *Science*, **302**, 639-42.

283. Lupas, A. (1996) Coiled coils: new structures and new functions. *Trends Biochem Sci*, **21**, 375-82.

284. Lupardus, P.J., et al. (2002) A requirement for replication in activation of the ATR-dependent DNA damage checkpoint. *Genes Dev*, **16**, 2327-32.

285. Ward, I.M., K. Minn, and J. Chen. (2004) UV-induced ataxia-telangiectasia-mutated and Rad3-related (ATR) activation requires replication stress. *J Biol Chem*, **279**, 9677-80.

286. Ira, G., et al. (2004) DNA end resection, homologous recombination and DNA damage checkpoint activation require CDK1. *Nature*, **431**, 1011-7.

287. Maude, S.L. and G.H. Enders. (2005) Cdk inhibition in human cells compromises chk1 function and activates a DNA damage response. *Cancer Res*, **65**, 780-6.

288. Dephoure, N., et al. (2008) A quantitative atlas of mitotic phosphorylation. *Proc Natl Acad Sci U S A*, **105**, 10762-7.

289. Stevenson-Lindert, L.M., P. Fowler, and J. Lew, *Substrate Specificity of CDK2-Cyclin A: WHAT IS OPTIMAL?* 2003. p. 50956-50960.

290. Xu, X., et al. (2008) The basic cleft of RPA70N binds multiple checkpoint proteins, including RAD9, to regulate ATR signaling. *Mol Cell Biol*, **28**, 7345-53.

291. Michael, W.M., et al. (2000) Activation of the DNA replication checkpoint through RNA synthesis by primase. *Science*, **289**, 2133-2137.

292. Stokes, M.P., et al. (2002) DNA replication is required for the checkpoint response to damaged DNA in Xenopus egg extracts. *J. Cell Biol.*, **158**, 863-872.

293. Kim, S.M., et al. (2005) Phosphorylation of Chk1 by ATM- and Rad3-related (ATR) in Xenopus egg extracts requires binding of ATRIP to ATR but not the stable DNA-binding or coiled-coil domains of ATRIP. *J Biol Chem*, **280**, 38355-64.

294. Lovejoy, C.A., et al. (2006) DDB1 maintains genome integrity through regulation of Cdt1. *Mol Cell Biol*, **26**, 7977-90.

295. Dodson, G.E., Y. Shi, and R.S. Tibbetts. (2004) DNA replication defects, spontaneous DNA damage, and ATM-dependent checkpoint activation in replication protein A-deficient cells. *J Biol Chem*, **279**, 34010-4.

296. Wu, X., S.M. Shell, and Y. Zou. (2005) Interaction and colocalization of Rad9/Rad1/Hus1 checkpoint complex with replication protein A in human cells. *Oncogene*, **24**, 4728-35.

297. Yoshioka, K., Y. Yoshioka, and P. Hsieh. (2006) ATR kinase activation mediated by MutS[alpha] and MutL[alpha] in response to cytotoxic O6-methylguanine adducts. *Mol. Cell*, **22**, 501-510.

298. Stauffer, M.E. and W.J. Chazin. (2004) Structural mechanisms of DNA replication, repair, and recombination. *J Biol Chem*, **279**, 30915-8.

299. Lee, S.E., et al. (1998) Saccharomyces Ku70, mre11/rad50 and RPA proteins regulate adaptation to G2/M arrest after DNA damage. *Cell*, **94**, 399-409.

300. Haring, S.J., et al. (2008) Cellular functions of human RPA1. Multiple roles of domains in replication, repair, and checkpoints. *J Biol Chem*, **283**, 19095-111.

301. Jacobs, D.M., et al. (1999) Human replication protein A: global fold of the N-terminal RPA-70 domain reveals a basic cleft and flexible C-terminal linker. *J Biomol NMR*, **14**, 321-31.

302. Olson, E., et al. (2007) The Mre11 complex mediates the S-phase checkpoint through an interaction with replication protein A. *Mol Cell Biol*, **27**, 6053-67.

303. Collins, I. and M.D. Garrett. (2005) Targeting the cell division cycle in cancer: CDK and cell cycle checkpoint kinase inhibitors. *Curr. Opin. Pharmacol.*, **5**, 366-373.

304. Kaelin, W.G. (2005) The concept of synthetic lethality in the context of anticancer therapy. *Nature Rev. Cancer*, **5**, 689-698.

305. Kohn, E.A., et al. (2002) Abrogation of the S phase DNA damage checkpoint results in S phase progression or premature mitosis depending on the concentration of 7-hydroxystaurosporine and the kinetics of Cdc25C activation. *J Biol Chem*, **277**, 26553-64.